STUDIA UNIVERSITATIS
BABEŞ-BOLYAI

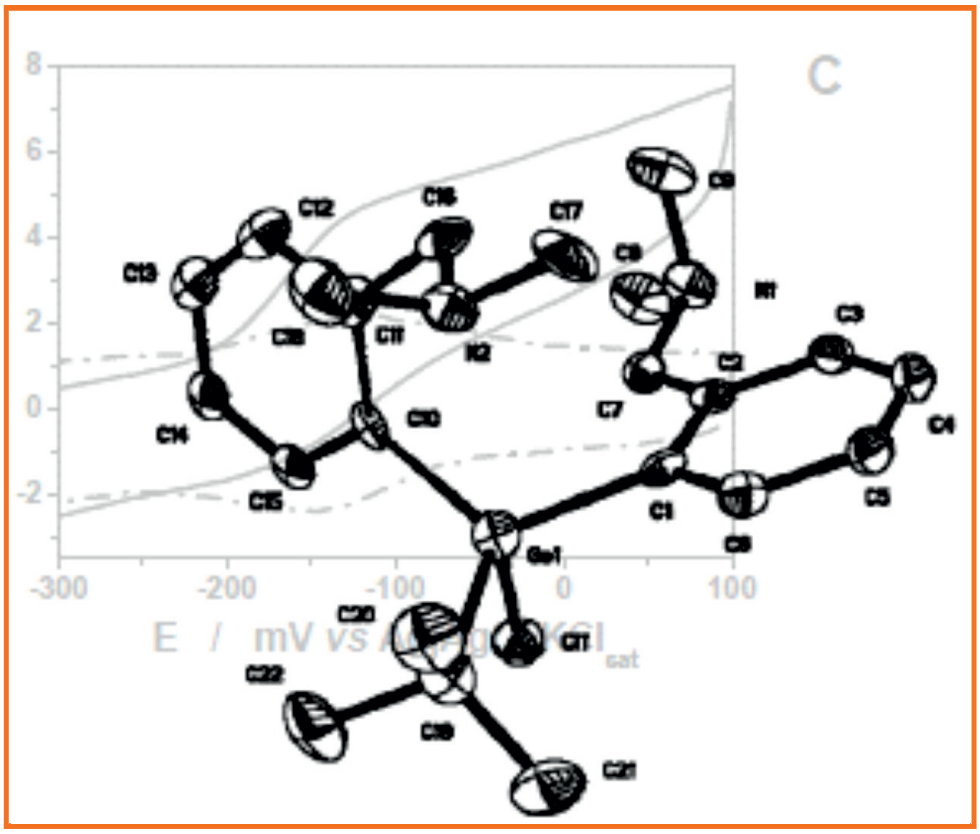

CHEMIA

2/2012

YEAR **(LVII) 2012**
MONTH **JUNE**
ISSUE **2**

S T U D I A
UNIVERSITATIS BABEŞ–BOLYAI

CHEMIA

2

Desktop Editing Office: 51ST B.P. Hasdeu, Cluj-Napoca, Romania, Phone + 40 264-40.53.52

CUPRINS – CONTENT – SOMMAIRE – INHALT

Studia Universitatis Babes-Bolyai Chemia has been selected for coverage in Thomson Reuters products and custom information services. Beginning with V. 53 (1) 2008, this publication is indexed and abstracted in the following:

- Science Citation Index Expanded (also known as SciSearch®)
- Chemistry Citation Index®
- Journal Citation Reports/Science Edition

This year Professor Ionel Haiduc, Member of the Roumanian Academy, celebrates his 75th birthday. Born in Cluj on May 9th, 1937, Ionel Haiduc graduated the Faculty of Chemistry of the University of Cluj in 1959. In 1964, he obtained the equivalent of a PhD in chemistry at the M.V. Lomonosov Institute of Fine Chemicals Technology in Moscow under a guidance of the Academician K.A. Andrianov. From 1959 until the present time the scientific life of Acad. Ionel Haiduc was developed at the Faculty of Chemistry of the University of Cluj. Full professor at the age of 36, he completed his formation as a researcher, in U.S.A., between 1966 and 1972, during three postdoctoral stages. Between 1990 and 1993 he was the Rector of "Babes-Bolyai" University of Cluj-Napoca and the vice-president of National Conference of Rectors. The passion for science in general and for chemistry in particular, the joy of sharing knowledge was appreciated by generations of students who often would have liked the courses to be never-ending stories. He is an outstanding professor and mentor recognized by the whole academic community.

The scientific areas covered by Professor Ionel Haiduc are Coordination and organometallic chemistry of Main Group elements, Supramolecular organometallic chemistry, Inorganic rings, Biologically active metal compounds (including antitumor activity), Inorganic chemistry nomenclature and systematization.

Faculty of Chemistry and Chemical Engineering of Babes-Bolyai University Cluj-Napoca has now a well known School of Organometallic Chemistry developed by Professor Ionel Haiduc starting the early 70's.

Professor Ionel Haiduc was always connected to the different aspects of the chemists' community life. Like a member of many academic bodies, he was involved in Science policy and management, as an active actor fighting for quality in the academic life and as author of publications.

The scientific work of Professor Ionel Haiduc is covered by 9 books (published in Romanian, Polish, English and Greek), 25 chapters in collective volumes and more than 400 scientific and review articles.

The most recent book published "Supramolecular Organometallic Chemistry" (co-authored by F. Edelmann), with the Foreword written by Jean-

Marie Lehn, Nobel prize winner, describes not only a major field of chemistry, but also a vivid interface between chemistry, biology, physics, and materials science. The prestigious ACS journal Crystal Growth & Design quoted: "As a discrete field, supramolecular organometallic chemistry did not exist until the publication of Haiduc and Edelmann's book *Supramolecular Organometallic Chemistry"*.

His brilliant career received a fully deserved recognition. The Romanian Academy offered him the "Gh. Spacu" prize in 1974 and elected him as corresponding member in 1990 and as full member in 1991. He was president of the Cluj-branch (1995-2006) and vice-president of the Romanian Academy (1998-2000). Starting 2006 he is the President of the Romanian Academy. Many other national and international awards and prizes mark the exceptional carrier of Ionel Haiduc. To name only a few of them: Humboldt Forschungsaufenthalt (1997), Gauss Professorship, Göttingen Academy (1998-1999), "Pro Colaboratione" Award, Hungarian Academy of Sciences, Debrecen Branch (1999), Honour Diploma, Presidium of the Moldavian Academy of Sciences (1999), Honorary Member of the Academy of Sciences of Moldova (2002), elected member of Academia Europaea (London) (2002), *Doctor honoris causa,* Technical Univerity "Gh. Assachi", Iasi, Romania (2002) and Polytechnical Univeristy of Timisoara, Romania (2004), Prize of Romanian Chemical Society (2004).

He also was awarded by the Presidents of Romania with "*Star of Romania*" ["Steaua Romaniei"] (2000 – mare ofiter, 2006 "mare cruce") and in 2006 and the "*Order of Honour,"* by the President of Republic Moldova.

With his scientific horizon, his sense of humor and his kindness, he was a perfect ambassador of the Romanian school of chemistry.

At his 75th anniversary, the Editorial Board of Studia Universitatis Babes-Bolyai, Series Chemia presents to Professor Ionel Haiduc the very best wishes for a long healthy and fruitful life and many successes in the years to come.

Editorial Board

STUDIA UBB CHEMIA, LVII, 2, 2012 (p. 7 - 20)

ANALYSIS IN TERMS OF THE MODIFIED UNIFAC (DORTMUND) GROUP CONTRIBUTION MODEL OF THE EXPERIMENTAL VAPOR - LIQUID EQUILIBRIUM DATA IN BINARY AND TERNARY SYSTEMS CONTAINING (1*R*,4*S*)-(+)-FENCHONE, METHYL CHAVICOL AND *trans*-ANETHOLE

IOAN BATIU[a,*], GEORGE M. PANAITESCU[b]

ABSTRACT. The experimental vapor-liquid equilibrium data (VLE) in binary and ternary systems which contain (1*R*,4*S*)-(+)-fenchone, methyl chavicol and *trans*-anethole, reported in previous papers, were used to check the predictive capability of the Modified UNIFAC (Dortmund) group contribution model in mixtures containing terpenoids. A comparison with the experimental VLE data was done. The Mod. UNIFAC (Do) group contribution model predicts satisfactory VLE data in all the binary and ternary systems but inadequately the values of the excess Gibbs energy. The Modified UNIFAC (Dortmund) group contribution model is the most useful model to predicts vapor-liquid equilibrium data.

Keywords: *Mod. UNIFAC (Dortmund), Vapor - liquid equilibria, Terpenoids, excess Gibbs energy.*

INTRODUCTION

Reliable phase equilibrium information of the system to be separated is most important for the development, design and optimization of separation processes. Since experimental data are often missing or of poor quality, group contribution methods became increasingly valuable.

The most common group contribution methods for the prediction of phase equilibria are: ASOG [1, 2, 3], original UNIFAC [4, 5, 6], Modified UNIFAC (Dortmund) [7, 8, 9], Modified UNIFAC [10] (Lyngby) and DISQUAC [11, 12].

While ASOG and the original UNIFAC method were developed mainly for the prediction of vapor-liquid equilibria (VLE) and azeotropic data, the modified versions of UNIFAC also reliable predict excess enthalpies, (h^E), solid-liquid equiilibria (SLE) of eutectic systems, activity coefficients at infinite dilution (γ^{∞}) and liquid-liquid equilibria (LLE).

[a] "Babeş-Bolyai" University of Cluj-Napoca, Faculty of Chemistry and Chemical Engineering, Arany Janos Street 11, 400028 Cluj-Napoca, Romania, * batiu@chem.ubbcluj.ro
[b] Petroleum-Gas University of Ploieşti, Bd. Bucureşti nr. 39, 100680 Ploieşti, Romania

According to the Mod. UNIFAC (Do) model the molecules are decomposed in structural groups. Each structural group is characterized by van der Waals volume, R_k and van der Waals surface area, Q_k.

The equations used in Mod. UNIFAC (Do) model to calculate activity coefficients, γ_i, vapor-liquid equilibria (VLE) or excess Gibbs energy, G^E, are the same as in original UNIFAC [4, 5].

The activity coefficient is the sum of a combinatorial part, essentially due to differences in size and shape of the molecules in the mixture, and a residual part, essentially due to energy interactions:

$$\ln \gamma_i = \ln \gamma_i^C + \ln \gamma_i^R \tag{1}$$

The combinatorial part was changed in an empirical way to made it possible to deal with compounds very different in size:

$$\ln \gamma_i^C = 1 - V_i^{'} + \ln V_i^{'} - 5q_i\left(1 - \frac{V_i}{F_i} + \ln\left(\frac{V_i}{F_i}\right)\right) \tag{2}$$

The parameter $V_i^{'}$ can be calculated by using the relative van der Waals volume, R_k of the different groups:

$$V_i^{'} = \frac{r_i^{3/4}}{\sum_j x_j r_j^{3/4}}; r_i = \sum \nu_k^{(i)} R_k \tag{3}$$

All others parameters, V_i, F_i, r_i, q_i are calculated in the same way as for the original UNIFAC model, i.e.

$$V_i = \frac{r_i}{\sum_j x_j r_j}; r_i = \sum \nu_k^{(i)} R_k \tag{4}$$

$$F_i = \frac{q_i}{\sum_j x_j q_j}; q_i = \sum \nu_k^{(i)} Q_k \tag{5}$$

where: r_i, is van der Waals volume of the molecule i, q_i, is van der Waals surface area of the molecule i. x_i, mol. fr. of the molecule i in mixture, $\nu_k^{(i)}$ is the number of groups of type k in molecule i.

In comparison to the original UNIFAC model, only the van der Waals properties, R_k, Q_k were changed slightly.

The residual part can be obtained by using the equations (eqs. 6, 7):

$$\ln \gamma_i^R = \sum_k \nu_k^{(i)} \left(\ln \Gamma_k - \ln \Gamma_k^{(i)} \right) \tag{6}$$

$$\ln \Gamma_k = Q_k \left[1 - \ln \left(\sum_m \theta_m \psi_{mk} \right) - \sum_m \frac{\theta_m \psi_{km}}{\sum_n \theta_n \psi_{nm}} \right] \tag{7}$$

where: Γ_k is the group residual activity coefficient, and $\Gamma_k^{(i)}$ is the residual activity coefficient of group *k* in a reference solution containing only molecules of type *i*, ψ_{nm} is the interaction parameters between main groups *n* and *m*. In equation (6) the term $\Gamma_k^{(i)}$ is necessary to obtain the normalization that activity coefficient γ_i becomes unity as $x_i \to 1$.The group area fraction, θ_m and group mole fraction, X_m are given by the following equations:

$$\theta_m = \frac{Q_m X_m}{\sum_n Q_n X_n}; \quad X_m = \frac{\sum_j \nu_m^{(j)} x_j}{\sum_j \sum_n \nu_n^{(j)} x_j} \tag{8}$$

One of the main differences between original UNIFAC (eq. 9) and Modified UNIFAC (Do) (eq. 10) is the introduction of temperature dependent of the interaction parameters, ψ_{nm} to permit a better description of the real phase behavior (activity coefficients) as a function of temperature:

$$\text{Original UNIFAC: } \psi_{nm} = \exp\left[-\frac{a_{nm}}{T} \right] \tag{9}$$

$$\text{Mod. UNIFAC (Do): } \psi_{nm} = \exp\left[-\frac{a_{nm} + b_{nm}T + c_{nm}T^2}{T} \right] \tag{10}$$

The Mod. UNIFAC (Do) is revised and extended periodicaly [13-19] to improve the capability of prediction.

(1*R*,4*S*)-(+)-Fenchone [(1*R*,4*S*)-(+)-1,3,3-trimethylbicyclo[2.2.1]heptan-2-one], methyl chavicol [4-allyl-1-methoxybenzene] and *trans*-anethole [*trans*-1-methoxy-4(prop-1-en-1-yl) benzene] are the main components of the essential oil from the fruits of bitter fennel (*Foeniculum vulgare Mill, fam. Umbelliferae*). Both the raw essential oils and its isolated pure components are used in perfumery, cosmetics, pharmacy, aromatherapy and food industry [20].

Generally, essential oil components belong to the terpenoid class. Terpenoids are natural products comprising a large number of compounds with

complicate chemical structures. Due to their chemical structure the compounds present complex intermolecular interactions.

In previous paper [21] has been examinated intermolecular interactions in binary systems containing: (S)-(+)-carvone + (+)-limonene; (-)-beta-pinene + eucalyptol; (R)-(-)-carvone + eucalyptol; *n*-octane + (+)-limonene; (R)-(-)-carvone + *n*-decane; *n*-decane + (-)-menthone, *n*-decane + (+)-fenchone and (-)-beta-pinene + (+)-fenchone and has been analyzed the applicability of the group contribution models, DISQUAC and Mod. UNIFAC (Do) to predict VLE data and excess Gibbs energy in the same mixtures.

In [22], the thermodynamic properties of the mixtures containing (1R,4S)-(+)-fenchone, methyl chavicol and *trans*-anethole have been examined in terms of intermolecular forces.

The chemical structures of the compounds are presented in Figure 1.

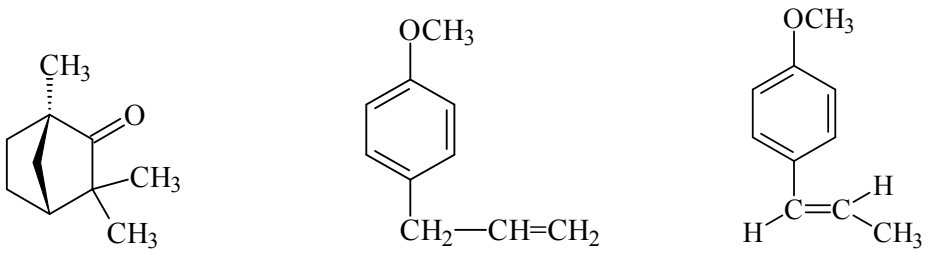

(1*R*,4*S*)-(+)-Fenchone Methyl chavicol *trans*-Anethole

Figure 1. Chemical structure of (1*R*,4*S*)-(+)-fenchone, methyl chavicol and *trans*-anethole

The names of the components referred to in this paper are: (+)-fenchone, methyl chavicol and *trans*-anethole.

The literature [23, 24] is very poor in vapor-liquid equilibrium data in the field of terpenoids. Since VLE data are often missing we check the capability of the Mod. UNIFAC (Do) model to predict VLE data in systems containing terpenoids.

Terpenoids and nonterpenoid compounds, main components of the essential oils, frequently contain oxygenated functional groups, some of them being in mesomeric relationship or being subjected to other electronic effects, steric hindrance effects or proximity effects.

One of the main objectives of the planned research work referred to the Mod. UNIFAC (Do) model is the consideration of the proximity and isomeric effects.

RESULTS AND DISCUSSION

(+)-Fenchone is a bi-cyclic terpenoid ketone while methyl chavicol and *trans*-anethole are two *semi*-aromatic ethers which do not belong to the terpenoid class.

Assessment of geometrical parameters

The molecules of (+)-fenchone, methyl chavicol and *trans*-anethole have been decomposed in structural groups according to the Mod. UNIFAC (Do) model. Table 1 lists the van der Waals values of R_k and Q_k for the all groups referred to in this paper.

Table 1. R_k and Q_k parameters and group assignment for the Modified UNIFAC (Dortmund) Method [8]

Main group	Subgroup	No	R_k	Q_k
1 “CH_3”	CH_3	1	0.6325	1.0608
	CH_2	2	0.6325	0.7081
	CH	3	0.6325	0.3554
	C	4	0.6325	0.0000
2 “C=C”	CH_2=CH	5	1.2832	1.6016
	CH=CH	6	1.2832	1.2489
	CH=C	7	1.2832	0.8962
3 ‘ACH”	ACH	9	0.3763	0.4321
	AC	10	0.3763	0.2113
9 “CH_2CO”	CH_3CO	18	1.7048	1.6700
	CH_2CO	19	1.7048	1.5542
	CCO		1.7048	1.5542
13. “CH_2O”	CH_3O	24	1.1434	1.6022
42 “c-CH_2”	c-CH_2	78	0.7136	0.8635
	c-CH	79	0.3479	0.1071
	c-C	80	0.3470	0.0000

The Mod. UNIFAC (Do) model [8] does not define a CCO subgroup for (+)-fenchone. For this subgroup we have considered the existing van der Waals properties, R_k and Q_k defined for the CH_2CO (19) subgroup. The CCO subgroup is sterically hindered by three adjacent methyl groups.

Table 2. Modified UNIFAC (Dortmund) group interaction parameters [8] and revised Modified UNIFAC (Dortmund) group interaction parameters [9] for the main group 42 (c-CH_2) with the main groups 1, 2, 3, 9 and 13.

n	m	a_{nm} (K)	b_{nm}	c_{nm} (K^{-1})	a_{mn} (K)	b_{mn}	c_{mn} (K^{-1})
1	2	189.66	-0.2723	0.000E+00	-95.418	0.0617	0.000E+00
1	3	114.2	0.0933	0.000E+00	16.07	-0.2998	0.000E+00
1	5	2777	-4.674	1.551E-03	1606	-4.7460	9.181E-04
**1	9	433.6	0.1473	0.000E+00	199	-0.8709	0.000E+00
1	13	233.1	-0.3155	0.000E+00	-9.654	-0.0324	0.000E+00
*1	42	-117.10	0.5481	-0.00098	170.90	-0.8062	0.00129
2	3	174.1	-0.5886	0.000E+00	-157.2	0.6166	0.000E+00
2	5	2649	-6.5080	4.822E-03	1566	-5.809	5.197E-03
**2	9	179.8	0.6991	0.000E+00	91.811	-0.7171	0.000E+00
**2	13	733.3	-2.509	0.000E+00	-844.3	2.945	0.000E+00
*2	42	2.4060	-0.1882	0.00	60.20	0.1565	0.00
**3	9	146.2	-1.237	4.237E-03	-57.53	1.212	-3.715E-03
3	13	-87.08	-0.1859	0.000E+00	179	0.0562	0.000E+00
*3	42	134.60	-1.2310	0.00149	-2.6190	1.0940	-0.00156
**9	13	3645	-26.91	4.757E-02	695.8	-0.9619	-2.462E-03
*9	42	168.20	-0.8197	0.00	464.50	0.1542	0.00
*13	42	397.00	-1.3790	0.00	-214.10	1.1340	0.00

* Revised Mod. UNIFAC (Do) group interaction parameters
** unpublished revised Mod. UNIFAC (Do) group interaction parameters

Assessment of interaction parameters

We used the group interaction parameters published in [8]. For the main group (42) we used the revised group interactions parameters published in [9]. Table 2 lists the Modified UNIFAC (Do) Group Interaction Parameters [8] and revised Modified UNIFAC (Do) Group Interaction Parameters [9] of the main group 42, ("c-CH_2"), with the main groups 1 ("CH_3"), 2 ("C=C"), 3 ("ACH"), 9 ("CH_2CO") and 13 ("CH_2O"), respectively. It should be pointed out that some revised interactions parameters (between 1-9, 2-9, 2-13, 3-9 and 9-13 groups) are not published, being used only inside the UNIFAC Consortium. It was not possible to use these revised interactions parameters to predict VLE data in the systems referred to in this paper.

Comparison with experiment

A comparison between experimental VLE data (*T-P-x-y*) and predicted VLE data is presented in Table 3. The excess Gibbs energy, G^E provides a more accurate comparison (Figs. 2 – 5). More discussions are necessary for each binary mixture.

Table 3. Comparison between experimental isobaric VLE data *T-x-y* and predicted isobaric VLE data *T-x-y* using Mod. UNIFAC (Do) model in binary and ternary systems containing (+)-fenchone, methyl chavicol and *trans*-anethole at *P*=4000 Pa and *P*=4270 Pa*, respectively.

System/Mod. UNIFAC (Do)	*AMD(y)* (mol. fr.)	*AMD(T)* (K)
Binary systems:		
(+)-fenchone + methyl chavicol	0.01	0.44
*(+)-fenchone + methyl chavicol	0.01	0.81
(+)-fenchone + *trans*-anethole	0.007	0.22
methyl chavicol + *trans*-anethole	0.002	1.00
Ternary system		
(+)-fenchone + methyl chavicol + *trans*-anethole	0.01	1.13

AMD(y) - Absolute mean deviation in the vapor phase compositions*;*
AMD(T) - Absolute mean deviation in temperature.

Binary system (+)-fenchone + methyl chavicol

The Mod. UNIFAC (Do) model, using the existing geometrical parameters van der Waals, R_k and Q_k defined for the "CH_2CO" (19) subgroup, is appropriate to predict the VLE data in the binary system (+)-fenchone + methyl chavicol (Table 3). The absolute mean deviation in the vapor phase composition, *AMD(y)* (mol.fr.) is 0.01 and the absolute mean deviations in temperature, *AMD(T)* (K) is smaller than 0.81.

The experimental excess Gibbs energy, $G^E_{\exp}$ presents positive and negative deviations from ideality (Figs. 2, 3). At *T* = 375.35 K, the equimolecular $G^E_{\exp}$ is ca. -50 ($Jmol^{-1}$) (*P*=4000 Pa) while at *T* = 377.75 K, the equimolecular $G^E_{\exp}$ is ca. -65 ($Jmol^{-1}$) (*P*=4270 Pa), negative deviations at both pressures.

The Mod. UNIFAC (Do) model predicts small deviations from ideality. At *T*=375.35 K the equimolecular G^E prediction is ca. 15 ($Jmol^{-1}$) (*P*=4000 Pa), respectively at *T* = 377.75 K, the equimolecular G^E prediction is ca. 5 ($Jmol^{-1}$) (*P*=4270 Pa), positive deviations at both pressures.

It should be noted the continue variation of the G^E prediction, presenting negative deviations from ideality until the equimolecular composition of the liquid phase, x_i and positive deviations after the equimolecular composition. At small compositions of (+)-fenchone in mixture, the unlike dipole/dipole interactions, >CO/-O-, as well as the dipole/induced dipole interactions, >CO/π, from $-C_6H_4-$ and $-CH=CH_2$ does not compensate the like weak dipole/dipole, -O-/-O- interactions, the dipole/induced dipole interactions, –O-/π, from $-C_6H_4-$ (phenylene) and $-CH=CH_2$ (double bonds) and the induced dipole/induced dipole interactions, π/π, from $-C_6H_4-/-C_6H_4-$, $-C_6H_4-/-CH=CH_2$

and -CH=CH_2/-CH=CH_2 in methyl chavicol [22]. Hence, the G^E predictions could not be negative until the equimolecular composition of the liquid phase. The conclusion is that the G^E predictions are unsatisfactorily.

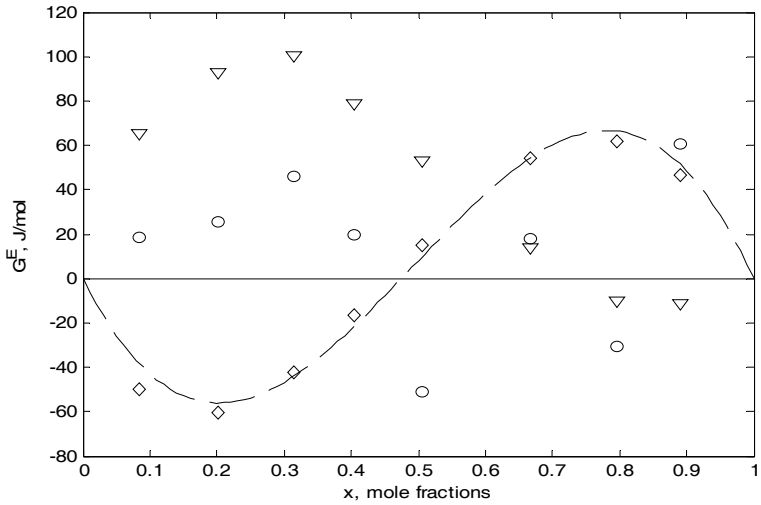

Figure 2. Variation of the molar excess Gibbs energy, G^E with mole fraction x_i, for the binary system (+)-fenchone (1) + methyl chavicol (2) at the constant pressure P=4000 Pa. (o) - experimental, (◊) - Mod. UNIFAC (Do) model, (∇) - calculated using binary parameters of the NRTL model.

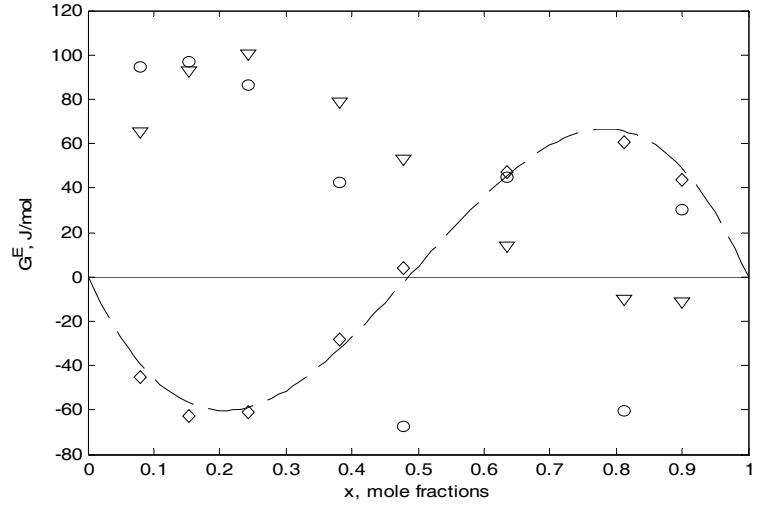

Figure 3. Variation of the molar excess Gibbs energy, G^E with mole fraction x_i, for the binary system (+)-fenchone (1) + methyl chavicol (2) at a constant pressure P=4270 Pa. (o) - experimental, (◊) - Mod. UNIFAC (Do) model, (∇) - calculated using binary parameters of the NRTL model.

The mesomeric effect in methyl chavicol, extended on the ether group, -O- and phenylene, -C_6H_4-, decrease the values of the excess Gibbs energy, $G^E_{\exp}$. Between phenylene, –C_6H_4- and double bond, -CH=CH_2 there is a proximity effect.

Binary system (+)-fenchone + trans-anethole

A very good prediction of the VLE data, using Mod. UNIFAC (Do) model, was found for the mixture (+)-fenchone + *trans*-anetole (Table 3). The absolute mean deviations in the vapor phase composition, *AMD(y)* (mol. fr.) is 0.007 and absolute mean deviations in temperature, *AMD(T)* (K) is 0.22.

The experimental excess Gibbs energy, $G^E_{\exp}$ presents negative deviations from ideality (Figure 4). At *T*=378.45 K, the equimolecular $G^E_{\exp}$ is ca. -20 (Jmol^{-1}).

The Mod. UNIFAC (Do) model predicts small deviations from ideality. At *T*=378.45 K, the predicted equimolecular G^E is ca. 4 (Jmol^{-1}).

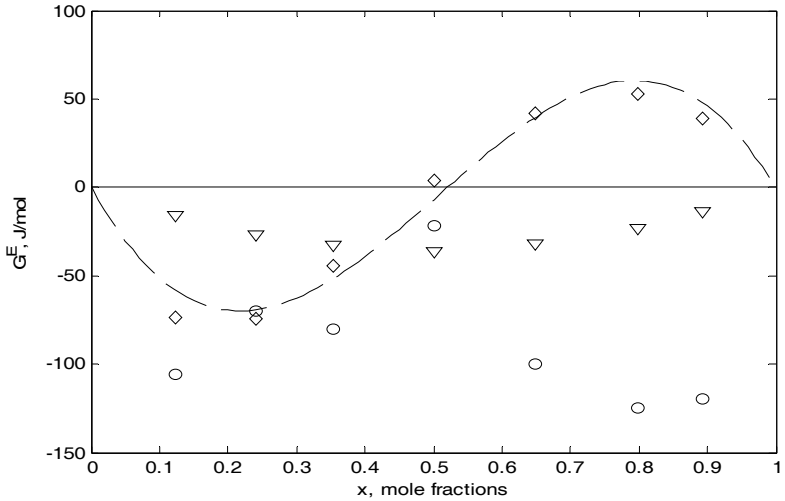

Figure 4. Variation of the molar excess Gibbs energy, G^E with mole fraction x_i, for the binary system (+)-fenchone (1) + *trans*-anethole (2) at a constant pressure *P*=4000 Pa. (o) -experimental, (◊) - Mod. UNIFAC (Do) model, (∇) – calculated using binary parameters of the NRTL model.

It should be noted the continue variation of the G^E predictions, presenting negative deviations from ideality until the equimolecular composition of the liquid phase, x_i and positive deviations after the equimolecular composition. At small compositions of (+)-fenchone in mixture, the unlike dipole/dipole

interactions, >CO/-O-, as well as the dipole/induced dipole interactions, >CO/π, from -C_6H_4- and -CH=CH_2 does not compensate the like weak dipole/dipole, -O-/-O- interactions, the dipole/induced dipole interactions, –O-/π, from -C_6H_4- (phenylene) and –CH=CH- (double bonds) and the induced dipole/induced dipole interactions, π/π, from -C_6H_4-/-C_6H_4-, -C_6H_4-/-CH=CH- and -CH=CH-/-CH=CH- in *trans*-anetole [22]. Hence, the G^E predictions could not be negative until the equimolecular composition of the liquid phase. The conclusion is that the G^E predictions are unsatisfactorily.

The mesomeric effect in *trans*-anethole, extended on the ether group, -O- and phenylene -C_6H_4- as well as on the double bond, -CH=CH-, decrease the values of the experimental excess Gibbs energy $G^E_{\exp}$.

Because the –O-C_6H_4-CH=CH- dipole in *trans*-anethole is stronger than the –O-C_6H_4- dipole in methyl chavicol, the binary system (+)-fenchone + *trans*-anethole show negative deviation from ideality on the whole range of compositions of the liquid phase (Fig. 4).

Binary system methyl chavicol + trans-anethole

In binary system methyl chavicol + *trans*-anethole the Mod. UNIFAC (Do) model predicts very accurate the composition of the vapor phase, y_i. The absolute mean deviation, *AMD(y)* (mol. fr.) is 0.002. The absolute mean deviation in temperature, *AMD(T)* (K) is 1.00. (Table 3).

The big difference between the boiling temperatures of the two isomeric compounds, methyl chavicol (216 ^oC/760 mmHg) and of it more stable isomer, *trans*-anethole (236 ^oC/760 mmHg), due to the more extended mesomeric effect in *trans*-anethole, explain the poor accuracy of the temperature prediction using the Mod. UNIFAC (Do) model.

The experimental excess Gibbs energy, $G^E_{\exp}$ presents positive deviations from ideality (Figure 5). At T=394.95 K, the equimolecular $G^E_{\exp}$ is ca. 160 (Jmol^{-1}).

The Mod. UNIFAC predictions, G^E are negative on the whole range of the liquid phase compositions. The G^E values are very close to zero. At T=394.95 K, the equimolecular G^E predictions is ca. -2 (Jmol^{-1}). The conclusion is that the G^E predictions are unsatisfactorily.

The Mod. UNIFAC (Do) model predicts satisfactory the composition of the vapor phase, y_i. (Table 3). The absolute mean deviation in the vapor phase composition, *AMD(y)* (mol.fr.) is 0.01. The absolute mean deviation in temperature, *AMD(T)* (K) is 1.13. The mesomeric effect in methyl chavicol and *trans*-anethole, explain the poor accuracy of the temperature prediction using the Mod. UNIFAC (Do) model.

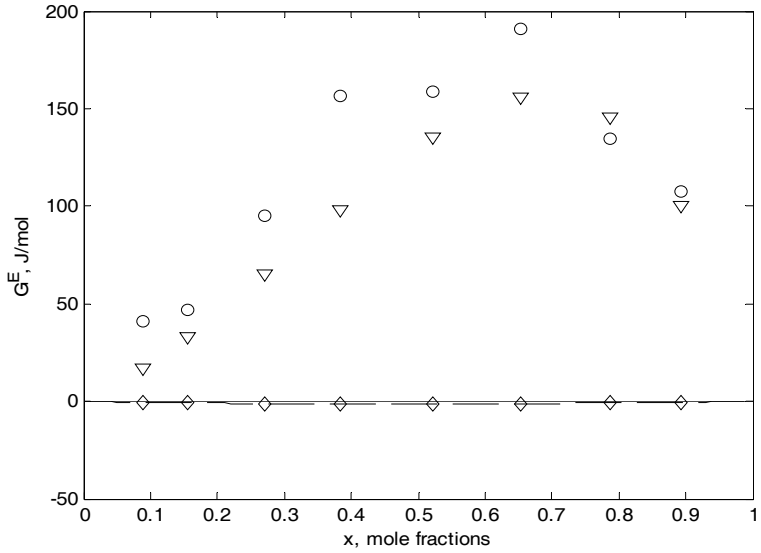

Figure 5. Variation of the molar excess Gibbs energy, G^E with mole fraction x_i, for the binary system methyl chavicol (1) + *trans*-anethole (2) at a constant pressure P=4000 Pa (o) - experimental, (◊) - Mod. UNIFAC (Do) model, (∇) - calculated using binary parameters of the NRTL model.

Ternary system {(+)-fenchone + methyl chavicol + trans-anethole}

Due to the hydrocarbon part of the involved molecules, *hydrophobic interactions* could not be negligible. The hydrophobic effect arises mainly from the attractive forces between hydrophobic parts of the molecules. It creates a higher degree of local order, producing a decrease in entropy that leads to an unfavorable Gibbs energy. The *hydrophobic interactions*, in addition with van der Waals and π/π attractions, contribute to positive and negative deviations from ideality in the binary system (+)-fenchone + methyl chavicol (Figs. 2, 3) and only negative deviations from ideality in the binary system (+)-fenchone + *trans*-anethole (Fig. 4) and only positive deviations from ideality in the binary system methyl chavicol + *trans*-anethole (Fig. 5) [22].

The dispersion of the experimental values of G^E (Figs. 2 - 5) is owing to the small values of G^E_{exp} and to the errors of the temperature measurements, (σ_T = 0.1 K) and of the vapor and liquid phase compositions measurements ($\sigma_{x,y}$ = 0.003 mol. fr.) as well as due to maintaining the pressure, P within 30 Pa around the desired values (σ_P = 60 Pa). The values of G^E were calculated using the binary parameters of the NRTL model published in [25].

CONCLUSIONS

The present investigation set out to check the capability of the Modified UNIFAC (Dortmund) group contributions model to predict the VLE data and excess Gibbs energy in binary and ternary systems containing (+)-fenchone, methyl chavicol and *trans*-anethole. Due to the various intermolecular interactions, mesomeric effects, steric hindrance effects and proximity effect the predictions are seriously affected. The Mod. UNIFAC (Do) group contribution model predicts satisfactory VLE data in all the binary and ternary systems but inadequately the values of the excess Gibbs energy. The poor predictions are due to of the complex structure of the investigated molecules.

EXPERIMENTAL SECTION

In previous papers [26, 27, 28] we reported experimental vapor-liquid equilibrium data for the following binary and ternary systems: methyl chavicol + (+)-fenchone; *trans*-anethole + (+)-fenchone; methyl chavicol + *trans*-anethole; methyl chavicol + *trans*-anethole + (+)-fenchone.

A series of isobaric *T-x-y* measurements were performed at (4000±30) Pa [26, 27, 28]. Another series of *T-P-x* measurements were performed at three constant liquid-phase compositions [26, 27]. For the binary system methyl chavicol + (+)-fenchone a series of isobaric *T-x-y* measurements were performed at (4270±30) Pa [26].

VLE data in binary systems were found to be thermodynamically consistent as tested by using the maximum likelihood multimodel fitting method described by Panaitescu [29]. The standard deviations for pressure, temperature and liquid and vapor phase compositions were set to σ_P = 60 Pa, σ_T = 0.1 K, σ_x = 0.003 mol. fr. and σ_y = 0.003 mol. fr., respectively. According to this test the isobaric *T-x-y* measurements are considered consistent if the values of the statistic criterion of selection of the each experimental point (*Ro*) and of the all experimental points (*global Ro*) are less than 2.45. At both pressure *P* (Pa) = (4000±30) and respectively *P* (Pa) = 4270±30), the values of the (*global Ro*) criterions and of the all values of the (*Ro*) criterions are less than 2.45. The thermodynamic consistency of the isobaric *T-x-y* measurements in the ternary system was checked using the McDermott-Ellis method [30] modified by Wisniak and Tamir [31]. According to these references two experimental points *a* and *b* are considered thermodynamically consistent if the local deviation, *D* is less than maximum deviation, D_{max}. For all the experimental points reported, *D* never exceeded 0.156 while the smallest value of D_{max} was 0.500.

REFERENCES

1. E.L. Derr, C.H. Deal, *Inst. Chem. Eng. Symp. Ser. (London),* **1969**, *32*, 40.
2. K. Kojima, K. Tochigi, "Prediction of Vapor-Liquid Equilibria by the ASOG Method", Kodansha-Elsevier Tokyo, **1979**.
3. K. Kojima, D. Tiegs, J. Gmehling, K. Tochigi*, J. Chem. Eng. Jpn.,* **1990**, *23*, 453.
4. Aa. Fredenslund, R.L. Jones, J.M. Prausnitz, *AIChE Journal,* **1975**, *21*, 1086.
5. Aa. Fredenslund, J. Gmehling, P. Rasmussen, „Vapor-Liquid Equilibria Using UNIFAC", Elsevier-Amsterdam, **1977**, chapter 4.
6. H.K. Hansen, P. Rasmussen, Aa. Fredenslund, M. Schiller, J. Gmehling, *Ind. Eng. Chem. Res.,* **1991**, *30*, 2352.
7. U. Weidlich, J. Gmehling, *Ind. Eng. Chem. Res.,* **1987**, *26*, 1372.
8. J. Gmehling, J. Li, M. Schiller, *Ind. Eng. Chem. Res.,* **1993**, *32*, 178.
9. J. Gmehling, J. Lohmann, A. Jakob, J. Li, R. Joh, *Ind. Eng. Chem. Res.,* **1998**, *37*, 4876.
10. B.L. Larsen, P. Rasmussen, Aa. Fredenslund, *Ind. Eng. Chem. Res.,* **1987**, *26*, 2274.
11. H.V. Kehiaian, J-P.E. Grolier, G.C. Benson, *Journal of Chimie Physique,* **1978**, *75*, 1031.
12. H.V. Kehiaian, B. Marongiu, *Fluid Phase Equilib.*, **1988**, *40*, 23.
13. J. Lohmann, R. Joh, J. Gmehling, *Ind. Eng. Chem. Res.,* **2001**, *40*, 957.
14. R. Wittig, J. Lohmann, R. Joh, S. Horstmann, J. Gmehling, *Ind. Eng. Chem. Res.,* **2001**, *40*, 5831.
15. J. Lohmann, J. Gmehling, *J. Chem. Eng. Jpn.,* **2001**, *34*, 43.
16. J. Gmehling, R. Wittig, J. Lohmann, R. Joh, *Ind. Eng. Chem. Res.,* **2002**, *41*, 1678.
17. R. Wittig, J. Lohmann, J. Gmehling, *AIChE Journal*, **2003**, *49*, 530.
18. A. Jakob, H. Grensemann, J. Lohmann, J. Gmehling, *Ind. Eng. Chem. Res.,* **2006**, *45*, 7924.
19. S. Nebig, J. Gmehling, *Fluid Phase Equilib*, **2010**, *294*, 206.
20. G. Radoias, A. Bosilcov, I. Batiu, "Odorante Naturale în Parfumeria Modernă" ("Natural Fragrances in Modern Parfumery"), Editura Casa Cărţii de Ştiinţă Cluj-Napoca, **2005**, chapter 4.
21. I. Batiu, *Fluid Phase Equilib.,* **2005**, *227*, 113.
22. I. Batiu, *Studia UBB Chemia,* **2012**, *LVII*, 195.
23. I. Wichterle, J. Linek, Z. Wagner and H.V. Kehiaian,"Vapor-Liquid Equilibrium Bibliographic Database". 9th Ed. CD-ROM, ELDATA, Paris, France, **2004**.
24. I. Wichterle, J. Linek, Z. Wagner, J.-C. Fontaine, K. Sosnkowska-Kehiaian and H.V. Kehiaian, „Vapor-Liquid Equilibrium in Mixtures and Solutions". Landolt-Boernstein Numerical Data and Functional Relationships in Science and Technology, New Series. W. Martienssen, Springer-Verlag, Berlin-Heidelberg, Germany, **2007** Ed.,Vol.IV/13A.

25. I. Batiu, *Studia UBB Chemia,* **2011**, *LVI*, 35.
26. I. Batiu, E. Jurgea, G.M. Panaitescu, *ELDATA: Int. Electron. J. Phys.-Chem. Data,* **1995**, *1*, 39.
27. I. Batiu, G.M. Panaitescu, M. Peia, *ELDATA: Int. Electron. J. Phys.-Chem. Data*, **1995**, *1*, 117.
28. I. Batiu, *ELDATA: Int. Electron. J. Phys.-Chem. Data,* **1995**, *1*, 303.
29. G.M. Panaitescu, *Rev. Chim.,* **1982**, 33 (*12*), 1110-1113; *Ind. Chem. Eng.* **1985**, *25*, 68.
30. C. Mc Dermott, S.R.M. Ellis, *Chem. Eng. Sci*., **1965**, *20*, 293.
31. J. Wisniak, A. Tamir, *J. Chem. Eng. Data,* **1977**, *22*, 253.

STUDIA UBB CHEMIA, LVII, 2, 2012 (p. 21 - 28)

INVESTIGATION OF METALLIC NANOPARTICLES PRODUCED BY LASER ABLATION METHOD AND THEIR CATALYTIC ACTIVITY ON CVD DIAMOND GROWTH

ZAHRA KHALAJ[a], MAHMOOD GHORANNEVISS[a,*]

ABSTRACT. The synthesis of high quality diamond films is one of the particular interests due to the material's outstanding physical and mechanical properties. In CVD diamond we found a new process parameter window where the growth of diamond films can be stabilized without the use of diamond powder on substrates. Using suitable catalyst and etching gas would enhance the diamond nucleation and therefore, increase the quality of the films. A laser ablation was conducted by using an optical system for producing the metallic nanoparticles. A light source with a first harmonic generator (FHG) of an Nd:YAG laser were used with the wavelength of 1064 nm, pulse duration: 6 ns and repetition rate of 10 Hz. Au and Ag nanoparticles were dried on the Si and glass wafers as a catalyst and etching treated by hydrogen plasma for 30 minutes. Topography of the wafers was analyzed using Atomic Force Microscopy (AFM) and shows a good distribution of the nanoparticles on the substrate surface. Diamond films were deposited on substrates coated metal using a Hot Filament Chemical Vapor Deposition (HFCVD) system. Crystallinity of the samples was observed by X-ray diffraction (XRD) method. Results show good quality diamond crystals with crystallinity of (311) structures, grown on substrate surface. According to the Scherrer formula, the grain size (L_{hkl}) of diamond nano crystals were calculated by $L_{hkl}=K\lambda/B\cos\theta_{hkl}$, where B is the FWHM in radians and λ is the wavelength in nm.

Keywords: *Nd:YAG laser, NNP, CVD diamond.*

INTRODUCTION

Carbon is one of the most important natural elements, which has several allotropes [1,2] such as carbon nanotubes [3], carbon nanowalls [3], diamond-like carbon [4], etc. Among different hybridizations [5], the sp^3 form is involved in the diamond structure. Due to its outstanding properties, diamond is the unique material with various applications in life and technology. By developing the Chemical Vapor Deposition (CVD) technology, the deposition of nanocrystalline diamond films (NDFs) by various CVD techniques has became the topic of wide research [6-9]. The quality and purity of nano structures in CVD techniques are very important. There are some possibilities

[a] Plasma Physics Research Center, Science and Research Branch, Islamic Azad University, Tehran, Iran, *Correspondent: Ghoranneviss@gmail.com

for increasing the quality and quantity of these deposits. The nucleation and growth of diamond coating can be dramatically improved with different surface treatments [10]. There are several methods for the enhancement of diamond nucleation, including mechanical and chemical treatment processes. One of the effective methods is the use of a catalyst layer for diamond deposition [10]. Using a catalyst layer can increase the rate of diamond nucleation and provide a carbon diffusion barrier layer to increase the needed carbon concentration for diamond nucleation [11, 12]. Using suitable catalyst and etching gas can enhance the diamond nucleation and therefore, increase the quality of the films.

In this paper, gold and silver nanoparticles were produced using laser ablation method and dried on the Si and glass wafers as a catalyst and compared with silicon with no pretreatments. All samples were etching treated by hydrogen plasma by Plasma Enhanced Chemical Vapor Deposition (PECVD) and grown using Hot Filament Chemical Vapor Deposition (HFCVD) system. The formation of metallic nanoparticles has been characterized by a variety of physical techniques such as, UV–vis spectroscopy and Atomic Force Microscopy (AFM). The crystallinity of the samples was studied by XRD (Cukα, λ=0.154nm, D/Max=2200, X-ray diffractometer) analysis. Fourier transform infrared (FT-IR) spectroscopy was used to characterize the coating.

RESULTS AND DISCUSSION
MORPHOLOGY OF THE FILMS

Figure 1 shows the measured absorption bands of the pure Au and Ag nanoparticles. The solution of pure Au nanoparticles, prepared by the laser ablation method, shows a reddish brown in color. The color of the solution is yellow for the silver nanoparticles, obtained in acetone. A sharp Plasmon band attributable to silver nanoparticles was observed around 400 nm. Observe that the surface Plasmon bands display a symmetrical configuration.

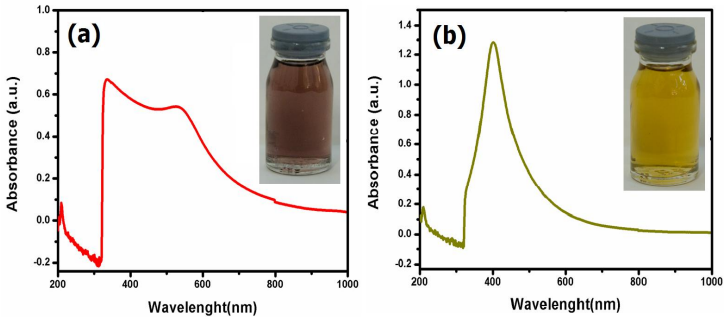

Figure 1. UV–vis spectra of (a) gold (b) silver, nanoparticles prepared by laser ablation in acetone solutions

Atomic force microscopy was performed on silicon coated nanoparticles in contact mode on 3μmx 3μm area. Figure 2 shows 3D images of the silicon coated by gold (S_1) and silicon coated by silver (S_2). Three dimensional images in both samples show different topography, which result in different average roughness for each sample. Therefore, as we can see in Figure 2(b) the distribution of size for silver nanoparticles is homogeneous while the homogeneity is less for Au NPs, Figure 2(a).

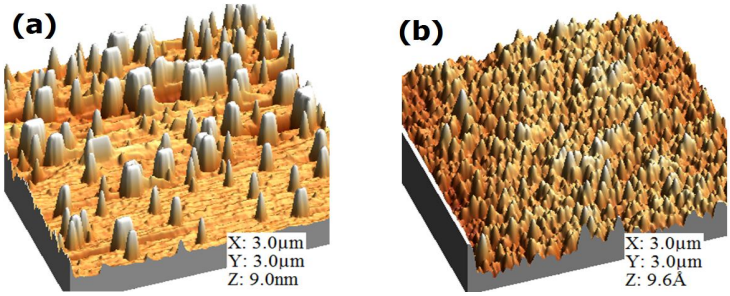

Figure 2. Three dimensional AFM images of silicon coated by (a) Gold and (b) silver nanoparticles.

Figure 3 shows the histograms of the size distribution of the metallic nanoparticles on the silicon surface. As the Gaussian diagram shows for S_2, the distribution of the Ag nanoparticles on substrates is homogenous. This homogeneity is less for S_1 because of the sharp difference between the distribution sizes of the nanoparticles. Moreover, S_1, particles are rather isolated from each other while there is a continuous distribution for S_2. This observation suggests that the particles seen at S_1 are fairly clusters of crystallites. In addition, the width of the peak in S_2 is larger than in S_1. It means that there is a high distribution in size of nanoparticles in S_2. Moreover surface roughness is low in this case.

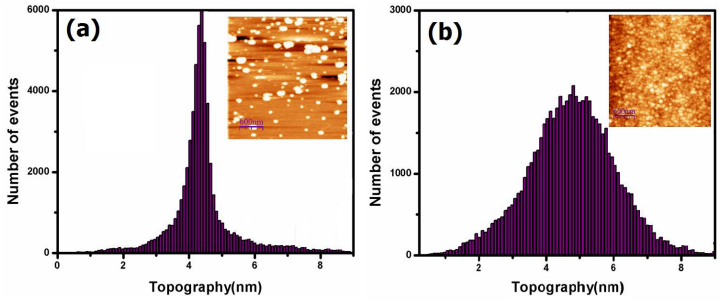

Figure 3. 2D AFM image and histogram of the size distribution of silicon coated by (a) gold and (b) silver nanoparticles.

The Root-Mean-Squared roughness (R_{rms}) of surface is one of the most important parameters for characterization of surface structure [4]:

$$R_{rms} = \sqrt{\frac{\sum_{n=1}^{N}(Z_n - \bar{Z})^2}{N-1}}$$

$$\bar{Z} = \frac{1}{N}\sum_{n=1}^{N} Z_n$$

with N being the number of data points [4]. The results of AFM studies after etching treatments are listed in Table 1.

Table 1. AFM studies of the silicon coated metallic particles

No.	Sample	Rms rough. (nm)	Ave. rough. (nm)	Ave. height
S_1	Si-Au	1.33	0.77	4.34
S_2	Si-Ag	0.19	0.15	0.63

The AFM results show that the RMS roughness of the samples decreases from S_1 to S_2. Therefore the substrate surface becomes smoother which is suitable for diamond nucleation.

XRD patterns of the diamond crystals deposited for 120 minutes at 25 Torr are shown in Figure 4. Based on Figure 4, a diffraction peak was found in the spectra for S_1 at 92.10°. One can observe the spectrum is dominated by intense peaks located at 2θ= 92.12° for S_2 which could be identified with reflections from (311) plane of diamond. The Full Width Half Maximum (FWHM) of the diamond peaks could be used for distinguishing the quality of diamonds. The sharp peaks with small FWHM indicate high crystal quality. The FWHM (B) of these peaks was used to calculate the grain size (L_{hkl}) from the well-known Scherrer's equation:

$$L_{hkl} = \frac{K\lambda}{B\cos\theta_{hkl}}$$

Here K=0.9, λ=0.154nm and θ is the Brag angle.

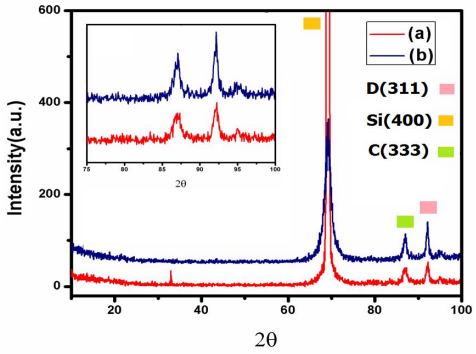

Figure 4. The XRD pattern for NCD films on: (a) S_1 and (b) S_2

Table 2 shows some calculations for the grain size of the diamond in both samples.

Table 2. XRD studies for the diamond crystals grown on different substrates

Sample	Operating Pressure (Torr)	Orientation of plane	2Θ (deg.)	FWHM (deg.)	$\Delta(2\Theta)\cos(\Theta)$ $x10^{-3}$ (rad.)	T (nm)
S_1	25	(311)	92.10	0.7210	0.0086	16.11
S_2	25	(311)	92.12	0.3302	0.0039	35.53

Due to the lower FWHM and higher intensity, the quality of the diamond in S_2 is better than S_1. In addition, the AFM data show that the RMS in S_1 and S_2 was 1.33nm and 0.19 nm, respectively. Therefore, the substrate surface in S_2 was smoother than S_1 which is more suitable for diamond growth. That is AFM and XRD results confirm each other. There was no peak observed for diamond coating on pure silicon.

Fourier Transform Infrared (FTIR) spectroscopy is a spectroscopic technique used to characterize the chemical bonds, molecular structures and C-H_n (n=1, 2, 3) bonding configurations in carbon materials. The typical infrared spectra of the diamond films deposited on S_2 substrate, in the range of 1000-4000 cm^{-1}, are shown in Figure 5. It shows an absorption band in CVD diamond in the "C-H stretch "region, with the peak at 2932.49 cm^{-1}, which is believed to be caused by symmetric C-H_2 stretching vibrations.

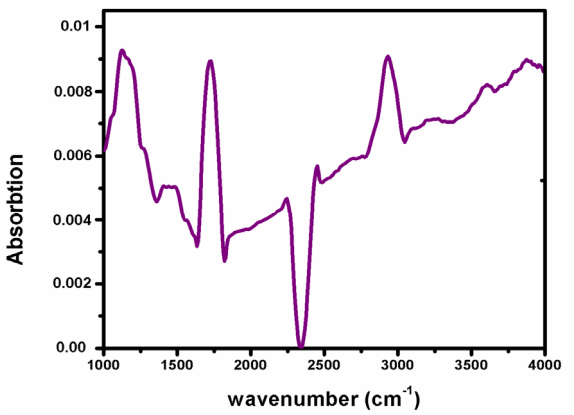

Figure 5. Typical FTIR absorbance spectra of the diamond films grown on S_2

EXPERIMENTAL DETAILS AND METHODOLOGY
SUBSTRATE TREATMENTS AND FILM SYNTHESIS

Diamond films were synthesized on P-type Silicon wafers (100) in the size of 5mm×5mm. All the substrates were cleaned in acetone and rinsed with ethanol prior to deposition. Two methods were used for diamond films, ND: YAG laser and CVD systems. Au and Ag nanoparticles were prepared by laser ablation of high purity targets in acetone using a first harmonic (1064 nm) Nd:YAG pulse laser with a repetition rate of 10 Hz, pulse width of 6 ns and a fluency of 1.5 J/cm^2. The laser beam strikes the surface vertically after passing throughout an optical window and the liquid. Figure 6 shows a schematic diagram for the laser ablation of a target in liquid. Au and Ag nanoparticles were dried on the Si wafers and were named S_1 and S_2 respectively.

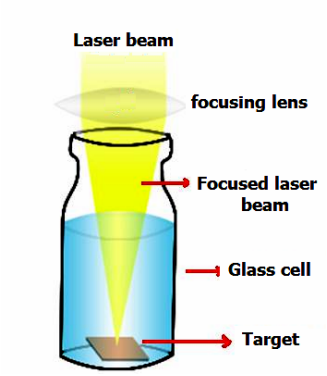

Figure 6. Schematic diagram for the laser ablation of target in liquid phase

CVD diamond growth was performed on the DC-Plasma Enhanced Chemical Vapor Deposition (PECVD) and Hot Filament Chemical Vapor Deposition (HFCVD) systems. S_1, S_2 and a silicon substrate with no catalyst pretreatments (S_3) were load to the central part of the DC-PECVD which is a cylindrical chamber with a diameter of 28cm consisting of a base and a cover. On the top of the system cover the DC source is flanged. The chamber can be opened for substrate handling by vertical shifting the aluminum cover on top. The temperature of the substrates is monitored by a thermocouple. A Hydrogen gas was inserted to the system for 30 minutes to create suitable sites for diamond growth. Using H_2 as etching gas would increase the diamond nucleation by creating suitable sites on substrate surface.

The substrate temperature, flow rate, and etching pressure were about: 200°C, 135 sccm, and 10 Torr, respectively. The samples were moved to the HFCVD system for diamond growth. This system consists of a horizontal stainless steel (S.S.316) cylinder as a reaction chamber, a furnace and filament (see Figure 7) [13].

After getting the base pressure, we feed the substrate with source gases through a steel nozzle. The substrate temperature, T_S, was increased up to 600°C, gradually. The temperature of the filament, T_F, was increased up to 1600°C. A combination of CH_4/H_2 with 5% flow ratio was fed into the reaction chamber. The reaction pressure and maximum temperature of the filament for the growth were 25 Torr and ≈1700°C, respectively. The duration of time was 120 minutes. Due to the high ionization energy of the hot filament, good quality diamond films were produced.

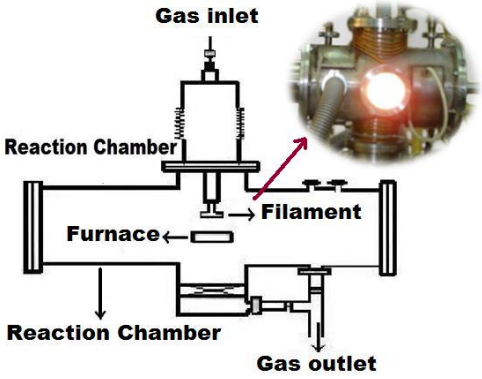

Figure 7. Schematic diagram of the HFCVD system

CONCLUSION

In this work, we have investigated the growth of diamond nanocrystals on silicon substrate with a new method. Using ND: YAG laser, we produced Au and Ag nanoparticles in acetone solution. Silicon wafers coated by Au and Ag nanoparticles were compared by pure silicon with no treatments. Using DC-PECVD and HFCVD techniques, high quality diamond nanocrystals with crystallinity of (311) were grown on pretreated substrates. The XRD patterns show the diamond nanocrystals grown on Si covered Ag have a higher quality, as shown by their high intensity and small FWHM in diamond peaks. The FTIR analysis for silicon coated by Ag shows an absorption band in CVD diamond with the peak at 2932.49 cm^{-1}, which is believed to be caused by symmetric C-H_2 stretching vibrations. There was no diamond coating on pure silicon.

The results show that the ionization rate of reaction gases and substrate pretreatments have a great influence on diamond nucleation. Using gold and silver coatings on silicon substrates had a good influence on diamond nucleation in this experiment.

ACKNOWLEDGEMENTS

The authours would like to thank the Iran National Science Foundation (INSF) for supporting this project.

REFERENCES

1. N.G. Shang, F.C.K. Au, X.M. Meng, C.S. Lee, I. Bello, S.T. Lee, *Chem. Phys. Lett.*, **2002**, *358*, 187-191.
2. E.C. Almeida, A.F. Azevedo, M.R. Baldan, N.A. Braga, J.M. Rosolen, N.G. Ferreira, *Chem. Phys. Lett.,* **2007**, *438*, 47-52.
3. P. Alizadeh Eslami, M. Ghoranneviss, Sh. Moradi, P. Abroomand Azar, S. Abedini Khorrami, S. Nasiri Laheghi, *Fuller Nanotub Car N,* **2011**,*19*, 237-249.
4. E. Vaghri, Z. Khalaj, M. Ghoranneviss, M. Borghei, *J. Fusion Energ.,* **2011**, *30,* 447-452.
5. S. Ghosh, D.K. Avasthi, A. Tripathi, D. Kabiraj, S. Singh, D.S. Misra, *Nucl. Instrum. Methods Phys. Res. B,* **2004**, *219–220*, 973–979.
6. Z. Khalaj, S. Z. Taheri, S. N. Laheghi and P. A. Eslami, *IPJ*, **2009**, *3-1*, 19.
7. K. Yamazaki, K. Furuichi, I. Tsumura and Y. Takagi, *J.Cryst. Growth*, **2008**, *310*, 1019-1022.
8. L.L. Melo, J.R. Moro, R.M. Castro, E.J. Corat and V.J. Trava Airoldi, *J. Surf Coat Tech.*, **2007**, *201*, 7382-7386.
9. H. Zhoutong, Y. Shumin, L. Qintao, Z. Dezhang and G. Jinlong, *J. Nucl. Sci. Tech.,* **2008**, *19*, 83-87.
10. Yongqing Fu, Bibo Yan, Nee Lam Loh, *Surf. Coat. Technol.,* **2000**, *130*, 173-185.
11. H.P. Lorenz, *Diamond Relat. Matter.*, **1995**, *4*, 1088-1092.
12. I.Y. Konyashin, M.B. Guseva, V.G. Babaev, V.V. Khvostov, G.M. Lopez, A.E. Alexenko, *Thin Solid Films*, **1997**, *300*, 18-24.
13. Z. Khalaj, M. Ghoranneviss, S. Nasirilaheghi, Z. Ghorannevis, R. Hatakeyama, *CJCP*, **2010**, *23*, 689-692.

STUDIA UBB CHEMIA, LVII, 2, 2012 (p. 29 - 45)

VAPOR - LIQUID EQUILIBRIA IN THE BINARY SYSTEM (3*R*)-(-)-LINALOOL + (3*S*)-(-)-BETA-CITRONELLOL

IOAN BATIU[a,*], GEORGES RADOIAS[b] AND ALIN BOSILCOV[b]

ABSTRACT. Vapor-liquid equilibrium data (VLE) have been measured for the binary system (3*R*)-(-)-linalool + (3*S*)-(-)-beta-citronellol. The vapor-liquid equilibrium data were correlated by means of the Wilson, NRTL and UNIQUAC equations. The binary parameters of the corresponding models were calculated. The vapor-liquid equilibrium data were used to discuss the thermodynamic properties of the mixture taking into account the intermolecular forces, proximity effect and the effect of the steric hindrance. The Modified UNIFAC (Dortmund) group contribution model was used to check their predictive capability in mixtures containing (3*R*)-(-)-linalool and (3*S*)-(-)-beta-citronellol.

Keywords: *Vapor - liquid equilibria, Terpenoids, excess Gibbs energy, Mod. UNIFAC (Dortmund), Wilson, NRTL, UNIQUAC.*

INTRODUCTION

Following up our program on measuring the vapor-liquid equilibrium data in mixtures containing terpenoids, the present work was focused on: 1. the measurement of vapor-liquid equilibria (VLE) for the binary mixtures of (3*R*)-(-)-linalool + (3*S*)-(-)-beta-citronellol; and 2. thermodynamic modeling of the experimental vapor-liquid equilibrium data of the mixtures (3*R*)-(-)-linalool + (3*S*)-(-)-beta-citronellol.

(3*R*)-(-)-Linalool [(-)-3,7-Dimethylocta-1,6-dien-3-ol] and (3*S*)-(-)-beta-citronellol [3,7-Dimethyloct-6-en-1-ol] and geraniol [3,7-Dimethylocta-2,6-dien-1-ol] are among the main components of the essential oil of geranium (*Pelargonium graveolens L, fam. Geraniaceae*), an important perfumery material. The raw essential oil is also used to isolate (3*S*)-(-)- beta-citronellol and geraniol of high purity.[1].

The chemical structures of the main components of the essential oils of geranium are presented in Figure 1. The names of the components referred to in this paper are: (-)-linalool, (-)-beta-citronellol and geraniol.

[a] "Babeş-Bolyai" University of Cluj-Napoca, Faculty of Chemistry and Chemical Engineering, Arany Janos Street 11, 400028 Cluj-Napoca, Romania, * batiu@chem.ubbcluj.ro
[b] Brüder Unterweger Essential Oils**,** Quality Assurance Dept., A-9911 Thal-Assling, Austria

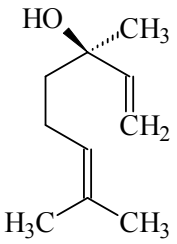

(3*R*)-(-)-Linalool

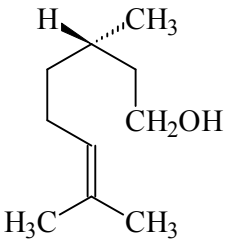

(3*S*)-(-)-beta-Citronellol

Figure 1. Chemical structure of (3*R*)-(-)-linalool, (3*S*)-(-)-beta-citronellol

Generally, essential oil components belong to the terpenoid class. Terpenoids are natural products comprising a large number of compounds with complicate chemical structures. Many essential oil components are monoterpenoids (C_{10}) and sesquiterpenoids (C_{15}), acyclic, monocyclic or bicyclic, saturated or unsaturated.

The main components of the essential oils - high value added chemicals - separate from raw essential oils by batch distillation function of their boiling points. Accurate isobaric vapor-liquid equilibrium data are necessary for the design and optimized the batch distillation column. The literature [2, 3] is very poor in the experimental vapor-liquid equilibrium data in the field of terpenoids.

No experimental VLE data are available for the binary system (-)-linalool + (-)-beta-citronellol [2, 3].

RESULTS AND DISCUSSION

Terpenoids frequently contain oxygenated functional groups, some of them being subjected to the electronic effects. Intermolecular interactions as well as steric hindrance effects or proximity effects may occur between the various functional groups.

(-)-Linalool is a acyclic terpenoid tertiary alcohol, while (-)-beta-citronellol is a acyclic terpenoid primary alcohol (Fig. 1).

The boiling points of the components

The direct experimental boiling temperature *T* of the pure terpenoids (-)-linalool and (-)-beta-citronellol were measured and presented in Table 1. The *T-P* measurements were correlated with the following Antoine equations (eqs. 1, 3).

Table 1. The experimental boiling temperatures *T/*(K) of the pure terpenoids (-)-linalool and (-)-beta-citronellol.

(-)-Linalool		(-)-beta-Citronellol	
P (Pa)	$T_{exp.}$ (K)	*P* (Pa)	$T_{exp.}$ (K)
666	343.45	666	368.55
1,333	355.55	1,333	380.80
2,000	363.10	2,000	388.25
4,000	377.25	4,000	402.70
6,666	388.45	6,666	414.15
10,000	398.45	10,000	423.25
13,332	405.65	13,332	430.85
19,998	416.55	19,998	442.20
26,664	424.85	26,664	450.25
39,996	437.45	39,996	462.85
53,328	446.65	53,328	472.25
101,325	470.15	101,325	496.40

(-)-Linalool, 12 points in the pressure range from 666 Pa to 101,325 Pa.

$$\ln(P/Pa) = 21.02499 - \frac{3{,}472.56}{(T/K) - 104.400} \tag{1}$$

In the range between 15,230 Pa and 88,730 Pa our (-)-linalool data agree well with literature data [4]. Absolute mean deviation in temperature, *AMD*(*T*) (K) was 0.50 while maximum deviation was 0.92.

Absolute mean deviation, *AMD*(*k*) was calculated using eq. (2)

$$AMD(k) = \sum_{i=1}^{N} \left| k_{\exp,i} - k_{calc,i} \right| / N \tag{2}$$

where: *k* stands for *T*, *P* or *y* representing respectively, the temperature and the pressure and the mole fraction composition of the vapor phase, while *N* is the number of experimental points.

(-)-beta-Citronellol, 12 points in the pressure range from 666 Pa to 101,325 Pa.

$$\ln(P/Pa) = 20.79777 - \frac{3{,}356.04}{(T/K) - 134.000} \tag{3}$$

The data reported in [5] for (-)-beta-citronellol, in the range between 2,000 Pa and 101,325 Pa, are 0.3 K to 2.70 K higher while in the range between 666 Pa and 2,000 Pa, are 0.57 K to 1.90 K lower than our measurements. Absolute mean deviation, *AMD*(*T*) (K) was 1.68 while maximum deviation was 2.70.

Vapor – liquid equilibrium data

A series of isobaric *T-x-y* measurements was performed at (3,333±30) Pa. The isobaric *T-x-y* measurements together with the activity coefficients, γ_i and the molar excess Gibbs energies, G^E are reported in Tab. 2 and Figs. 2 and 3.

Table 2. Experimental vapor - liquid equilibrium data of the binary system (-)-linalool (1) + (-)-beta-citronellol (2) at P = (3,333±30) Pa

T (K)	x_1	y_1	γ_1	γ_2	G^E (Jmol^{-1})
399.60	0.0000	0.0000	1.4414	1.0000	0.00
396.55	0.0350	0.1210	1.2468	1.0023	33.00
393.30	0.1030	0.3050	1.2190	1.0000	67.00
391.00	0.1590	0.4200	1.1965	1.0000	90.00
387.70	0.2450	0.5580	1.1866	1.0043	145.00
384.45	0.3460	0.6770	1.1740	1.0054	188.00
382.00	0.4250	0.7450	1.1726	1.0302	269.00
381.45	0.4460	0.7600	1.1684	1.0370	284.00
379.95	0.5100	0.8020	1.1539	1.0505	307.00
377.55	0.6250	0.8620	1.1298	1.0940	345.30
377.20	0.6470	0.8710	1.1208	1.1081	345.00
375.25	0.7840	0.9250	1.0761	1.1769	289.00
374.40	0.8840	0.9550	1.0257	1.3811	186.00
373.25	1.0000	1.0000	1.0000	1.5800	0.0000

Boiling temperature T, liquid phase, x_i and vapor phase, y_i compositions (mole fractions), activity coefficients γ_i and molar excess Gibbs energy G^E

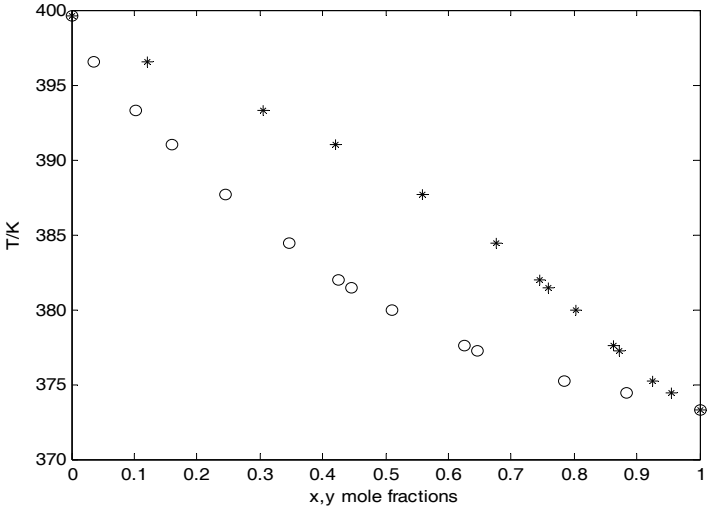

Figure 2. Experimental vapor - liquid equilibrium diagram for the binary system (-)-linalool (1) + (-)-beta-citronellol (2) at constant pressure P=3,333 Pa, temperature T/(K) as a function of the liquid phase x_i (o), or vapor phase y_i (*), mole fraction composition of component 1.

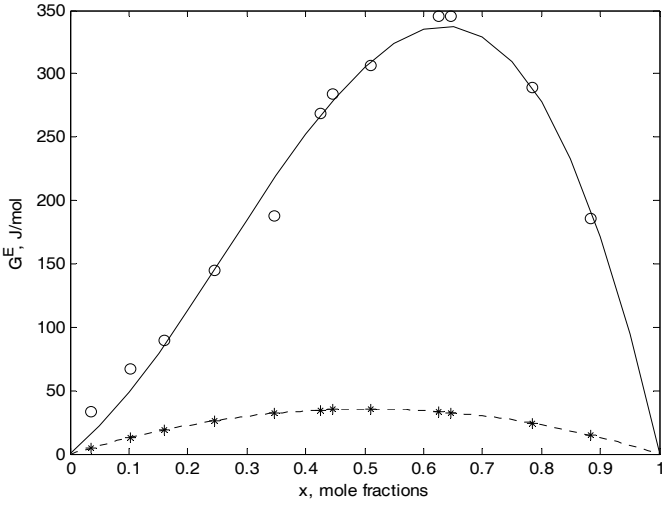

Figure 3. Variation of the molar excess Gibbs energy, G^E with mole fraction x_i, for the binary system (-)-linalool (1) + (-)-beta-citronellol (2) at a constant pressure P=3333 Pa (o) -experimental, (*) – predicted by Mod. UNIFAC (Do) model

The experimental activity coefficients γ_i were calculated by [6] (eq. 4):

$$\ln \gamma_i = \ln \frac{y_i P}{x_i P_i^0} + \left[\frac{\left(B_{ii} - V_i\right)\left(P - P_i^0\right) + P\delta_{ij} y_j^2}{RT} \right] \quad i,j=1,2 \qquad (4)$$

where: $\delta_{ij} = 2B_{ij} - B_{ii} - B_{jj}$ $\quad i,j=1,2$

The standard state for the calculation of activity coefficients is the pure component at the pressure and temperature of the solution.

The second virial coefficients B_{ii} and B_{ij} were calculated by the method of Pitzer and Curl [7]. The Rackett equation (eq. 5) was used to calculate the liquid molar volumes V_i.

$$V = \frac{RT_c}{P_c}\left(0.29056 - 0.08775\omega\right)^a ; a = 1 + (1 - T_r)^{\frac{2}{7}} \qquad (5)$$

where: T_c, P_c, T_r are critical temperature, critical pressure and reduce temperature, respectively; ω is acentric factor.

The critical properties for (-)-linalool and (-)-beta citronellol were estimated by the method proposed by Bae et al. [8] and by Joback's group contribution method [9].

The molar excess Gibbs energies, G^E (J mol^{-1}) were calculated from (eq. 6):

$$G^E = RT\sum x_i \ln \gamma_i \quad (6)$$

In the binary system (-)-linalool + (-)-beta-citronellol the values of the experimental activity coefficients, γ_i range from ca. 1.00 to ca. 1.58. The experimental fugacity coefficients, φ_i are very closed to unity. This means a quasi-ideal behavior of the liquid phase and ideal behavior of the vapor phase. The binary system (-)-linalool + (-)-beta-citronellol shows positive deviations from ideality (Fig. 3). The molar excess Gibbs energies, G^E calculated from the isobaric *T-x-y* measurements range from 0 ($Jmol^{-1}$) to ca. + 345 ($Jmol^{-1}$)

Another series of *T-P* measurements was performed at four constant liquid phase compositions, x_i (mol.fr.). For the mixtures of (-)-linalool (1) + (-)-beta-citronellol (2): x_1=0.1590±0.001; x_1=0.4250±0.001; x_1=0.5100±0.001; x_1=0.7840±0.001. The *T-P-x* measurements are reported in Tab. 3.

Table 3. Experimental vapor - liquid equilibrium data of the binary system (-)-linalool (1) + (-)-beta-citronellol (2).

T (K)	x_1	*P* (Pa)
362.35	0.1590	666
374.35	0.1590	1,333
381.55	0.1590	2,000
387.15	0.1590	2,666
391.75	0.1590	3,333
354.15	0.4250	666
365.75	0.4250	1,333
372.95	0.4250	2,000
378.15	0.4250	2,666
383.15	0.4250	3,333
349.65	0.5100	666
361.75	0.5100	1,333
370.05	0.5100	2,000
375.25	0.5100	2,666
379.75	0.5100	3,333
344.55	0.7840	666
357.05	0.7840	1,333
364.55	0.7840	2,666
376.45	0.7840	3,333

Boiling temperature *T*, liquid phase compositions, x_i (mol.fr.) and pressure *P*.

Check the thermodynamically consistency

The isobaric *T-x-y* measurements of the mixtures (-)-linalool + (-)-beta-citronellol were found to be thermodynamically consistent as tested by using the maximum likelihood multimodel fitting method described by Panaitescu [10]. The objective function (S) is defined as follows (eq. 7):

$$S = \sum_{i=1}^{N} \left[\left(P_{ie} - P_{ic}\right)^2 / \sigma_P^2 + \left(T_{ie} - T_{ic}\right)^2 / \sigma_T^2 + \left(x_{ie} - x_{ic}\right)^2 / \sigma_x^2 + \left(y_{ie} - y_{ic}\right)^2 / \sigma_y^2 \right] \quad (7)$$

where: N is the number of experimental points; P_{ie}, T_{ie}, x_{ie} and y_{ie} are the experimental data and P_{ic}, T_{ic}, x_{ic} and y_{ic} are the corresponding calculated values for pressure, temperature, and the liquid and the vapor phase compositions, respectively; σ_P, σ_T, σ_x and σ_y are the standard deviations for pressure, temperature and liquid and vapor phase compositions. In this paper, the standard deviations were set to: σ_P = 60 Pa, σ_T = 0.05 K, σ_x = 0.001 mol. fr. and σ_y = 0.001 mol. fr., respectively. According to this test the isobaric *T-x-y* measurements are considered consistent if the values of the statistic criterion of selection of the each experimental point (*Ro*) and of the all experimental points (*global Ro*) are less than 2.45. At *P* = (3,333±30) Pa the values of the (*global Ro*) criterions were: 0.487 (Wilson), 0.622 (NRTL) and 1.154 (UNIQUAC), while the all values of the (*Ro*) criterions are less than 2.45.

The thermodynamic consistency of the isobaric *T-x-y* measurements was also checked against the point-to-point test of Van Ness, modified by Fredenslund [11] using a fourth order Legendre polynomial. According to this test, the data are considered consistent if the absolute mean deviation in *y*, *AMD(y)* (mol.fr.) is less than 0.01. At *P*=(3,333±30) Pa we found *AMD(*y) (mol.fr.) = 0.00387.

Reduction of the experimental VLE data by non-electrolyte solutions models

The experimental VLE data of the binary system (-)-linalool + (-)-beta-citronellol have been correlated by means of the Wilson [12], NRTL [13, 14] and UNIQUAC [15] equations. The equations used are the same as in others applications, see for example [16] and need not to be repeated here.

The binary parameters of the models were obtained from the isobaric *T-x-y* measurements and from the *T-P-x* measurements. They were calculated by minimizing the following objective functions (***S***): the maximum likelihood multimodel fitting method [10] (eq. 7) (B_{12}, B_{21}) and the boiling points condition, (eq. 8) (A_{12}, A_{21}):

$$S = \sum_{i=1}^{N} [1 - (P_1^0 / P) x_1 \gamma_1(A_{12}, A_{21}) - (P_2^0 / P) x_2 \gamma_2(A_{12}, A_{21})]_i = \min. \quad (8)$$

where: N is the number of experimental points, P is the total pressure, P_1^0 and P_2^0 are the vapor pressures of the pure components 1 and 2, A_{12} and A_{21} are, respectively, the binary parameters of the Wilson, NRTL and UNIQUAC models, γ_1 and γ_2 are the activity coefficients, x_1 and x_2 are the mole fractions of the pure components 1 and 2 in the liquid phase.

The purport of the calculated binary parameters (B_{12}, B_{21}) (eq. 7) is: $[(\lambda_{12}-\lambda_{11}),(\lambda_{21}-\lambda_{22})]$ (Wilson); $[(g_{12}-g_{22}),(g_{21}-g_{11})]$ (NRTL) and $[(u_{12}-u_{22})/R,\ (u_{21}-u_{11})/R]$ (UNIQUAC). The purport of the calculated binary parameters (A_{12}, A_{21}) (eq.8) is: $[\Lambda_{12},\Lambda_{21}]$ (Wilson); $[\tau_{12},\tau_{21}]$ (NRTL) and $[(u_{12}-u_{22}),(u_{21}-u_{11})]$ (UNIQUAC).

The values of the binary parameters of each model (B_{12}, B_{21}), respectively (A_{12}, A_{21}), the statistic criterions of the all experimental points (*global Ro*), the absolute mean deviations in the vapor phase compositions, *AMD(y)* (mol. fr.) and in pressure, *AMD(P)* (Pa) are reported in Tables 4 and 5.

Table 4. Binary parameters (B_{12}, B_{21}) of the Wilson and NRTL (α = 0.3) and UNIQUAC models for the binary system (-)-linalool (1) + (-)-beta-citronellol (2) obtained from isobaric *T-x-y* measurements at constant pressure *P*=3,333 Pa (the object function - the maximum likelihood multimodel fitting method). (*A_{12}, *A_{21}) are the corresponding binary parameters calculated from (B_{12}, B_{21}).

Models	T-P-x-y		*global Ro*
	B_{12}/(*A_{12})	B_{21}/(*A_{21})	
Wilson	-1757.99/	4981.51/0.487	
	*1.75904	*0.21474	
NRTL (α=0.3)	5565.46/	-2796.93/ 0.622	
	*1.73669	*-0.87278	
UNIQUAC	220.81/	-159.41/ 1.154	
	*1835.81	*-1325.33	

(B_{12}, B_{21}): Wilson $[(\lambda_{12}-\lambda_{11}),\ (\lambda_{21}-\lambda_{22})]$ and NRTL $[(g_{12}-g_{22}),\ (g_{21}-g_{11})]$ parameters unit (Jmol^{-1}); UNIQUAC $[(u_{12}-u_{22})/R,(u_{21}-u_{11})/R]$ parameter unit (K); (*A_{12}, *A_{21}) Wilson and NRTL dimensionless parameters; UNIQUAC parameter unit (Jmol^{-1}). The statistic criterion of the all experimental points (*global Ro*).

It should be noted that the values of the binary parameters of the Wilson, NRTL and UNIQUAC models, for the same isobaric *T-x-y* measurements, are not identical when the two objective functions are used. Using the same objective function - the boiling points condition – the calculated binary parameters from the isobaric *T-x-y* measurements and from *T-P-x* measurements are different. This fact do not affect the vapor-liquid prediction if the binary parameters are used only to calculate vapor-liquid equilibrium data at the same pressure or at others pressures. Consequently, the vapor phase compositions, y_i (mol. fr.) at the pressure of *P*=3,333 Pa, calculated using the Wilson, NRTL and UNIQUAC binary parameters, obtained from our *P-T-*x_i measurements, are in good agreement with our *P-T-*x_i-y_i experimental data. The absolute mean deviations in the vapor phase composition, *AMD(y)* (mol.fr.) are: 0.01 (Wilson); 0.01 (NRTL) and 0.007 (UNIQUAC), respectively. The absolute mean deviations in pressure, *AMD(P)* (Pa) are: 130 (Wilson); 124 (NRTL) and 35 (UNIQUAC), respectively.

Table 5. Binary parameters (A_{12}, A_{21}) of the Wilson and NRTL (α = 0.3) and UNIQUAC models for the binary system (-)-linalool (1) + (-)-beta-citronellol (2) obtained from isobaric *T-x-y* measurements at constant pressure *P*=3,333 Pa, respectively from *T-P-x* measurements (the object function - the boiling points condition).

Models	**T-P-x-y**		*AMD(y)* (mol. fr.)	*AMD(P)* (Pa)	**T-P-x**		*AMD(P)* (Pa)
	A_{12}	A_{21}			A_{12}	A_{21}	
Wilson	1.98464	0.13072	0.0035	13	2.65891	0.01148	57
NRTL (α=0.3)	16.8535	18.8344	0.0143	84	2.97777	-1.33218	57
UNIQUAC	607.230	405.87	0.0048	21	725.885	-465.710	60

Absolute mean deviations in the vapor phase composition, *AMD(y)* and in pressure, *AMD(P)*; Wilson and NRTL dimensionless parameters; UNIQUAC parameter unit ($Jmol^{-1}$)

Table 7. Modified UNIFAC (Dortmund) group interaction parameters [24]

n	m	a_{nm} (K)	b_{nm}	c_{nm} (K^{-1})	a_{mn} (K)	b_{mn}	c_{mn} (K^{-1})
1	2	189.66	-0.2723	0.000E+00	-95.418	0.0617	0.000E+00
1	5	2777	-4.674	1.551E-03	1606	-4.7460	9.181E-04
2	5	2649	-6.5080	4.822E-03	1566	-5.809	5.197E-03

Boiling points correlation

The boiling points of the binary systems (-)-linalool + (-)-beta-citronellol were correlated by the equation proposed by Wisniak and Tamir [17] (eq. 9).

$$T/K = \sum_{i=1}^{n} x_i T_i^0 / K + \sum_{i,j=1}^{n} \{x_i x_j \sum_{k=0}^{m} C_k (x_i - x_j)^k\} + \\ + x_1 x_2 x_3 \{A + B(x_1 - x_2) + C(x_1 - x_3) + D(x_2 - x_3)\} \quad (9)$$

where: n is the number of components (n = 2 or 3), T_i^0 is the boiling point of the pure components i and m is the number of terms in the series expansion of $(x_i - x_j)$, C_k are the binary constants while A, B, C, D are ternary constants.

Root mean square deviation (RMSD) is defined by eq. (10)

$$RMSD(T) = \left[\sum_{i=1}^{i=N} (T_{i,\exp} - T_{i,calc.})^2 / (N-1) \right]^{1/2} \quad (10)$$

For the binary system (-)-linalool + (-)-beta-citronellol, with 4 coefficients *C(i)* (eq. 9): C(1) =-23.01009; C(2) = 1.22011; C(3) =-0.29773; C(4)=9.98300, the absolute mean deviation *AMD*(*T*) (K) (eq. 2) and the root mean square deviation *RMSD*(*T*) (K) (eq. 10) are 0.057 and respectively 0.021.

Check the predictive capability of the Modified UNIFAC (Dortmund) group contribution model

The most common group contribution methods for the prediction of phase equilibria are: ASOG [18, 19, 20], original UNIFAC [11, 21, 22], Modified UNIFAC (Dortmund) [23, 24, 25], Modified UNIFAC [26] (Lyngby) and DISQUAC [27, 28].

The Modified UNIFAC (Dortmund) group contribution model is the most useful model to predicts vapor-liquid equilibrium data.

According to the Mod. UNIFAC (Do) model the molecules are decomposed in structural groups. Each structural group is characterized by van der Waals volume, R_k and van der Waals surface area, Q_k.

The equations used in Modified UNIFAC (Dortmund) model [24] to calculate activity coefficients, γ_i, VLE data or G^E are the same as in the original UNIFAC [11, 21].

The Mod. UNIFAC (Do) is revised and extended periodicaly [29-35] to improve the capability of prediction.

One of the main differences between original UNIFAC (eq. 9) and Modified UNIFAC (Do) (eq. 10) is the introduction of temperature dependent of the interaction parameters, ψ_{nm}, between main structural groups n and m,

to permit a better description of the real phase behavior as a function of temperature:

$$\text{Original UNIFAC: } \psi_{nm} = \exp\left[-\frac{a_{nm}}{T}\right] \tag{9}$$

$$\text{Mod. UNIFAC (Do): } \psi_{nm} = \exp\left[-\frac{a_{nm} + b_{nm}T + c_{nm}T^2}{T}\right] \tag{10}$$

Assessment of geometrical parameters

The molecules of (-)-linalool and (-)-beta-citronellol have been decomposed in structural groups according to the Mod. UNIFAC (Do) model. Table 6 lists the van der Waals values of R_k and Q_k for the all structural groups referred to in this paper.

Table 6. R_k and Q_k parameters and group assignment for the Modified UNIFAC (Dortmund) Method [24]

Main group	Subgroup	No	R_k	Q_k
1 "CH_3"	CH_3	1	0.6325	1.0608
	CH_2	2	0.6325	0.7081
	CH	3	0.6325	0.3554
	C	4	0.6325	0.0000
2 "C=C"	CH_2=CH	5	1.2832	1.6016
	CH=C	7	1.2832	0.8962
5. "OH"	OH(p)	14	1.2302	0.8927
	OH(t)	82	0.6895	0.8345

Assessment of interaction parameters

We used the group interaction parameters published in [24].Table 7 lists the Modified UNIFAC (Do) Group Interaction Parameters.

Comparison with experiment

A comparison between experimental VLE data (*T-P-x-y*) and predicted VLE data (the vapor phase compositions y_i and the temperatures T_i) is done. More discussions are necessary for the binary mixture (-)-linalool + (-)-beta-citronellol.

The Mod. UNIFAC (Do) model predicts satisfactory the composition of the vapor phase, y_i. The absolute mean deviation in the vapor phase composition, *AMD(y)* (mol.fr.) is 0.009. The absolute mean deviation in temperature, *AMD(T)* (K) is 1.52. We appreciate that the temperature prediction is rather poor.

The excess Gibbs energy, G^E, provides a more accurate comparison. The experimental excess Gibbs energy, $G^E_{\exp}$ presents positive deviations from ideality (Figure 3). At ca. *T*=377.55 K, $G^E_{\exp}$ (*x* = 0.6250) is ca. 345 (Jmol^{-1}).

The Mod. UNIFAC (Do) model predicts small deviations from ideality. The excess Gibbs energy predictions, G^E_{UNI} are positive on the all range of the compositions of the liquid phase, x_i. At ca. *T*=377.55 K, the equimolecular G^E_{UNI} is ca. 35 (Jmol^{-1}) (Fig. 3) The conclusion is that the excess Gibbs energy predictions are unsatisfactorily.

Analysis in terms of intermolecular forces of the thermodynamic properties of the mixtures containing (-)-linalool + (-)-beta-citronellol

Thermodynamic properties of any pure substance are determined by intermolecular forces that operate between the molecules of that substance. Thermodynamic properties of the mixtures depend on intermolecular forces that operate between the molecules belonging to the same component, but also to interaction between dissimilar molecules of the mixture. Frequently, the theory of intermolecular forces gives us no more than a qualitative, or perhaps semiquantitative basis for understanding phase behaviour, but even such a limited basis can be useful for understanding and correlating experimental results. A brief discussion of the intermolecular forces in molecular thermodynamics of fluid-phase equilibria [36] and in supramolecular chemistry [37] was done.

Literature describes different types of intermolecular forces [36], but for our purpose here, only *induction forces* (between an induced dipole – e.g. a dipole induced in a molecule with polarizable electrons), *dispersion forces* (forces of attraction between nonpolar molecules based on *hydrophobic interactions*) and, respectively *specific (chemical) forces* leading to hydrogen bonds were considerated. Also we take into consideration the van der Waals forces [37] and the steric hindrance effect.

The calculated dipole moment of the (-)-linalool is 1.42 D, while the calculated dipole moment of the (-)-beta-citronellol is 2.50 D, indicating possible strong electrostatic forces of associations between these two compounds. The values of the calculated dipole moments were obtained using, for geometry optimization - hamiltonian: B3LYP (density functional theory); basis set: 6-31G(d) (Gaussian98) and for dipole moment - hamiltonian: B3LYP; basis set: 6-31G(d) (Gaussian98).

(-)-Linalool and (-)-beta-citronellol contain two active functional groups, hydroxyl, –OH and double bonds, -CH=CH$_2$ and/or –CH=C<. In (-)-linalool hydroxyl group, –OH is sterically hindered by methyl group, -CH$_3$. Between hydroxyl group, –OH and double bond, -CH=CH$_2$ there is a proximity effect.

The major contribution to the non-ideality of the mixture comes from the hydrogen bonds between hydroxyl groups, and from the like weak dipole/ dipole, -O-/-O- interactions, due to non bonding electrons from the hydroxyl group.

When a strongly hydrogen-bonded substance is dissolved in a nonpolar solvent (such as hexane o cyclohexane), hydrogen bonds are broken until all the molecules exist as monomers rather then dimers, trimers, or higher aggregates. The solvation of the alcohol broke the hydrogen bond and, such braking requires energy, much heat is absorbed (positive deviations from ideality) [36].

Linear primary alcohols exhibit large deviations from ideality, e.g. binary system (1-butanol + hexane) has a G^E (x_1=0.50) of the order of 1186 (J mol^{-1}) at 333 K, respectively, binary system (1-butanol + cyclohexane) has G^E (x_1==0.50) of the order of 1100 (J mol^{-1}) at 318 K [38]. *Tertiary alcohols*, due to the steric hindrance, exhibit smaller deviations than primary linear alcohols, e.g. binary system {2-methyl-2-propanol (*tert*-butanol) + cyclohexane} has G^E (x_1=0.50) of the order of 935 (J mol^{-1}) at 318 K [38].

In a mixture of two alcohols, the hydrogen bonds compensate and this results in small deviation from ideality. Binary system (ethanol + 2-propanol) has G^E (x_1==0.50) of the order of 35 (J mol^{-1}) at 313.15 K [38].

In (-)-linalool due to additional alkyl groups and to the two double bonds, to the like weak dipole/dipole, -O-/-O- interactions, the dipole/induced dipole interactions, –O-/π, from H_2C=CH- and >C=CH- (double bonds) and the induced dipole/induced dipole interactions, π/π, from H_2C=CH-/H_2C=CH-, H_2C=CH-/>C=CH- and respectively >C=CH-/>C=CH- are added. In mixture with primary linear alcohols, e.g. in the binary system (linalool + 1-butanol), the (-)-linalool's interactions are added and this results in a relatively higher deviation from ideality. At 357 K, G^E (x_1=0.69) is ca. 213 (J mol^{-1}) [4].

In (-)-beta-citronellol, due to additional alkyl groups and to the one double bond, to the like weak dipole/dipole, -O-/-O- interactions, the dipole/ induced dipole interactions, –O-/π, from >C=CH- (double bond) and the induced dipole/induced dipole interactions, π/π, from >C=CH-/>C=CH- are added. In the binary system (-)-linalool + (-)-beta-citronellol}, the (-)-beta-citronellol's interactions are added and this results in a relatively higher deviation from ideality. At ca 377 K, G^E (x_1=0.625) is ca. 345 (J mol^{-1}) (Fig.3) (this paper).

Due to the important hydrocarbon part of the involved molecules, *hydrophobic interactions* could not be negligible [36, 37]. The hydrophobic effect arises mainly from the attractive forces between hydrophobic parts of the molecules. Hydrophobic effects generally relate to the exclusion from polar solvent of large particles or those are weekly solvated (e.g. hydrogen bonds or dipolar interactions). This can produce effects resembling attraction between one organic molecule and another, although there are in addition van der Waals and π/π attractions between organic molecules themselves. The hydrophobic

effect creates a higher degree of local order, producing a decrease in entropy that leads to an unfavorable Gibbs energy. The entropic contribution, TS^E to the excess Gibbs energy, G^E is even larger than the enthalpic contribution, H^E [36].

CONCLUSIONS

This paper has reported original vapor - liquid equlibrium data in binary system (-)-linalool + (-)-beta-citronellol.

Reduction of the vapor-liquid equlibrium data was carried out by means of the Wilson, NRTL and UNIQUAC equations. The binary parameters of the corresponding models were calculated from the isobaric *T-x-y* measurements and from the *T-P-x* measurements.

The Modified UNIFAC (Dortmund) group contribution model was used to check their predictive capability in mixtures containing (3*R*)-(-)-linalool and (3*S*)-(-)-beta-citronellol. The Mod. UNIFAC (Do) model predicts satisfactory the composition of the vapor phase, y_i. We appreciate that the temperature prediction is rather poor.

(-)-Linalool, (-)-beta-citronellol, main components of the essential oils of geranium are molecules containing various functional groups. It was presented an analysis in terms of intermolecular forces of the thermodynamic properties of the mixtures containing (-)-linalool, (-)-beta-citronellol taking into consideration the values of the molar excess Gibbs energy, G^E.

EXPERIMENTAL SECTION

Chemicals

(-)-Linalool [(-)-3,7-Dimethylocta-1,6-dien-3-ol], CAS RN 78-70-6, Brüder Unterweger GmbH, Austria, material of started purity >99.4 %, tested by Hewlett-Packard 6890 gas-chromatograph, was used without further purification.

(-)-beta-Citronellol [3,7-Dimethyloct-6-en-1-ol], CAS RN 106-22-9, Brüder Unterweger GmbH, Austria, material of started purity >99.4 %, tested by Hewlett-Packard 6890 gas-chromatograph, was used without further purification.

Apparatus and procedure

An all-glass 240-cm^3 recirculation still (Sieg and Röck Type, Normag Labor-und Verfahrenstechnik GmbH & Co., Hofheim am Taunus, Germany) was used. The equilibrium temperature *T* was measured by means of a termistor thermometer connected to a digital multimeter (YSI 4600, USA) calibrated against ITS-90, within $\sigma(T)$ (K)=0.05. A pressure controller (Normag) maintained the pressure *P* within 30 Pa around the desired values. *P* was measured using a mercury-filled U-tube together with a cathetometer within $\sigma(P)$ (Pa)=30. Atmospheric pressure was measured by a barometer with an accuracy of $\sigma(P)$ (Pa)=13.

Prior to an experimental run, the equilibrium still was thoroughly cleaned and evacuated. It was then charged with the appropriate amounts of components and pressure was adjusted to the required value by means of a vacuum pump. Equilibrium was attained under continuous stirring and recirculation of the two phases for 1 h. Samples of the liquid and condensed vapor were taken after pressurizing the apparatus to atmospheric pressure.

The equilibrium still (Stage Type, i-Fischer Labodest, Model 602-D, Germany) was also used. These equilibrium still does not work properly to obtain accurate vapor-liquidequilibrium data in the field of terpenoids.

Sample analysis

The equilibrium vapor and liquid compositions were determined by gas chromatography, carried out on two different instruments.

Dual channel analysis was performed on a Hewlett-Packard 5890 Series II gas-chromatograph, equipped with flame ionization detectors (GC-FID), using two fused silica capillary columns coated with stationary phases of different polarity: Supelcowax TA-10, (60m x 0.32 mm i.d., film thickness 0.5 μm) (polar) and SPP – 1, (60 m, 0.32 mm i.d., film thickness 0.25 μm) (nonpolar). Oven temperature was programmed as follows: 333 °K (held 3 min), then at a rate of 4°K/min to 483 °K and held 20 min. Injector and detector temperatures were 533 K, respectively 543 K. Hydrogen was used as carrier gas at a pressure of 1.2 bar. Injection volume was 0.5×10^{-3} mL (split mode), at a split ratio of 1:20.

A Hewlett-Packard 6890 gas-chromatograph equipped with a flame ionization detector (GC-FID) was also used. The semi-polar system consisted of a HP-5 fused silica capillary column (30m x 0.25 mm i.d., film thickness 0.25 μm). The temperature program was: 323 °K (held 2 min) at 2 °K/min to 453 °K, and then at 20 °K/min to 523 °K and held 2 min. Carrier gas was He at a flow rate of 1 mL/min. Injector and detector temperatures were 523 °K. Injection volume was 0.5×10^{-3} mL (split mode), with a split ratio of 1:20.

Calibration was performed using gravimetrically prepared solutions. The response factor of the detector was 0.973 (polar column), 1.036 (non-polar column) and 1.05 (semi-polar column). Very good separations were achieved under these conditions. The precision of the analyses was generally within $\sigma(x_i) = \sigma(y_i) = 0.001$ in mole fraction, at any concentration.

ACKNOWLEDGMENTS

The authors gratefully acknowledges to Dr. Răzvan Podea (S.C. Natex S.R.L. Cluj-Napoca, Romania) and Dr. Szücs-Balàzs Jòzsef-Zsolt (“Babeş-Bolyai” University of Cluj-Napoca, Romania) for their help in the analytical work and to M.Sc. Ing. Jesus Manuel Flores Arizaca (Universidad Nacional Amazónica Madre de Dios, Puerto Maldonado, Perú) for their help in the experimental work.

REFERENCES

1. G. Radoias, A. Bosilcov, I. Batiu, “Odorante Naturale în Parfumeria Modernă (Natural Fragrances in Modern Parfumery)”, Editura Casa Cărţii de Ştiinţă, Cluj-Napoca, **2005**, chapter 4.
2. I. Wichterle, J. Linek, Z. Wagner and H.V. Kehiaian, “Vapor-Liquid Equilibrium Bibliographic Database”, 9th Ed. CD-ROM, ELDATA, Paris, France, **2004**.
3. I. Wichterle, J. Linek, Z. Wagner, J.-C. Fontaine, K. Sosnkowska-Kehiaian and H.V. Kehiaian, „Vapor-Liquid Equilibrium in Mixtures and Solutions”. Landolt-Boernstein Numerical Data and Functional Relationships in Science and Technology, New Series. W. Martienssen Ed., Vol. IV/13A. Springer-Verlag, Berlin-Heidelberg, Germany, **2007**.
4. D. Dongshun, L. Haoran, H. Shijun, *J. Chem. Thermodynamics,* **2002**, *34*, 1431.
5. ◊ ◊ ◊ “Perry’s Chemical Engineer’s Handbook”, Seventh Edition, McGraw-Hill, Late Editor, R.H. Perry, Editor D.W. Green, Assoc. Editor J.O. Malonay, New York, **1997**, section 2.
6. H.C. Van Ness and M.M. Abbott, “Classical Thermodynamics of Non-electrolyte Solutions”, Mc Graw-Hill Book Co. New York, **1982**.
7. K.S. Pitzer and R.F. Curl, *J. Am. Chem. Soc*., **1957**, *79*, 2369.
8. H.K. Bae, S.Y. Lee and A.S. Teja, *Fluid Phase Equilib*., **1991**, *66*, 225.
9. R.C. Reid, J.M. Prausnitz and B.E. Poling. “The Properties of Gases and Liquids”, 4th Ed. Mc Graw-Hill, Book Company USA, New York, **1987**.
10. G.M. Panaitescu, *Rev. Chim.,* **1982**, *33*, 1110; *Ind. Chem. Eng.,* **1985**, *25*, 68.
11. Aa. Fredenslund, J. Gmehling and P. Rasmunsen, “Vapor-Liquid Equilibria using UNIFAC, A Group Contribution Methods”, Elsevier, Amsterdam, **1977**, chapter 4.
12. G.M. Wilson, *J. Am. Chem.Soc.,* **1964**, *86*, 127.
13. H. Renon and J.M. Prausnitz, *A.I.Ch.E. J.,* **1968**, *14*, 135.
14. H. Renon and J.M. Prausnitz, *Ind. and Eng. Chem. Process. Des. Dev.,* **1969**, *8*, 413.
15. D.S. Abrams and J.M. Prausnitz, *A.I.Ch.E. J*., **1975**, *21*, 116.
16. I. Batiu, *Studia UBB Chemia,* **2011**, *LVI*, 37.
17. J. Wisniak, A. Tamir *Chem. Eng Sci*., **1976**, 31, 631.
18. E.L. Derr, C.H. Deal, *Inst. Chem. Eng. Symp. Ser.* (London), **1969**, *32*, 40.
19. K. Kojima, K. Tochigi, “Prediction of Vapor-Liquid Equilibria by the ASOG Method”, Kodansha-Elsevier Tokyo, **1979**.
20. K. Kojima, D. Tiegs, J. Gmehling, K. Tochigi*, J. Chem. Eng. Jpn.,* **1990**, *23*, 453.
21. Aa. Fredenslund, R. L. Jones, J. M. Prausnitz, *AIChE Journal*, **1975**, *21*, 1086.
22. H.K. Hansen, P. Rasmussen, Aa. Fredenslund, M. Schiller, J. Gmehling, *Ind. Eng. Chem. Res.,* **1991**, *30*, 2352.
23. U. Weidlich, J. Gmehling, *Ind. Eng. Chem. Res.,* **1987**, *26*, 1372.
24 J. Gmehling, J. Li, M. Schiller, *Ind. Eng. Chem. Res.,* **1993**, *32*, 178.

25. J. Gmehling, J. Lohmann, A. Jakob, J. Li, R. Joh, *Ind. Eng. Chem. Res.,* **1998**, *37*, 4876.
26. B.L. Larsen, P. Rasmussen, Aa. Fredenslund, *Ind. Eng. Chem. Res.,* **1987**, *26*, 2274.
27. H.V. Kehiaian, J-P.E. Grolier, G.C. Benson, *Journal of Chimie Physique,* **1978**, *75*, 1031.
28. H.V. Kehiaian, B. Marongiu, *Fluid Phase Equilib.*, **1988**, *40*, 23.
29. J. Lohmann, R. Joh, J. Gmehling, *Ind. Eng. Chem. Res.,* **2001**, *40*, 957.
30. R. Wittig, J. Lohmann, R. Joh, S. Horstmann, J. Gmehling, *Ind. Eng. Chem. Res.,* **2001**, *40*, 5831.
31. J. Lohmann, J. Gmehling, *J. Chem. Eng. Jpn,* **2001**, *34*, 43.
32. J. Gmehling, R. Wittig, J. Lohmann, R. Joh, *Ind. Eng. Chem. Res.,* **2002**, *41*, 1678.
33. R. Wittig, J. Lohmann, J. Gmehling, *AIChE Journal*, **2003**, *49*, 530.
34. A. Jakob, H. Grensemann, J. Lohmann, J. Gmehling, *Ind. Eng. Chem. Res.,* **2006**, *45*, 7924.
35, 36. S. Nebig, J. Gmehling, *Fluid Phase Equilib*, **2010**, *294*, 206.
36. J.M. Prausnitz, R.N. Lichtenthaler, E.G. Azevedo, "Molecular Thermodynamics of Fluid-Phase Equilibria" Printece Hall PTR Printice-Hall Inc. Upper Saddle River, New Jersey, **1999**, chapter 4.
37. J.W. Steed, J.L. Atwood "Supramolecular Chemistry", John Wiley & Sons, Ltd, Baffins Lane, Chickester, **2009**, chapter 1.
38. D.R. Lide, H.V. Kehiaian "CRC Handbook of Thermophysical and Thermochemical Data" CRC Press Inc. Boca Raton Ann Arbor London Tokyo, **1994**, section 3.

STUDIA UBB CHEMIA, LVII, 2, 2012 (p. 47 - 57)

EVALUATION OF IRON AND NICKEL-BASED OXYGEN CARRIERS FOR NATURAL GAS CHEMICAL LOOPING COMBUSTION SYSTEMS

IULIA-MARIA BODEA[a], CALIN-CRISTIAN CORMOS[a]

ABSTRACT. Chemical looping combustion (CLC) is a innovative technology used to capture CO_2, in which a solid oxygen carrier is circulated between two interconnected bed reactors. A fuel gas is oxidized to carbon dioxide and water by the oxygen carrier. The reduced oxygen carrier is transported to the air reactor where it is oxidized back to its original state by air. This paper investigates two natural gas CLC processes using ferric oxide and nickel oxide as oxygen carriers. The oxygen carriers are reduced in the temperature range 750-850°C while the oxidation temperature is between 850-950°C. The processes studied have the net electrical efficiencies in the range of 41-42% and the CO_2 capture rate is about 99%.

Keywords: *Chemical looping combustion (CLC), Power generation, Oxygen carriers, Carbon Capture and Storage (CCS)*

INTRODUCTION

The effect of carbon dioxide emissions for exacerbating the greenhouse effect is well known [1]. Carbon dioxide emissions derived from human activities have increased the concentration of greenhouse gases in the atmosphere, contributing to global climate change and increasing global temperature [2]. About a third of the global CO_2 emissions comes from the burning of fossil fuels in power generation sector [1].

Chemical Looping Combustion (CLC) is one promissing techniques used to combine fuel combustion and pure CO_2 production in situ allowing for CO_2 sequestration [3]. This technology was first proposed primarily for the combustion of gaseous fuels and only recently been considered for solid fuels such as coal without gasification of the coal first to syngas [4]. CLC is a two-step gas combustion process that produces a pure CO_2 stream, ready for compression and sequestration [5]. The process is composed of two fluidized bed reactors, an air reactor and a fuel reactor, as shown in Figure 1. The fuel is introduced to the fuel reactor where it reacts with an oxygen carrier to CO_2

[a] "Babeş-Bolyai" University of Cluj-Napoca, Faculty of Chemistry and Chemical Engineering, Arany Janos Street 11, 400028 Cluj-Napoca, Romania; Emails: iulyya_b@yahoo.com, cormos@chem.ubbcluj.ro

and H_2O. The reduced oxygen carrier is transported to the air reactor where it is oxidized back to its original state by air. As a result, CO_2 can be inherently separated in this combustion process. The total amount of heat released in the air and the fuel reactor is equal to the heat released from normal combustion thus separating CO_2 without any losses in energy [6-7].

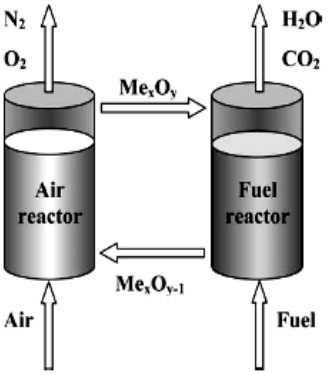

Figure 1. Chemical looping combustion (CLC)

In the fuel reactor, the metal oxide is reduced by the following general chemical reaction for a hydrocarbonated fuel (like natural gas or other hydrocarbons) [1]. The same reactions can take place also in case of syngas resulted from gasification of catalytic reforming processes.

$$(2n+m)\ Me_xO_y + C_nH_{2m} \rightarrow (2n+m)\ Me_xO_{y-1} + n\ CO_2 + m\ H_2O \quad (1)$$

Me_xO_y is a metal oxide and Me_xO_{y-1} represents its reduced form.

The particles of oxygen carrier are transferred to the air reactor where they are regenerated by taking up oxygen from the air.

$$Me_xO_{y-1} + ½\ O_2 \rightarrow Me_xO_y \quad (2)$$

The oxidized oxygen-carrier is transported back to the fuel reactor and is reduced again. The reduction of the oxygen-carrier (1) can be either endothermic or exothermic, depending on the metal oxide and the fuel, while the oxidation (2) is exothermic [1-2]. Ideally, the number of reduction–oxidation cycles of the oxygen carrier (OC) would be infinite. However, the OC material must be renewed as a consequence of particle attrition/fragmentation or reactivity loss during the reduction/oxidation cycles and a makeup flow of new material is necessary.

The properties of the oxygen carrier are vital for the practice of the process of CLC. Metal oxides with their reduced oxides or metals should have a strong affinity for reaction with gaseous fuel as well as a high rate of oxidation by air [3]. Metal oxides of Fe, Ni, Co, Cu, Mn, and Cd have been discussed

in the literature for CLC of gaseous fuels such as natural gas and CH_4 [4]. Iron oxide is cheaper than other metal oxides [1] but Ni-based oxygen carriers have been the most extensively materials analysed in the literature because they have very high reactivity and good performance working at high temperatures [5]. Beside of promising energy efficiencies, the chemical looping systems are also reducing significantly the emissions of nitrogen oxides resulted from fuel conversion. The main responsible for this fact is the decoupling the air environment (air reactor) from fuel (fuel reactor). Also, the high temperature heat recovery of chemical systems is implying higher pressure and temperature of the generated steam which means more power generated in the steam turbine.

RESULTS AND DISCUSSION

This paper describes two processes of the carbon dioxide capture using a natural gas-based chemical looping combustion system. The processes are identical in design, the difference is in terms of substance used as oxygen carrier. The oxygen carriers used are ferric oxide (Fe_2O_3) and nickel oxide (NiO). The process is composed of two interconnected fludized bed reactors [6,8] as shown in Figure 2.

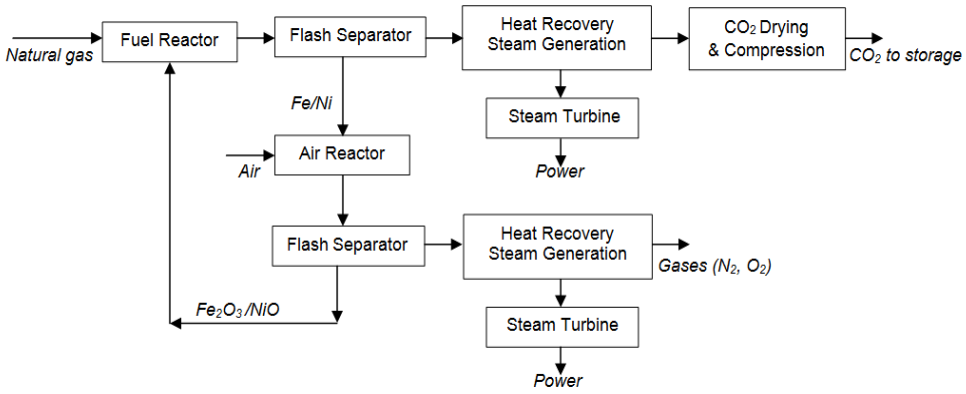

Figure 2. Chemical looping combustion for power generation

The natural gas having 30°C and 15 bar comes in contact with the oxygen carrier in the fuel reactor. The reduction of the oxygen carrier takes place at about 750-850°C and 15 bar, according to the chemical reactions (3) and (4) [8-9]:

$$4Fe_2O_{3(s)} + 3CH_{4\ (g)} \rightarrow 8Fe_{(s)} + 3CO_{2(g)} + 6H_2O_{(g)} \quad (3)$$

$$4NiO_{(s)} + CH_{4(g)} \rightarrow 4Ni_{(s)} + CO_{2(g)} + 2H_2O_{(g)} \quad (4)$$

The stream which leaves the reactor is sent to a flash separator where the solid phase is separated from the gas phase. The rich CO_2 stream leaves the flash to the top and is sent to a heat recovery steam generation. The CO_2 hot stream is then cooled down with cooling water, at around 40°C, the temperature is achieved by using a series of heat exchangers (heat recovery steam generator - HRSG). The steam obtained in heat recovery steam generators by cooling the hot streams reaches a steam turbine where heat is converted into electricity. The exhausted steam leaves the turbine, then it is condensed and recycled back in the cycle (steam – Rankine cycle).

The CO_2 cooled stream is sent to a compression unit, which has 3 compression stages with intercoolers. In the first stage the gas is compressed from 14 bar to 20 bar. The stream is cooled at 40°C and enters in a flash separator, used to remove the water from the process. Cooling and separation are made after each stage of compression. In the second stage the pressure is increased from 20 bar to 70 bar, then the pressure reaches in the third stage 120 bar. The compression stages were used instead of one compressor because one compressor needs more energy to achieve 120 bar than 3 compression stages. Another argument is to avoid the overheating of the compressors.

The solid stream coming from the bottom of the flash separator is sent to the air reactor where is oxidized with air at 850-950°C, according to the reactions (5) and (6).

$$4Fe_{(s)} + 3O_{2\,(g)} \rightarrow 2Fe_2O_{3(s)} \quad (5)$$

$$4Ni_{(s)} + 2O_{2(g)} \rightarrow 4NiO_{(s)} \quad (6)$$

The oxygen carrier obtained (ferric oxide/nickel oxide) is recycled to the reduction reactor. The gas stream leaves the flash separator to the top and is sent, like the CO_2 stream, to a integrated combined cycle. Nitrogen makes up the main part of air but is inert in the reaction equation (5) and (6). Therefore, the gas phase leaving the air reactor consist of nitrogen and excess oxygen [10-11].

The natural gas composition and the equipments main design assumptions used in the mathematical modeling and simulation are presented in Table 1. ChemCAD was used as simulation software.

The material balances for the two processes are given in Tables 2 and 3. The inlet and outlet mass flow represents the mass flow of the components entering and leaving the reactors. Table 2 and 3 shows that the natural gas is fully oxidized to CO_2 and water. The conversion of ferric oxide to iron is about 98.6 % in the fuel reactor while the oxidation of iron to ferric oxide is complete in the air reactor (Table 2). Regarding the process using nickel oxide as oxygen carrier, in the fuel reactor the reduction of nickel oxide to nickel is 100 % and the oxidation of nickel to nickel oxide is also complete (Table 3). These results are in line with experimental data reported in the literature [2-3].

Table 1. Main design assumptions

	Parameters	Fe_2O_3/Fe	NiO/Ni
Natural gas	Temperature (°C)	30.00	
	Pressure (bar)	15.00	
	Gas composition (% vol.)		
	Methane	89.00	
	Nitrogen	0.89	
	Carbon dioxide	2.00	
	Ethane	7.00	
	Propane	1.00	
	I-Butane	0.05	
	N-Butane	0.05	
	I-Pentane	0.005	
	N-Pentane	0.004	
	Hexane	0.001	
	Hydrogen Sulfide	0.00001	
	Calorific value (MJ/kg dry)		
	Gross (HHV)	51.473	
	Net (LHV)	46.502	
Fuel reactor	Reactor type	Gibbs	Gibbs
	Temperature (°C)	750.00-850.00	750.00-850.00
	Pressure (bar)	15.00	15.00
	Pressure drop (bar)	1	1
Air reactor	Temperature (°C)	850.00-950.00	850.00-950.00
	Pressure (bar)	14.00	14.00
	Fractional conversion	>99%	>99%
Heat exchangers	Minimum temperature difference (°C)	10.00	10.00
Expander	Expander efficiency (%)	65.00	65.00
CO_2 compression	Delivery pressure (bar)	120.00	120.00
	Compressor efficiency (%)	85.00	85.00
	Number of compression stages	3	3

Table 2. Material balance for CLC using ferric oxide as oxygen carrier

Parameters	Fuel reactor		Air reactor	
	Inlet	Outlet	Inlet	Outlet
Pressure (bar)	15.00	14.00	14.00	14.00
Temperature (°C)	799.68	850.00	267.56	949.74
Total mass flow (t/h)	655.68	655.68	3057.37	3057.37
Solid mass flow (t/h)	606.83	426.18	426.18	606.83
Gas mass flow (t/h)	48.85	229.48	2631.19	2450.56
Solid phase composition (% wt.)				
Ferric oxide	100.00	1.37	1.37	100.00
Iron	0.00	98.63	98.63	0.00

Parameters	Fuel reactor		Air reactor	
	Inlet	Outlet	Inlet	Outlet
Gas phase composition (% vol.)				
Carbon dioxide	2.00	34.66	0.03	0.03
Methane	89.00	0.00	0.00	0.00
Oxygen	0.00	0.00	20.73	15.50
Nitrogen	0.89	0.28	77.29	82.39
Water	0.00	65.05	1.03	1.09
Hydrogen sulfide	0.00001	0.00	0.00	0.00
Argon	0.00	0.00	0.90	0.90
Ethane	7.00	0.00	0.00	0.00
Propane	1.00	0.00	0.00	0.00
N-Butane	0.05	0.00	0.00	0.00
N-Pentane	0.004	0.00	0.00	0.00
N-Hexane	0.001	0.00	0.00	0.00
I-Butane	0.05	0.00	0.00	0.00
I-Pentane	0.005	0.00	0.00	0.00

Table 3. Material balance for CLC using nickel oxide as oxygen carrier

Parameters	Fuel reactor		Air reactor	
	Inlet	Outlet	Inlet	Outlet
Pressure (bar)	15.00	14.00	14.00	14.00
Temperature (°C)	727.00	850.00	216.98	950.29
Total mass flow (t/h)	892.21	892.21	3292.48	3292.48
Solid mass flow (t/h)	843.36	662.73	662.73	843.36
Gas mass flow (t/h)	48.85	229.48	2629.75	2449.12
Solid phase composition (% wt.)				
Nickel oxide	100.00	0.00	0.00	100.00
Nickel	0.00	100.00	100.00	0.00
Gas phase composition (% vol.)				
Carbon dioxide	2.00	34.66	0.03	0.03
Methane	89.00	0.00	0.00	0.00
Oxygen	0.00	0.00	20.73	15.50
Nitrogen	0.89	0.28	77.29	82.39
Water	0.00	65.05	1.03	1.09
Hydrogen sulfide	0.00001	0.00	0.00	0.00
Argon	0.00	0.00	0.90	0.90
Ethane	7.00	0.00	0.00	0.00
Propane	1.00	0.00	0.00	0.00
N-Butane	0.05	0.00	0.00	0.00
N-Pentane	0.004	0.00	0.00	0.00
N-Hexane	0.001	0.00	0.00	0.00
I-Butane	0.05	0.00	0.00	0.00
I-Pentane	0.005	0.00	0.00	0.00

Table 4 presents the composition of the carbon dioxide stream for the 2 cases studied versus the proposed specification [12]. The proposed specification is considering the requirement of transport and storage options (Enhanced Oil Recovery – EOR storage option was considered being the most restrictive case). For both processes studied the CO_2 content is bigger than the proposed limit (95 % vol.).

Table 4. Quality specification of captured carbon dioxide stream

Composition (% vol.)	Proposed specification	Fe_2O_3/Fe	NiO/Ni
CO_2	>95.00	98.82	98.82
CO	<2000 ppm	0.00	0.00
N_2	<4.00	0.81	0.81
O_2		0.00	0.00
Ar		0.00	0.00
H_2		0.00	0.00
H_2S	<100 ppm	9 ppm	9 ppm
H_2O	<250 ppm	0.36	0.36

Table 5 presents the main plant performance indicators for the 2 evaluated cases. The methane input is 500 MW_{th} and it is expressed taking into consideration the lower heating value (LHV). The overall efficiency of the plant was calculated considering the difference between power generated and power consumed (net power output), divided by the fuel (natural gas) input.

Table 5. Overall plant performance indicators

Main plant data	Units	Fe_2O_3/Fe	NiO/Ni
Methane input (C=A*B/3600)	MW_{th}	500.00	500.00
Methane flow rate (A)	t/h	38.708	38.708
Natural gas LHV (B)	MJ/kg	46.502	46.502
Power generated (D)	MW_e	456.01	456.05
Steam turbine	MW_e	164.13	164.21
Purge gas expander	MW_e	291.87	291.84
Power consumed (E)	MW_e	247.11	246.49
Air compressors	MW_e	239.77	239.64
CO_2 compressors	MW_e	5.10	5.10
Process pumps	MW_e	1.28	1.28
Cooling water pumps	MW_e	0.94	0.45
CO_2 capture rate	%	99.07	99.07
Plant efficiency ((D-E)/C*100)	%	41.77	41.91

The results show that the processes studied have the gross efficiency in the range of 44-45 % and the net efficiency in the range of 41-42 %. Regarding the rate of carbon dioxide capture the two processes have the same capture rate, about 99%. To calculate the CO_2 capture rate was taken into consideration the amount of CO_2 in the water output stream and gas output stream. These results underline an important advantage of chemical looping systems namelly high efficiency in condition of a total decarbonisation of the fuel used. In term of the two evaluated metalic oxides, there is no significant difference between them in term of technical performances [13-14]. However, ferric oxide could be the most preferable choice considering the wide distribution and the potential integration of spent oxide into metalurgy sector.

The carefully heat and power integration is a fundamental pre-condition of the carbon capture technologies to reduce the ancillary energy consumptions. In this study, in order to evaluate the possibilities of integration of the chemical looping CO_2 capture process, a pinch analysis was performed. In the power cycle the hot streams are cooled with cooling water. A heat-integration problem involves transferring heat from hot streams to cold streams so that each stream reaches its desired target temperature while minimizing the utility consumptions (including heating and cooling utilities) [15-18].

The composite curves (Figures 3 and 5) represent the hot and cold streams on a single diagram and determine the minimum utility duties for the entire system. Horizontal lines represent constant-temperature utilities. For condensing and vaporizing streams as hot and cold streams, respectively, a 1°C temperature change was considered [15].

The grand composite curve (Figures 4 and 6) displays the net heat-flow characteristics of a process versus its temperature and provides the same overall energy target as the composite curves.

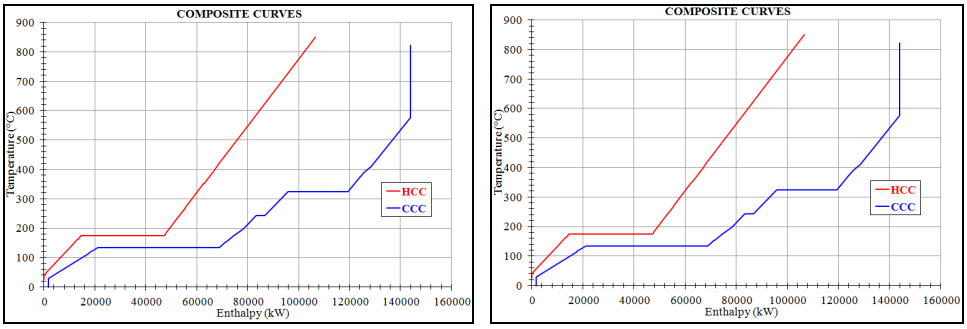

a b

Figure 3. Composite curves for heat recovery from CO_2 stream (fuel reactor)
a. CLC using ferric oxide; b. CLC using nickel oxide

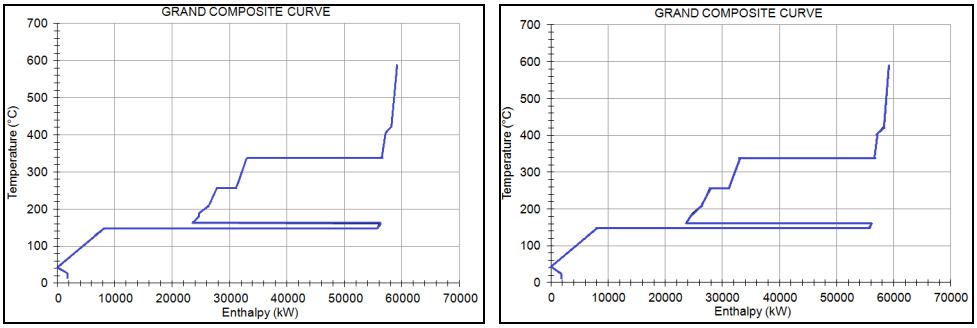

a b

Figure 4. Grand composite curve for heat recovery from CO_2 stream (fuel reactor) a. CLC using ferric oxide; b. CLC using nickel oxide

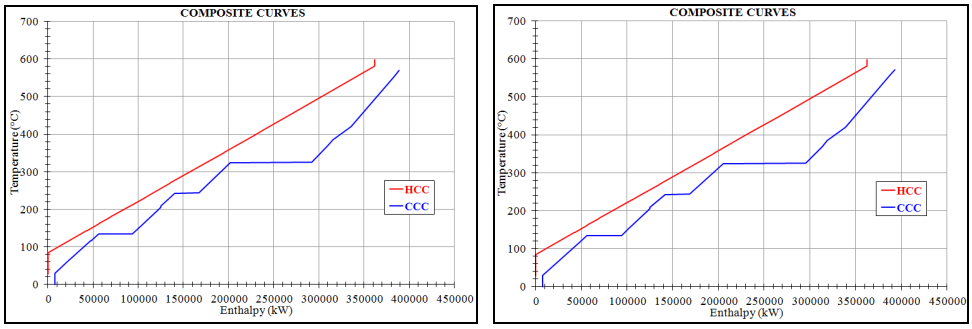

a b

Figure 5. Composite curves for heat recovery from spent air stream (air reactor) a. CLC using ferric oxide; b. CLC using nickel oxide

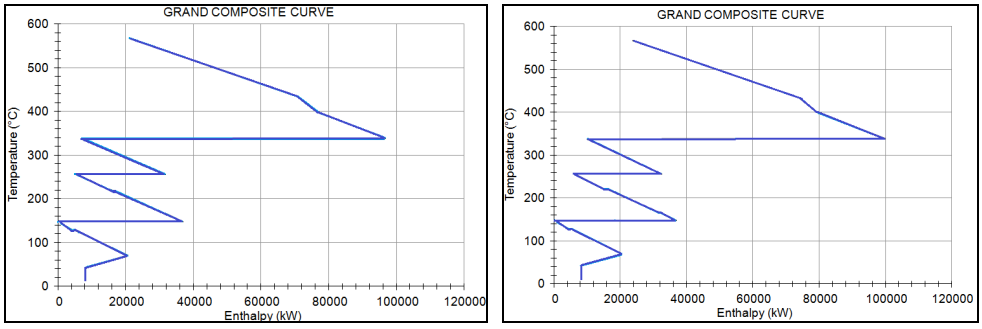

a b

Figure 6. Grand composite curve for heat recovery from spent air stream (air reactor). a. CLC using ferric oxide; b. CLC using nickel oxide

The grand composite curve shows that a large amount of heating utility with high temperature level is needed in the processes. The cold streams were heated by hot utilities below the pinch, while the hot streams were cooled by cold utilities above the pinch. The pinch analysis indicates that the pinch temperature is around 43°C for CO_2 stream resulted from fuel reactor (Figure 4) and around 147°C for exhaust air resulted from air reactor (Figure 6).

CONCLUSIONS

This paper investigates two oxygen carriers for natural gas chemical looping combustion processes using interconnected fluidized beds with inherent separation of CO_2. The technical evaluation of the processes was based on modeling and simulation work, the most important design characteristics being evaluated in this paper were: general configuration of the CLC system, CO_2 capture rate, heat and power integration issues of the main plant sub-systems, overall energy efficiency, performances of various oxygen carriers etc.

The results obtained after modeling and simulation show that the CLC-technique is a promissing thermo-chemical conversion providing high energy efficiencies in both cases either ferric oxide or nickel oxide as oxygen carriers.

ACKNOWLEDGMENTS

This work was supported by a grant of the Romanian National Authority for Scientific Research, CNCS – UEFISCDI, project ID PNII-CT-ERC-2012-1; 2ERC: "*Innovative systems for carbon dioxide capture applied to energy conversion processes*".

REFERENCES

1. A. Abad, T. Mattisson, A. Lyngfelt, M. Johansson*, Fuel*, **2007**, *86*, 1021–1035.
2. A. Abad, T. Mattisson, A. Lyngfelt, M. Ryden*, Fuel,* **2006**, *85*, 1174–1185.
3. L. Shen, J. Wu, J. Xiao, *Combustion and Flame*, **2008***.*
4. A. Rubel, K. Liu, J. Neathery, D. Taulbee, *Fuel*, **2009**, *88*, 876–884.
5. A. Abad, J. Adánez, F. García-Labiano, L.F. de Diego, P. Gayán, J. Celaya, *Chemical Engineering Science,* **2007**, *62*, 533–549.
6. H. Leion, T. Mattisson, A. Lyngfelt, *International Journal of Greenhouse Gas Control*, **2008**, *2,* 180–193.
7. M. Iggland, H. Leion, T. Mattisson, A. Lyngfelt, *Chemical Engineering Science,* **2010**, *65*, 5841–5851.
8. T. Mattison, M. Johansson, A. Lyngfelt, *Fuel*, **2006**, *85*, 736-747.

9. L.S. Fan, “Chemical Looping Systems for Fossil Energy Conversions”, Wiley-AIChE, **2010**, chapter 2.
10. J. Adanez, A. Abad, F. Garcia-Labiano, P. Gayan, L.F. de Diego*, Progress in Energy and Combustion Science*, **2012**, *38*, 215-282.
11. J. Wolf, M. Anheden, J. Yan, *Fuel*, **2005**, *84*, 993-1006.
12. E. De Visser, C. Hendriks, M. Barrio, M.J. Mølnvik, G. De Koeijer, S. Liljemark, Y. Le Gallo, *International Journal of Greenhouse Gas Control*, **2008**, *2*, 478-484.
13. K.S. Kang, C.H. Kim, K.K. Bae, W. Cho, S.H. Kim, C.S. Park, *International Journal of Hydrogen Energy*, **2010**, *35*, 12246-12254.
14. C. Dueso, M. Ortiz, A. Abad, F. García-Labiano, L.F. de Diego, P. Gayán, J. Adánez, *Chemical Engineering Journal*, **2012**, *188*, 142-154.
15. B. Linnhoff, D. Townsend, D. Boland, “*A User Guide to Process Integration for the Efficient Use of Energy*”, IChemE UK, **1982**.
16. J. Varghese, S. Bandyopadhyay, *Chemical Engineering Research Design*, **2012**, *90*, 213-219.
17. C.C. Cormos, *International Journal of Hydrogen Energy*, **2010**, *35*, 7485-7497.
18. C.C. Cormos, *International Journal of Hydrogen Energy*, **2010**, *35*, 2278-2289.

STUDIA UBB CHEMIA, LVII, 2, 2012 (p. 59 - 69)

SPECTROELECTROCHEMICAL STUDIES OF CARBON-BASED SCREEN-PRINTED ELECTRODES MODIFIED WITH POROUS GELS OF ZIRCONIUM, CLAYS AND CALIXARENES

CECILIA CRISTEA[a], NICOLAE BONCIOCAT[b], IULIU O. MARIAN[b,*], ROBERT SĂNDULESCU[a]

ABSTRACT. Electrochemical impedance spectroscopy (EIS) was applied in order to analyze the properties of carbon based screen-printed electrodes modified with clay, Zr porous gel. Parametric equations for Nyquist diagrams applicable in extreme domain of frequencies were used in the case of clay or Zr porous gel modifiers. The equations lead to an analysis of the curves around the frequency of 0.1 Hz. The terms expressing diffusion and charge transfer respectively, were calculated for the proposed electrodes. For comparison Nova 1.6 AUTOLAB soft was used to determining the electrochemical terms involved in Warburg classical circuits.

Keywords: *screen-printed electrodes, electrochemical impedance spectroscopy, clay, zirconium oxide nanoporous gel*

INTRODUCTION

Electrochemical impedance spectroscopy (EIS) is a powerful tool for monitoring the chemical and physical changes of interfacial properties on electrode surface [1]. Nyquist plot of EIS measurements are composed by a semicircle in the high – frequency region associated with resistance and capacitance and a straight line in the low-frequency region associated with the mass transfer [2]. Electrochemical impedance spectroscopy is a sensitive indicator of a wide variety of chemical and physical properties. An increasing trend towards the development of impedimetric biosensors is being currently observed. Impedimetric techniques have been performed to characterize the

[a] "Iuliu Hatieganu" University, Faculty of Pharmacy, Analytical Chemistry Dept., 4 Pasteur St. Cluj-Napoca, Romania
[b] Babeş-Bolyai University, Faculty of Chemistry, Physical Chemistry Dept., 11 Arany Janos St. Cluj-Napoca, Romania, * iomar@chem.ubbcluj.ro

fabrication of the biosensors and to monitor the catalyzed reactions of enzymes or the biomolecular recognition events of specific binding proteins, receptors, nucleic acids, whole cells, antibodies or antibody-related substances [3].

Nowadays there is considerable interest in the development of electroanalytical sensors (i.e., potentiometric, amperometric, electrochemical biosensors) for the detection of a wide range of analytes. Consequently, electrochemical impedance spectroscopy plays an important role in the characterization of many types of sensors. EIS has been used to provide information on various fundamental processes (i.e., adsorption/film formation, rate of charge transfer, ion exchange, diffusion, etc.) that occur at the electrode–electrolyte interface. [4].

Electrochemical impedance spectroscopy results were modeled by appropriate equivalent circuits for the aim of elucidating electrical properties of functionalized carbon-based electrodes [5].

To improve the sensibility and selectivity of the electrodes several modifiers could be used.

In this paper will be presented the electrochemical behavior studied with EIS of the clays and zirconia porous gel (ZPG) modifiers dispersed in thin films deposited on the surfaces of carbon-based screen printed electrodes (SPE). As reported in literature, the use of SPEs is a great simplification in the design and operation of analytical determinations, in accordance with the requirements of a decentralized assay [6-8]. Recently, the SPEs have demonstrated a great interest especially in the development of rapid analytical analysis and biosensor's fabrication.

Among different versions of composite electrodes for pharmaceutical compounds detection (acetaminophen, purine alkaloids etc.) the clay modified electrodes are interesting because they combine the adsorbent properties with ion exchange ability and with the hydration layer. The clays, collected from our geographical area (Valea Chioarului, Romania), were enriched, completely characterized (chemical composition, diffractometry, specific surface, ionic exchange capacity and thermal analysis) and separated by sedimentation, centrifugation and ultracentrifugation in samples with different particle sizes. The surface electrode was modified by adding a thin film of a mixture of polymer polyethyleneimine (PEI) and different amounts of clays. Polyethyleneimine is a linear polymeric cation and kept during several weeks a good permeability. It was used by various authors as entrapment material in the development of biosensors [9] and showed a good rate of electron transfer between the biocomponent and the electrode [10, 11].

The same procedure was used for the fabrication of the screen-printed electrodes modified with PEI and zirconia porous gel (ZPG). The advantage of using zirconium oxide nanoporous gels was exploited in the construction of biosensors due to their biocompatibility [12, 13]. Lately many approaches used zirconia porous gel to immobilize enzyme during polymerization or electro-deposition [14]. According to the literature, zirconium gel or thin film were used to immobilize hemoglobin, DNA, myoglobin and HRP at gold or carbon electrode. Zirconia porous gels were used to entrap the biomolecules due to their biocompatibility. (ZPG) was recently used for the entrapment of hemoglobin and myoglobin and the protein ZrO_2 film preserved their bioactivity and showed a good electrocatalytic behavior towards H_2O_2 reduction. The analytical characteristics of the developed biosensor proved that the nanogel preserved the catalytic activity and a good hydration microenvironment for the enzymes. Due to its lack of toxicity, good conductivity, affinity for groups containing oxygen, the ZrO_2 nanogels became attractive for the construction of biosensors [15]. In order to fully characterize the sensors besides cyclic voltammetry and amperometry, EIS studies were performed.

EIS method was applied in order to analyze the properties of mentioned above modified carbon based screen-printed electrodes. Parametric equations for Nyquist diagrams applicable in extreme domain of frequencies were used. The equations lead to an analysis of the curves around the frequency of 0.1 Hz. The terms expressing diffusion and charge transfer respectively, were calculated for some analyzed modified electrodes.

RESULTS AND DISCUSSIONS

In some previous papers, Bonciocat *et al.* [7, 8] have developed a new approach to the Electrochemical Impedance Spectroscopy (EIS), when only charge transfer and diffusion limitations are present. By using this approach some new results, concerning the parametric equations of Nyquist plots corresponding to redox multielectrodes, have been obtained. Thus in the domain of very small frequencies (around 0.1 Hz) these equations are:

$$\mathrm{Re}(t) = R_{sol} + A + \frac{J_1[\omega(t-\tau)]}{\sqrt{2\pi}} B\omega^{-1/2} \tag{1}$$

$$-\mathrm{Im}(t) = \frac{J_1^2[\omega(t-\tau)] + J_2^2[\omega(t-\tau)]}{2\pi} B^2 C_d + \frac{J_2[\omega(t-\tau)]}{\sqrt{2\pi}} B\omega^{-1/2} \tag{1'}$$

where $Z_{cell} = \mathrm{Re} + j\,\mathrm{Im}$, $\omega = 2\pi\upsilon$ represent the radial frequency of the alternating current, τ the moment of time when the alternating overtension $\tilde{\eta}$ is superimposed over the constant overtension η applied at t = 0, and t is the time when the Nyquist plot recording ends. C_d is the double layer capacity and J_1 and J_2 are the Fresnel integrals.

$$J_1[\omega(t-\tau)] = \int_0^{\omega(t-\tau)} \frac{\cos x}{x^{1/2}} dx \quad \text{respectively} \quad J_2[\omega(t-\tau)] = \int_0^{\omega(t-\tau)} \frac{\sin x}{x^{1/2}} dx \qquad (2)$$

whose values tend to $\sqrt{\pi/2} = 1.253$ for sufficiently great values of the product $\omega(t-\tau)$.

A and B express the charge transfer, respective diffusion limitations of the interface and have the meanings

$$1/A = \sum_i 1/A_i \qquad 1/B = \sum_i 1/B_i \qquad (3)$$

where the terms on the right sides of eqs. (3) refer to the individual electrode reactions occurring simultaneously at the interface.

The EIS allows the estimation of the total quantities A and B, characterizing the multielectrode as a whole, but doesn't permit the estimation of the individual quantities A_i, respective B_i.

If the product $\omega(t-\tau)$ is sufficiently great, we may accept the approximation

$$J_1[\omega(t-\tau)] \cong J_2[\omega(t-\tau)] \cong 1.253$$

even for the smallest radial frequency used, say $\omega_1 = 2\pi\upsilon_1 = 0.628 s^{-1}$.

Of course, the above condition may be fulfilled, because the interval of time $t-\tau$ is at our disposal.

Further, the double layer specific capacity is about 20μF/cm^2, if an indifferent electrolyte is present in excess in the solution. Therefore, the double layer capacity is C_d = 0.2 S, if the electrode surface S is given in m^2. Consequently, the first term on the right side of eq. (1') may be neglected if:

$$B \langle 1/0.2 S\omega^{1/2} \qquad (4)$$

For $\omega_1 = 0.628\, s^{-1}$ and S=12.56.10^{-6} m^2, we get B < 500·10^3 Ωs$^{-½}$, condition that generally, holds true. In these conditions the system of eqs. (1, and 1') becomes:

$$\mathrm{Re}(t) \cong R_{sol} + A + \frac{1}{2} B\omega^{-1/2} \quad (5) \quad \text{and} \quad -\mathrm{Im}(t) \cong \frac{1}{2} B\omega^{-1/2} \quad (5')$$

The latest term on the right side hand of eq. (5) represent the *Warburg diffusion resistance* of the interface

$$R_W(\omega) = \frac{1}{2} B\omega^{-1/2} \tag{6}$$

Both terms *A* and $R_W(\omega)$ are ohmic terms, which don't introduce a phase difference. As for the term $\frac{1}{2} B\omega^{-1/2}$ of eq. (5'), it represents *the capacitive reactance* of the interface

$$X_{C_W}(\omega) = \frac{1}{2} B\omega^{-1/2} \tag{7}$$

As we see, $R_W(\omega) = X_{C_W}(\omega)$ but, in the complex plane, the Warburg diffusion resistance is represented on the real axis, while $X_{C_W}(\omega)$, being negative, is represented downwards on the imaginary axis. The capacitive reactance is due to *the Warburg pseudo-capacitance* of the interface.

$$X_{C_W}(\omega) = \frac{1}{\omega C_W(\omega)} \tag{8}$$

and consequently:

$$R_W(\omega) C_W(\omega) = 1/\omega \tag{9}$$

Finally, writing eqs. (5 and 5') for $\omega = \omega_1 = 0.628 s^{-1}$

$$B = -\mathrm{Im}(\omega_1) \frac{2}{\omega_1^{-1/2}} = 1{,}58.[-\mathrm{Im}(\omega_1)] \; (\ \Omega s^{-1/2}) \tag{10}$$

$$R_{sol} + A = \mathrm{Re}(\omega_1) - [-\mathrm{Im}(\omega_1)] \tag{11}$$

Using a proposed theoretical model based on Volterra equation, charge transfer and diffusion terms were calculated for each modified electrode.

For comparison the electrochemical terms R_{ts}, $R_{s,}$ C_d, and W of classical Warburg circuit was calculated with Nova 1.6 Autolab software.

Electrodes modified with clays thin films

The electrochemical behavior of the home made SPE modified with thin films of clays was tested in the presence of some pharmaceutical compounds as ascorbic acid, acetylsalicylic acid and acetaminophen. Chemical composition studies as well as diffractometry, IR and X ray studies established the properties of several clays originated from the northern part of our country [16]. After some preliminary electrochemical studies it was decided to work with montmorillonite with under 0.2 μm particle dimensions. Thin films of PEI and clay were deposited on the surface of the working electrode in order to change the electrochemical characteristics of it. The electrochemical behavior of the clay modified electrodes was tested in the presence of potassium ferro/ferricyanide (Figure 1) and the charge transfer and diffusion terms are presented in Table 1.

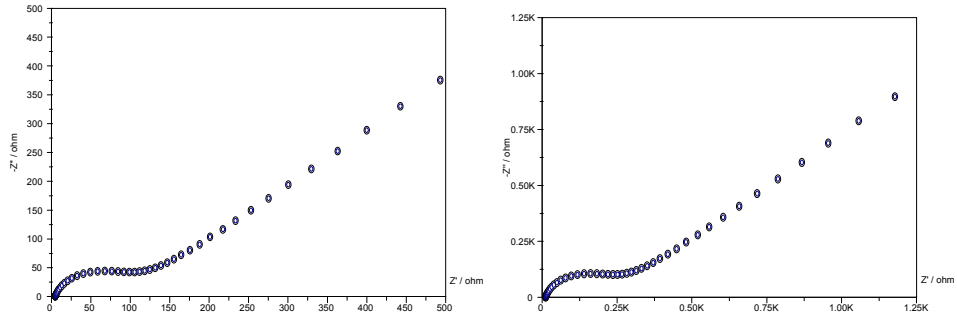

Figure 1. Impedance spectra of $0.5 \cdot 10^{-3}$ M potassium ferro/ferricyanide at unmodified (left) and clay modified SPE (right) in 0.25M KCl

Table 1. Charge transfer and diffusion terms for clay modified electrodes

Type of electrode	$Re(\omega_1)$ (Ω)	$-Im(\omega_1)$ (Ω)	$R_{sol} + A$ (Ω)	B ($\Omega\ s^{-1/2}$)
Unmodified SPE	493	375	118	592.5
Clay modified SPE	1180	897	283	1417.3

The terms R_{sol}+A and B was calculated considering the point situated at 0.1Hz in impedance spectra.

The experimental data was fitted by AUTOLAB soft and the electrical parameters of classical Warburg circuits are presented in Table 2

Table 2. Calculated values with Nova 1.6 Autolab for Warburg circuit

Type of electrode	R_{ts} (Ω)	C_d (μF)	R_{sol} (Ω)	W (Ω^{-1} $s^{1/2}$)	W^{-1} (Ω $s^{-1/2}$)
Unmodified SPE	80.2	5.91	5.2	$2095 \cdot 10^{-2}$	477.3
Clay modified SPE	191.6	2.473	12.42	$877 \cdot 10^{-3}$	1140.2

In Table 2 the term W^{-1} reflect the contribution of Warburg parameters at imaginary part of classical Warburg circuit. The W^{-1} term can be associated to the B term in accepted mathematical model. Without R_{sol}, R_{ts} and C_d terms contributions the differences between the calculated values in last columns in Table 1 and Table 2 are due probably to the proposed model.

However for unmodified SPE the relative error is 19.4% and for clay modified electrode the relative error is 19.5%.

Electrodes modified with ZPG thin films

The advantage of using zirconium oxide nanoporous gels was exploited in the construction of biosensors due to their biocompatibility [11]. Before developing the biosensors the characteristics of the new modified electrodes with thin films of PEI and ZPG were tested on the presence of a redox probe.

The electrochemical behavior of the ZPG modified electrodes was tested in the presence of potassium ferro/ferricyanide (Figure 2) and the charge transfer and diffusion terms are presented in Table 3.

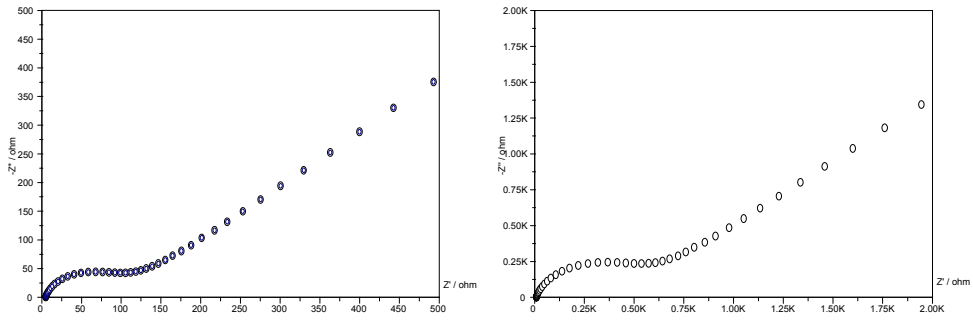

Figure 2. Impedance spectra of $0.5 \cdot 10^{-3}$ M potassium ferro/ferricyanide at unmodified SPE (left) and ZPG modified SPE (right) in 0.25 M KCl

Table 3. Charge transfer and diffusion terms for ZPG modified electrodes

Type of electrode	Re(ω1) (Ω)	-Im(ω1) (Ω)	Rsol + A (Ω)	B (Ω $s^{-1/2}$)
unmodified SPE	493	375	118	592.5
ZPG modified SPE	1943	1340	603	2117.2

The terms R_{sol}+A and B was calculated considering the point situated at the 0.1Hz in impedance spectra.

The experimental data was fited by AUTOLAB soft and the electrical parameters of classical Warburg circuits are presented in Table 4

Table 4. Values calculated with Nova 1.6 Autolab soft for Warburg circuit

Type of electrode	R_{ts} (Ω)	C_d (μF)	R_{sol} (Ω)	W (Ω^{-1} $s^{1/2}$)	W^{-1} (Ω $s^{-1/2}$)
Unmodified SPE	80.2	5.91	5.2	$2905 \cdot 10^{-6}$	477.3
ZPG modified SPE	400	2.634	9.38	$559 \cdot 10^{-6}$	1788.9

Like in the previous experiment by comparing the last columns of Table 3 and Table 4 the calculated relative error in the case of ZPG modified SPE is 15.4%.

On the other hand the modified SPE have another C_d because of thin film modifiers added on the surface of working electrode.

The modeling with parametric equations was in agreement with the results obtained by Nova 1.6 Autolab software, both for clay modified and ZPG modified SPEs.

EXPERIMENTAL

Thin films of polymer (polyethyleneimine) with various additives (clays, zirconia porous gel) were deposited on the surface of the carbon based screen-printed electrodes (SPE).

The graphite based SPEs (composed by graphite working electrode and graphite counter electrode and a silver pseudo-reference electrode obtained

by the screen-printed technique on an insulated plate) were purchased from Dropsens, Spain [11,15].

The clays, collected from our geographical area (Valea Chioarului, Romania), were enriched and completely characterized (chemical composition, diffractometry, specific surface, ionic exchange capacity and thermal analysis) and separated by sedimentation, centrifugation and ultracentrifugation of the different particle sizes [17].

The modified electrodes were prepared by mixing 5 mg polyethyleneimine (PEI) in125 μL dry ethanol and 120 μL distillate water with 6,5 μL (50 mg/mL) hydrated clays of 0.2 μm fraction.

A similar procedure was used for the fabrication of the SPE modified electrodes with PEI and ZPG.

The zirconia alcogel was prepared according to the literature [12]. The zirconia alcogel has been prepared, starting from 0.25M zirconium salt ($ZrO(NO_3)_2.xH_2O$) alcoholic solution by refluxing for 2 h at 90ºC then allowed to cool at room temperature. 5mg PEI with 125μl ethanol and 120μl distillated water were mixed for 15 min with vortex. 6.5μl porous gel were added and mixed another 15 min with vortex. Polyethyleneimine (MW 60000) from Aldrich was used without purification.

All the experiments were performed in the presence of electrolyte solutions (0.25M KCl, $0.5 \cdot 10^{-3}$ M potassium ferro/ferricyanide). The chemicals were provided by Sigma-Aldrich or Merck and they were of analytical grade. The electrochemical analysis was performed with AUTOLAB potentiostat PGSTAT 30 and FRA 2 module (frequency domain 0,1Hz to 100 kHz) by using unmodified and modified graphite screen-printed electrode as electrochemical cell. All impedance spectra were normalized to the surface area of working electrode. The working temperature was room temperature (25ºC).

CONCLUSIONS

Screen-printed electrodes modified with various compounds (clays and zirconia porous gel) included in a conductive polymer and directly deposited on the electrode surface were investigated. Two ways of investigations were proposed for clay or ZPG modified SPEs: parametric equations modeling and Nova 1.6 Autolab software.

By comparing the contribution of Warburg terms calculated in theoretical model proposed with contribution of Warburg terms calculated by Autolab soft for the same classical Warburg circuit reasonable relative errors results.

ACKNOWLEDGEMENTS

The financial supports of PN II IDEI 338/2011 grant program and UMF (young researchers grant) 27020/3/15.11.2011 is appreciated.

REFERENCES

1. S.M. Park, J.S. Yoo, *Anal. Chem.,* **2003**, *75*, 455A-461A;

2. J.Li, L. Xu, H. Huang, J. Zhou, E.S. Abdel-Halimb, J.R. Zhang, J.J. Zhu, *Talanta*, **2011**, *85*, 2113-2120;

3. J.G. Guana, Y.Q. Miao, Q.J. Zhanga, *Journal of Bioscience and Bioengineering,* **2004**, *97(4),* 219-226;

4. B. Pejcic, R. De Marco, *Electrochimica Acta*, **2006**, *51(18),* 6217-6229;

5. H. Saklya, R. Mlika, I. Bonnamour, F. Aouni, H. Ben Ouada, N. Jaffrezic Renault, *Electrochimica Acta*, **2007**, *52(11)*, 3697-3703;

6. J. Wang, *Analyst*, **1994**, *119,* 763-766;

7. N. Bonciocat, *Studia UBB Chemia*, **2008**, *LIII*, 31-42;

8. I.O. Marian, N. Bonciocat, C. Cristea, R. Săndulescu, M. Bucșa, M. Vlassa, *Electroanalysis,* **2010**, *22(5),* 542-548;

9. M.D. Rubianes, G.A. Rivas, *Eletrochem. Commun.* **2007**, *9*, 480-484;

10. E. Lojou, P. Bianco*, Electrochim. Acta*, **2007**, *52*, 7307-7314;

11. S. Laschi, E. Bulukin, I. Palchetti, C. Cristea, M. Mascini, *ITBM-RBM*, **2008**, *29*, 202-207;

12. S.Q. Liu, J.J. Xu, H.Y. Chen, *Colloid Surf. B*, **2004**, *36*, 155-159;

13. S.Q. Liu, J.J. Xu, H.Y. Chen, *Bioelectrochemistry,* **2002**, *57*, 149-154;

14. V. Sima, C. Cristea, F. Lăpăduș, I.O. Marian, A. Marian, R. Săndulescu, *J. Pharm. Biomed. Analysis*, **2008**, *48*, 1195-1200;

15. V. Sima, C. Cristea, E. Bodoki, G. Duţu, R. Săndulescu, *Central European Journal of Chemistry*, **2010**, *8(5),* 1034-1040;

16. A. Marian, I.O. Marian, C. Cristea, R. Săndulescu, Gh. Vasilie, *Studia UBB Ambientum*, **2009**, *LIV*, 81-90;

17. A. Maghear, C. Cristea, A. Marian, I.O. Marian, R. Săndulescu, *Clays and clay minerals,* **2012**, submitted.

STUDIA UBB CHEMIA, LVII, 2, 2012 (p. 71 - 81)

DETERMINATION OF CALCIUM, MAGNESIUM AND POLYPHENOLS IN HAWTHORN FRUITS FROM VULCAN COAL DUMP

ANDREEA BRAŞOVAN[a], RAMONA CÂMPEAN[b], VASILICA MÂNDROC[c], VLAD CODREA[a], NELI OLAH[d,*]

ABSTRACT. The study refers to the content determination of calcium, magnesium and polyphenols in hawthorn fruits collected from Vulcan coal dump. This dump was never covered by fertile soil or fertilizer containing nitrogen, potassium and phosphorus. The hawthorn fruits obtained from dump contains significantly high concentration of calcium and magnesium, compared with the already published data. The polyphenols were evaluated by spectral (UV-Vis spectrophotometry) and chromatographic (TLC and HPLC) methods. The total flavonoids and total polyphenols contents of dump fruits are similar with those obtained in fruits collected from hawthorn culture, being lower than the already published data. In both type of hawthorn fruits could be identified the hyperoside, as the main flavonoid. We found also rutoside, only in traces, in the culture sample.

Keywords: *coal dump, hawthorn fruits, calcium, magnesium, polyphenols.*

INTRODUCTION

Hawthorn (*Crataegus monogyna*) is appearing as a shrub or small tree widespread in Europe, Asia and North Africa. In our country it can be found in lowland and mountain forestry, on the border of meadows and crops and nearby coal dumps, sometimes grown for ornamental purpose. It belongs to the Rosaceae family. It is a shrub with spiny branches and can be identified by the following: ligneous, dark brown branches, having diameters of 1 to 2.5 mm; ovate leaves with pinnate or lobate limb, with a stem up to 2 cm and numerous small, white flowers, disposed in corymb. The flowers have a green-brown tubular calyx consisting in 5 free triangular sepals, a corolla composed of 5 white or yellowish-brown free petals, 15-20 stamens and a monocarpellary

[a] Babeş-Bolyai University, 1, Kogălniceanu Str., 400084, Cluj-Napoca, Romania
[b] Babeş-Bolyai University, 30, Fântânele Str., 400294, Cluj-Napoca, Romania
[c] Liviu Rebreanu Highschool, Tineretului Str., Turda, Romania
[d] "Vasile Goldis" West University of Arad, Faculty of Pharmacy, Department of Pharmaceutical Industry, 1 Feleacului Str., 300041, Arad, Romania and SC PlantExtrakt SRL, 407059 Rădaia, Romania; * olahdr@aol.com

ovary. The fruit is obovat or globular, with an overall length of 6-10 mm and 4-8 mm wide, red-brown or dark red colored. It has a single oblong brown seed, smooth and glossy. The fruit is a drupe [1-5].

In the last 40 years, hawthorn has become one of the most studied medicinal herbs. Researchers have discovered several active substances in flowers, leaves and fruits. The plant contains triterpens like crategic acid, ursolic acid; flavonoids; purinic bases; phytosterols; volatile oil, tannins, pectin, vitamin C. Flowers and leaves are rich in flavonoids, tannins, triterpene acids and essential oil. The bark contains aesculin, a glycoside from the coumarins group. The fruits are rich in amines, vitamin C, antocyanosides and other polyphenols, carotenoids, sorbitol, glucose and sucrose. These active ingredients are useful in treating cardiovascular diseases and sometimes can substitute the valerian [6-11].

Researches carried out by M. Nicolov have revealed the presence of 17 flavonoidic compounds in hawthorn. The presence of vitamin B and C, carotenoids, sorbitol, glucose, sucrose, chlorogenic and caffeic acid was demonstrated by Cekolinskaia. In order to demonstrate the pharmacological action of the chemical compounds of hawthorn, many experiments on dogs, rats and rabbits had been made. Hawthorn is used in various forms, entering in the soothing tea composition, the anti-asthma and hypertension tea also [6].

As hawthorn is rich in calcium and magnesium, it is recommended in nourishment and heart or brain treatment. The hawthorn preparations are recommended in heart degenerations and coronary sclerosis in the elderly, to treat a heart hypertonia, in myocardial insufficiency after infectious diseases and cardiac arrhythmias. It cause dilatation of blood vessels, in particular coronary blood vessels, reduced peripheral resistance and increased coronary circulation. The blood flow increases, the oxygen consumption is increased too, even efficiency in using oxygen is improved. It acts to eliminate extrasystole of any genesis and to remove any accesses of paroxysmal tachycardia. Crataegus has positive intropic, dromotropic and chronotropic effects, and negative bathmotropic effects. The cardiotropic effect of Crataegus is due by the increased membrane permeability for calcium as well as the inhibition of phosphodiesterase with an increase of intracellular c-AMP concentrations. Inhibitory effects on the sodium/potassium ATPase in vitro were most pronounced with application of Crataegus procyandidins, followed by Crataegus flavonoids, and least with Crataegus extracts [12-20].

The purpose of this paper is to determin the calcium and magnesium content respectively the polyphenols content in the Crataegus (hawthorn) fruits harvested from a sterile dump in comparison with the fruits collected from culture.

RESULTS AND DISCUSSION

The first step of the study was to determine the soil composition. In order to find out the responsible ions for hawthorn growth, was performed an elemental XRF analysis, which results are in Table 1.

Table 1. XRF elemental analysis results

Element	Si^{4+}	Al^{3+}	K^{+}	Ca^{2+}	Mg^{2+}
wt. %	46.9	20.6	5.08	6.09	1.03

The petrology of the coal dumps refers to clay, marl, shale and clay sandstone. After investigations by X-ray diffraction it could be demonstrated that the dump etiantrosoil is rich in quartz, calcite, feldspar and biotite. The coal dump was never covered by a soil layer, therefore the hawthorn was spread directly on the sterile.

The results presented in Table 1 show that the silicium ions are the most representative ions from soil. These ions are present in all soil types [21-23]. Aluminium and potassium are in the composition of the potassium feldspar and biotite. The latter contains magnesium, which can be released into the soil through alteration of the black mica in the presence of water. Calcium is present in calcite and is released into the soil also by chemical altering.

The main chemical elements necessary for the development of hawthorn are provided in the content within soil minerals. Some minerals could be chemical inactive or on the opposite, could be active in presence of water. Quartz is the main mineral found into the soil sample. Quartz have a hexagonal crystallization and assure a very compact and resistant structure, without cleavage. Featured properties of quartz particles prove that it is chemically inert acting as a neutral component.

Calcite is a typical mineral for sedimentary soils [24,25]. Calcite particles are influenced by water, which could release Ca^{2+} ions in aqueous solution, similarly to the process involved in cave formations. Hawthorn roots could easily assimilate Ca^{2+} ions from dump soil in presence of relative humidity due to larger amount of calcite particles founded there.

The biotite structure features hexagonal crystal planes of SiO_2 tetrahedra (which have a very high mechanical strength) bonded in multi – layers by Mg^{2+}, Al^{3+}, and K^{+} ions which trapped free valences of SiO_2 tetrahedra. The mechanical strength is weaker between the layers than inside of them, the inter–layer distance allows water to penetrate inside of biotite crystal and consequently to release some of the bonding ions. The released ions amount is favored by the presence of small micro – scaled particles [21-23]. The biotite is enough to release a significant amount of Mg^{2+} ions in the presence of water; similar, the amount of potassium feldspar represents an important source of K^{+} ions.

A fertile soil rich in humus can stabilize oligoelements such Ca and Mg as humic acid salts insoluble in water. Furthermore this colloidal suspension is absorbed by plants roots due to the cellular osmotic pressure [9, 10]. The dump soil is characterized by an acute lack of organic material and humus due to the pedogenesis. Furthermore the available minerals are released from parent minerals directly into the water present in dump soil. The hawthorn absorbs this mineralized water in the feeding circuit. There appear a strong interconnection between the Ca and Mg content in the soil samples and the amount in hawthorn.

The results of XRF elemental analysis are in fair agreement with the minerals identified in soil with XRD observation. All identified ions belong to these minerals. In this particular case we could calculate the Ca and Mg amount per solid soil sample as follows:

$$\begin{cases} Ca_{sol} = 6.09 \ \ gr/100gr\ sol \\ Mg_{sol} = 1.03 \ \ gr/100gr\ sol \end{cases} \tag{1}$$

This allows further to calculate the hawthorn fruit extraction coefficient, R, of Ca and Mg according to the relations (2) and (3):

$$R_{Ca} = \frac{Ca_{soil} - Ca_{brier}}{Ca_{soil}} \cdot 100 \ [\%] \tag{2}$$

$$R_{Mg} = \frac{Mg_{soil} - Mg_{brier}}{Mg_{soil}} \cdot 100 \ [\%] \tag{3}$$

The calcium content was determined based on the following calibration curve: A = 0.011 x C_{Ca} – 0.0004. The calcium content of hawthorn fruits collected from the Vulcan coal dump are ranging between 0.5204 and 0.5358, the average being 0.5258 g Ca/100g solid sample. Reference values are within 0.3046 and 0.4141 g Ca/100g solid sample.

The magnesium content was determined based on the following calibration curve: A = 0.573 x C_{Mg} – 0.0001. The magnesium content vary between 0.3421 and 0.3622, and the average is 0.3555 g Mg/100g solid sample. The reference value for the magnesium content ranges between 0.1502 and 0.1565 g solid sample mg/100g.

Finally results that the Ca extraction coefficient is 91% and Mg extraction coefficient is 65% for the hawthorn fruits growth on the dump soil. The calcite content is significantly increased, compared to biotite. The lesser amount of biotite conducts to an enhanced extraction coefficient for Mg. This proves that dump soil is able to assure an optimal amount of Ca and Mg for the hawthorn fruits situated far over the standard range. The lack of heavy

metals in the dump area is a favorable assumption for human use of hawthorn. This is a sufficient condition for a random and wild crop, suitable only for home application (brier marmalade, depurative and refreshing tea etc.).

The polyphenols were investigated by TLC (Figure1). The compounds separated from samples – hawthorn fruit extracts from coal dump respectively from culture were compared with the used standards: rutoside, hyperoside, chlorogenic acid and caffeic acid. In the used visualization condition the flavonoids show yellow to orange bands and the other polyphenols have blue to bluish-green bands.

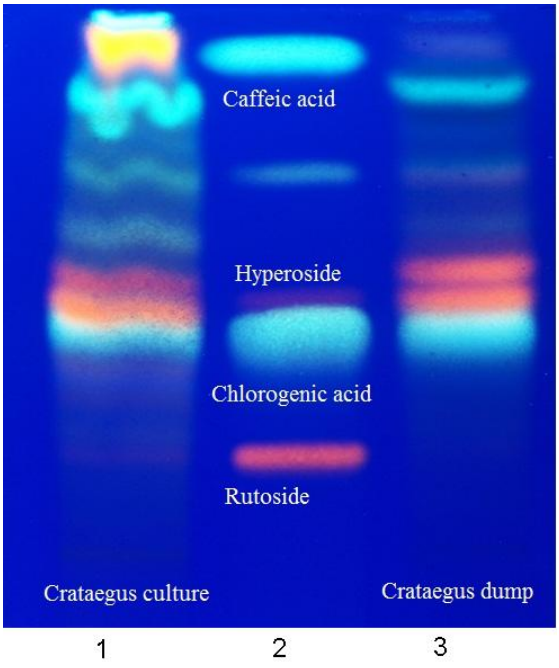

Figure 1. Polyphenols TLC chromatogram

The sample from culture contains trace of rutoside, that can not be identified in the coal dump sample. In both samples were identified based on the shape, position and color of bands the chlorogenic acid and the hyperoside. From TLC chromatogram can be observed that the culture sample is more rich in flavonoids that the coal dump sample, due by the presents of more blue, bluish-green and yellow-orange bands.

The quantitative determination of flavonoids (Table 2) is determined by calculating the content of total flavonoids expressed in rutoside in dry product, which according to Petricici and Servis must be between 1.1 – 2.28 % [25] and after laboratory investigations we obtained a total flavonoids content expressed

in rutoside of 0.31 mg % in the sterile dump sample and 0.38 mg % in the culture sample. The quantitative determination of polyphenols shown in Table 2, is determined by calculating the polyphenols content expressed in caffeic acid. For example, Tadić et al. have obtained 3.54 % polyphenols in hawthorn fruits [20], and after laboratory investigations, we obtained a content of total polyphenols expressed in caffeic acid of 0.22 mg % in the sterile dump sample and 0.23 mg % in the culture sample. The calculation of total flavonoids respectively polyphenols content were performed using the following calibration curves:

- Total flavonoids expressed in rutoside:
  - $A = 31.77 \times C_{rutoside} + 0.002$
- Polyphenols expressed in caffeic acid:
  - $A = 4.092 \times C_{caffeic\ acid} + 0.119$

Table 2. Total flavonoids content expressed in rutoside and polyphenols content expressed in caffeic acid

The determinations	Sterile dump	Culture	Reference value
Total flavonoids content, expressed in rutoside [mg%]	0.31	0.38	1.1 – 2.28
Polyphenols content, expressed in caffeic acid [mg%]	0.22	0.23	3.54

In Figure 2 are presented the HPLC chromatograms.

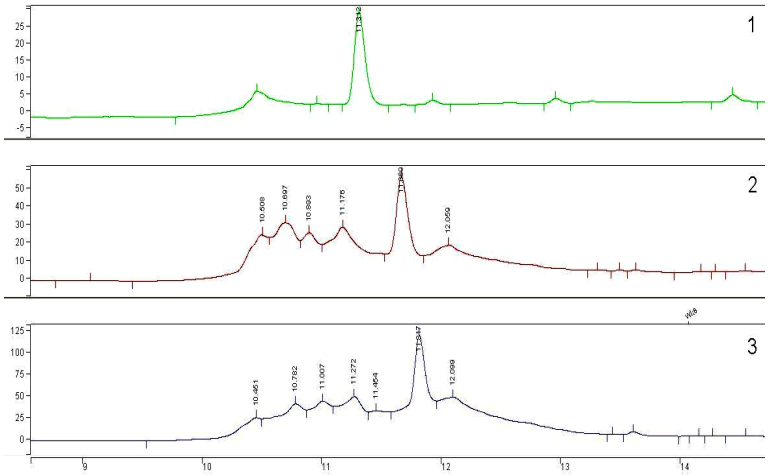

Figure 2. HPLC chromatogram of hyperoside (1) and Crataegus fruits from culture (2) and from sterile dump (3)

In Figure 3 is highlight the UV-Vis spectrum obtained during the HPLC analysis for: a) standard hyperoside; b) hyperoside from culture sample and c) hyperoside from sterile dump sample.

Comparing the HPLC chromatograms (the same retention time) and the obtained UV-Vis spectra (the same allure and absorbtion maximum) presented above we can conclude that both Crataegus fruits samples contains hyperoside.

Other therapeutically important polyphenols from hawthorn fruits are the procyanidines that were determined by calculating the content of procyanidine expressed in cyanidine chloride, according to European Pharmacopoeia and must be at least 1% [1]. According to our laboratory investigations was obtained a content of procyanidine of 0.98% for both samples, less than the prevision of Pharmacopoeia.

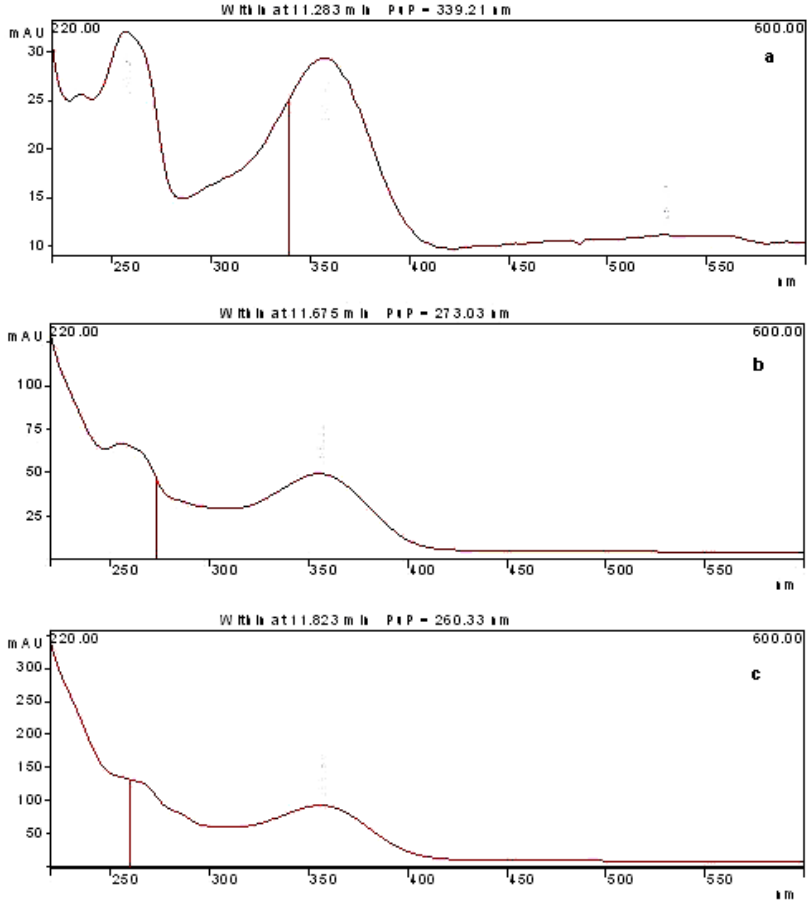

Figure 3. Hyperoside UV-Vis spectra – standard (a) and Crataegus samples (b – culture sample, c – dump sample)

Comparing the obtained results with those already published we can conclude that the calcium and magnesium contents of the dump hawthorn fruits contain 20% more calcium than those obtained by Boudraa et al. [26] and about 50% more calcium and twice more magnesium than those determined by Ozcan [11].

The results for total flavonoids obtained for the culture and dump sample are similar, but much lower than the reference data values. In case of polyphenols we obtained also similar values between the two samples and again, much lower than the reference value. Probably the content in polyphenols and flavonoids of the hawthorn fruits are influenced not just by the soil type, but also by the humidity during a year and the geographical position of the growing area. The culture and the sterile dump being situated in proximity the climatic influence was similar in both areas. This can be the explanation of the similar values obtained for total flavonoids and polyphenols content.

CONCLUSIONS

We can conclude that the hawthorn (Crataegus) fruits obtained from the culture and from the dump are similar, both containing smaller amounts of flavonoids and polyphenols, than the already published data. From the class of flavonoids can be identify the hyperoside in both samples, but the rutoside is present just in trace in culture sample. The calcium and the magnesium concentration are higher than usual in the dump sample, being more proper to be used in nourishment and heart or brain treatments. Based on these studies can be conclude that a soil more rich in calcium and magnesium minerals should be more proper for culture of hawthorn to obtain fruits more rich in these therapeutically important ions.

EXPERIMENTAL SECTION

Vegetal materials

The hawthorn fruits from the sterile dump were collected in the first half of September from the Vulcan coal dump (Petroşani Basin, Hunedoara County, Romania) and they were preserved according to the standard procedures SR 1631-1:2003.

The hawthorn fruits from the culture were collected in September.

The soil from sterile dump was collected in the same time with the fruits.

The soil analysis

The samples were dried at 80 ºC for 12 h, powdered (325 mesh) and mixed with boric acid in a 1:4 ratio (100 mg of sample and 400 mg of H_3BO_4). The mixture was pressed at 203 MPa for 10 minutes, obtaining 2,5 cm diameter pellets of 100 mg/cm^2 surface density.

The elemental soil analysis was performed according to the standard sampling and operating procedures using a S_4 Pioneer X-ray fluorescence spectrophotometer (XRF) in order to measure the main elements from beryllium to uranium. The results were expressed in percentage from soil.

The results are read with Spectra Plus software and the determination of elements is done using Dyna Match international database. Measurements were made according to EN ISO 9001:2000.

Three replicates were made for each sample.

The determination of calcium and magnesium

The vegetal material sample was mineralized using a Berghof microwave MWS_2 oven. The dry mineralization was achieved in three stages: first stage (T_1) at 145°C, for 10 minutes, the second stage (T_2) at 160°C, for 10 minutes and the third stage (T_3) at 190°C, for 20 minutes, using 80% of power. After mineralization the white ash was treated with 1% HNO_3 and diluted to 10 ml with deionized water. The obtained solution was used for the determinations of calcium and magnesium in the hawthorn fruit.

In order to establish the content of calcium and magnesium in the hawthorn fruits it was used atomic absorption spectrometry, AAS. It was used a Shimadzu atomic absorption spectrometer, AA 6300. The determinations were carried out according to EN 1134: 1994 respectively ISO 5725:1998, ISO 3696: 1987, ISO 3696: 1995. The AAS spectrophotometer uses calcium lamp, at 10 mA respectively a magnesium lamp, at 8 mA.

The determination of calcium was performed at 422.7 nm, using background compensation with deuterium lamp. The calibration curve was made between 0 - 2.5 ppm.

The determination of magnesium was performed at 285.2 nm, using background compensation with deuterium lamp. The calibration curve was made between 0 - 0.5 ppm.

Three replicates were made for each sample.

The TLC determination of polyphenols

The flavonoides and other polyphenols were determined by thin layer chromatography using a silica chromatographic plate with fluorescence indicator at 254 nm. The mobile phase was formic acid (Merck) – water – ethyl-methyl-cetone (Merck) - ethyl acetate (Merck), in proportion of 10:10:30:50 v/v.

The used standards were chlorogenic acid, hyperoside, caffeic acid and rutoside, each having 1 mg/mL in methanol. It was applied 30 µL from the samples and 10 µL from each standard.

After drying, the plate was sprayed with diphenyboriloxiethylamine (10 g/L) in methanol and then with polyethylenglycol 400 (50 mL/L) in ethanol. After 30 minutes the chromathogram was observed in fluorescence at 365 nm [27].

The HPLC determination of hyperoside

The determination was carried out by high performance liquid chromatography using a Varian Star HPLC system.

As standard was used hyperoside, 0.1 mg/mL in methanol.

The analysis conditions were: silica C18 column (Phenomenex, Luna C18, 150 x 4.6 mm, 5 μm); like mobile phase was used a binary gradient prepared from 0.1% (v/v) trifluoracetic acid (Merck) in water and acetonitril (Merck). The elution started with a linear gradient, beginning with isocratic elution followed for the next 15 minutes with 95 % trifluoracetic acid, then for 5 minutes with 5 % trifluoracetic acid and at the end for the 10 minutes with 95 % trifluoracetic acid. The flow rate was 1 mL/min. The DAD detector was operated at 270 nm and the injection volume was 10 μL.

The spectral determination of polyphenols

The polyphenols were determined using phosphotungstenic reagent, at 715 nm, according to Romanian Pharmacopoeia [28]. As standard was used the caffeic acid, 1 mg/mL in methanol. There was build a calibration curve from 0.002 to 0.013 mg/ml range.

The total flavonoids were determined using aluminium chloride 2.5 %, at 430 nm, according to Romanian Pharmacopoeia [28]. As standard was used the rutoside, 0.1 mg/ml in methanol. There was build a calibration curve from 0.004 to 0.016 mg/ml range.

The procyanidines were determined according to European Pharmacopoeia, using extraction in buthanol, at 545 nm. The results were expressed in cyanidine chloride [1].

REFERENCES

1. ***, “European Pharmacopoeia”, Ed. VII, Medpharm Scientific Publisher, Stuttgart, **2011**.
2. I. Hodişan, I. Pop, „Botanică sistematică”, Editura Didactică şi Pedagogică, Bucharest, **1976**, 324.
3. I. Pop, I. Hodisan, D. Mitotelu, L. Lungu, I. Cristurean, G. Mihai, “Botanică sistematică”, Didactică şi Pedagogică Press, Bucharest, **1983**, 301-306.
4. G. Racz, A. Racz, E. Cociu, “Plante medicinale şi aromatice”, Ceres Publishing House, Bucharest, **1970**, 172-174.
5. N. Ştefan, A. Oprea, „Botanică sistematică”, Alexandru Ioan Cuza University Press, Iaşi, **2007**, 552.

6. I. Ciulei, E. Grigorescu, U. Stănescu, „Plante medicinale, fitochimie şi fitoterapie – Tratat de farmacogzonie", Vol. I, Editura Medicală, Bucharest, **1993**, 452-458.
7. C. Pârvu, "Universul plantelor – Mică enciclopedie", Enciclopedică Press, Bucharest, **1997**, 471-472.
8. C.Pârvu, "Enciclopedia plantelor, Plante din flora României", Vol 3, Tehnică Press, Bucharest, **2004**, 678-681.
9. A. Radu, "Botanică farmaceutică", Didactică and Pedagogică Press, Bucharest, **1974**, 404-405.
10. I. Ciulei, L. Sommer, V. Istudor, „Farmacognozie", vol. I, IMF Press, Bucharest, **1979**.
11. M. Ozcan, H. Haciseferogullari, T. Maracoglu, D. Aslan, *Journal of Food Engineering*, **2005**, *68(4)*, 409-413.
12. G. Mohan, "Plante medicinale fitoterapie", All Publishing House, Bucharest, **1998**, 235-236.
13. G. Siegel, U. Gasper, F. Schnalke et al., *Phytother Res*, **1996**, *10*, S195-S198.
14. Anon, *Altern Med Rev*, **1998**, *3(2),* 138-139.
15. M. Schussler, J. Holzl, U. Fricke, *Arzneimittelforschung,* **1995**, *45(8),* 842-845.
16. M. Schussler et al., *Planta Med*, **1993**, *59(7)*, 88.
17. C. Mang, V. Herrmann, R. Butzer et al., *Eur J Clin Pharmacol*, **1997**, *52*, A59.
18. V.H.P.T. Ammon, R. Kaul, *Dtsch Apoth Z*, **1994**, *26*, 33-36, *27*, 21-35, *28,* 35-42.
19. G. Rohr, G. Meier, *Dtsch Apoth Z*, **1997**, *137(42),*104-116.
20. V.M. Tadić, S. Dobrić, G.M. Marković, S.M. Dordević, I.A. Arsić, N.R. Menković, T. Stević, *J Agric Food Chem*, **2008**, *56(17)*, 7700-9.
21. A. Brasovan, V. Codrea, V. Mândroc, R. Campean, N. Olah, *Analele Universitatii din Oradea, Fascicula Biologie*, **2009**, *XVI/2*, 40-42.
22. A. Brasovan, R.F. Campean, G. Arghir, V. Codrea, *Metalurgia International*, **2010**, *XV(7)*, 40-43.
23. A. Braşovan, V. Mândroc, R. Câmpean, I. Petean, V. Codrea, G. Arghir, *Analele Universităţii din Oradea, Fascicula Biologie*, **2011**, *XVIII/1*, 5-9.
24. M. Surpăţeanu, „Elemente de chimia mediului", Matrix Rom Press, Bucharest, **2004**, 176-215.
25. I. Petricici, L. Servis, *Acta Pharm. Jugosl.*, **1997**, *27*, 75.
26. S. Boudraa, L. Hambaba, S. Zidani, H. Boudraa, *Fruits Journal*, **2010**, *65 (2)*, 75-84.
27. ***, "Homoopathisches Arzneibuch", Deutscher Apotheker Verlag, Stuttgart, **2011**.
28. ***, "Farmacopeea Română", Ed. X, Editura Medicală, Bucharest, **1993**.

STUDIA UBB CHEMIA, LVII, 2, 2012 (p. 83 - 93)

COMPARATIVE STUDY OF DIFFERENT TLC-IMAGE ANALYSIS METHODS FOR QUANTITATIVE EVALUATION OF PARABENS IN PHARMACEUTICAL SUSPENSIONS

IOANA ANAMARIA TUHUŢIU[a], DORINA CASONI[a,*], COSTEL SÂRBU[a]

ABSTRACT. A high-performance thin-layer chromatographic method combined with a sample preparation procedure and digital images processing has been developed for simultaneous determination of parabens in pharmaceutical suspensions. For the quantitative evaluation of the chromatographic spots, three different software that combines 2D (ImageDecipher-TLC and Sorbfil TLC) and respectively 3D (JustTLC) image analysis were investigated. The statistical parameters of the linear relation between the applied concentrations and both the peaks area and volume respectively, revealed no statistical significant differences in terms of the regression determination coefficient (R^2). The lowest limits of detection and quantification values were obtained for ethylparaben and butylparaben using the ImageDecipher-TLC software. Also, by using ImageDecipher-TLC software with conversion of color images of chromatographic plates into grey scale, the precision of the developed method increased in all cases. The results obtained for commercial samples showed that the proposed method, using new UV-Vis TLC scanner device with ImageDecipher-TLC software, is suitable for rapid routine analysis of parabens in pharmaceutical suspensions.

Keywords: *quantitative evaluation, parabens, HPTLC, digital processing of images, method validation*

INTRODUCTION

The esters of para-hydroxybenzoic acid are called parabens and they are a class of chemicals widely used as preservatives in the cosmetic, pharmaceutical and food industries. Common parabens include methylparaben, ethylparaben, propylparaben and butylparaben, and less common parabens include isobutylparaben, isopropylparaben and benzylparaben. Parabens are effective preservatives in many types of formulas, being used primarily for their antibacterial and antifungal properties, against molds and yeast. Their efficacy as preservatives, in combination with the long history of their use, their low cost, broad spectrum of activity, inertness, worldwide regulatory

[a] Babeş-Bolyai University, Faculty of Chemistry and Chemical Engineering, Arany Janos Str. No 11, RO-400028 Cluj-Napoca, România, * casoni_dorina@yahoo.com

acceptance, biodegradability, and their excellent chemical stability in relation to pH and temperature [1], probably explains why parabens are so commonplace. However, they are becoming increasingly controversial, because they have been found in extremely low concentrations in breast cancer tumors [2]. Parabens have also displayed the ability to weakly mimic estrogen [2], however, no causal link between parabens and cancer has been established [3]. The most frequently used parabens in pharmaceutical products are methylparaben and propylparaben. Generally the first one is preferred because as the chain length of the ester group of the parabens increases, antimicrobial activity increases, but water solubility decreases [4]. Usually, the microbial replication occurs in the water phase and hence, the amount of paraben dissolved in the water phase determines the preservative ability [1].

Several methods such as gas chromatography (GC) [5, 6], high performance liquid chromatography (HPLC) [7–10], high performance thin-layer chromatography (HPTLC) [11, 12], micellar electrokinetic capillary chromatography [13, 14] and electrophoretic methods [15, 16] are presented in literature for the determination of parabens in pharmaceutical products. Among them, HPTLC is a widely accepted technique for its high accuracy, precision, reproducibility of results in addition to its low per sample operating cost, easy sample preparation, and short analysis time. The quantitative determination in HPTLC is usually performed in two ways: by slit-scanning or charge coupled (CCD) cameras devices. Standard slit-scanning densitometry measures the absorbance or fluorescence of the chosen tracks on the chromatogram. The main disadvantage of this method is unfavorable error propagation and low spatial resolution since slit-scanning operates by observing a small portion of light emanating from the chromatographic surface defined by the scanning slit [17, 18]. The CCD camera evaluates the TLC plates in several different modes like transmission [18, 19], reflectance [19] or fluorescence, and it has the advantage that the evaluation time is shorter than in slit-scanning densitometry [19]. Also, the comparison between CCD cameras and densitometry, presented in the literature, showed that the CCD cameras offer higher linear concentration ranges than densitometers [19]. In addition, new systems based on digital processing of images of chromatographic plates were recently reported in literature as important TLC methods for quantitative determination of various classes of compounds [20-23].

Therefore the aim of this work was to develop a simple, fast, precise, accurate and sensitive HPTLC method, in fluorescence quenching mode, for the quantitative determination of parabens in pharmaceuticals, using a UV scanner equipped with a CCD camera and specialized software for digital processing of images.

RESULTS AND DISCUSSIONS

Image analysis and chromatograms processing

The new UV scanner device for TLC analysis was used in this study for a quantitative evaluation of chromatographic plates. This device can detect visible and also weak fluorescent spots under UV light at 254nm or 365nm. The scanner captures the visible fluorescence or reflected light using a Charge Coupled Device (CCD) that turns the light into a proportionally electrical signal. Further the electric signal is transformed into digital information and the computer shows the information in an image. The brightness or grey degree is proportional with the concentration of the substance on the TLC plate. A good separation of compounds and a good scanning resolution of the chromatographic plate are very important for an accurate quantitative evaluation. The chosen HPTLC conditions have yielded to a good separation of the investigated parabens ($R_{F(Ethylparaben)}$ = 0.54, $R_{F(Propylparaben)}$ = 0.41, $R_{F(Butylparaben)}$ = 0.30) which appeared as dark spots on the chromatographic plates in UV light (λ = 254 nm). Examples of chromatograms obtained with three different software that combine 2D (ImageDecipher-TLC and Sorbfil TLC) and respectively 3D (JustTLC) image analysis, are presented in Figure 1.

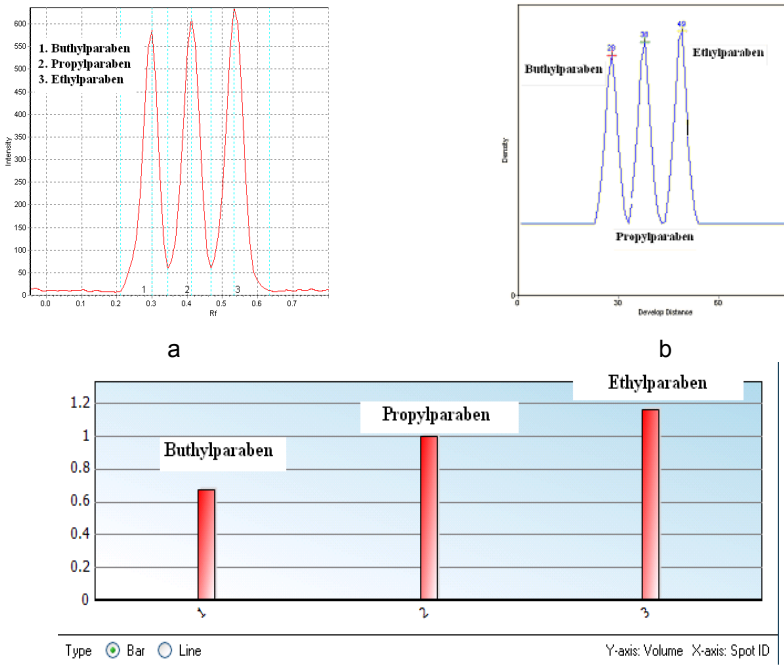

Figure 1. (a) Chromatogram obtained with Sorbfil TLC Videodensitometer software; (b) Chromatogram obtained with ImageDecipher-TLC software; (c) Chromatogram obtained with JustTLC software

Linearity, precision and accuracy of the method

The linear domain of the investigated parabens was studied using six different concentrations of parabens (applied in duplicates) by three different software for digital processing of images of chromatographic plates. The investigated linearity domain was in range 0.300 – 0.800 µg/spot for ethylparaben, propylparaben and butylparaben respectively. The statistical parameters of the linear relation between the applied concentrations and both the peaks area and volume respectively (Table 1), revealed no significant differences in terms of the regression determination coefficient (R^2). By a careful statistical investigation of the results (Table 1) we can observe slightly lower R^2 values in case of the software (JustTLC) that use the intergrated volume for the quantitative evaluation of the chromatographic spots.

The limit of detection (LOD) and quantification (LOQ) were calculated based on confidence bands generated from calibration experiments using ordinary least squares method and the results are presented in Table 1. The lowest LOD and LOQ values were obtained for ethylparaben and butylparaben using the ImageDecipher-TLC software.

The precision of the method was determined on five identical spots at three concentration levels (0.400 µg/spot, 0.600 µg/spot and 0.800 µg/spot) for all of the investigated parabens. The developed chromatographic plates were processed as described before, the precision of the method being estimated in terms of relative standard deviation in all cases. As we can see from the obtained results (Table 2), the best precision (for a quantitative evaluation of the chromatographic spots of parabens) seems to be provided by using ImageDecipher-TLC software. Also, by conversion of color images of chromatographic plates into grey scale, the precision of the developed method increased in all cases.

The accuracy of the proposed method, expressed in terms of recovery, was evaluated at two levels of concentration (0.400 µg/spot and 0.600 µg/spot) using the standard addition method. There have been analyzed solutions with no initial added concentration and solutions with known added concentration of parabens. The results (Table 3) showed no significant differences between recovery values estimated using the investigated software in case of butylparaben and slightly high differences in case of ethylparaben and propylparaben respectively.

Analysis of parabens in pharmaceutical suspensions

On account of the good results obtained for linearity, precision and accuracy of the proposed method, its applicability was assessed for pharmaceutical suspensions analysis (Maalox suspension, Theraplix France). Because the pharmaceutical suspension has a low content of parabens, a sample concentration and purification step was done before TLC analysis.

Table 1. Linearity range, linear regression equations and some statistical parameters for the proposed method

Compounds	Linearity range (µg/spot)	Software	Scale	Regression equation	R^2	LOD (µg/spot)	LOQ (µg/spot)
Ethylparaben	0.300 - 0.800	ImageDecipher-TLC	grey	y = 1506.9x + 225.40	0.9964	0.062	0.117
			red	y = 4562.6x + 753.59	0.9968	0.065	0.122
		Sorbfil	grey	y = 4666.0x + 958.37	0.9935	0.080	0.149
			red	y = 4885.7x + 946.19	0.9962	0.076	0.143
		JustTLC	grey	y = 1.9771x - 0.0158	0.9959	0.058	0.105
Propylparaben	0.300 - 0.800	ImageDecipher-TLC	grey	y = 1201.7x + 146.06	0.9918	0.070	0.131
			red	y = 3680.7x + 460.36	0.9923	0.088	0.164
		Sorbfil	grey	y = 4208.0x + 563.60	0.9964	0.073	0.138
			red	y = 4287.4x + 592.75	0.9937	0.076	0.143
		JustTLC	grey	y = 1.7157x - 0.0245	0.9901	0.093	0.163
Butylparaben	0.300 - 0.800	ImageDecipher-TLC	grey	y = 1391.9x - 18.271	0.9956	0.066	0.125
			red	y = 3973.7x + 146.96	0.9909	0.062	0.118
		Sorbfil	grey	y = 4221.4x + 241.88	0.9947	0.077	0.144
			red	y = 4277.1x + 274.90	0.9958	0.054	0.103
		JustTLC	grey	y = 1.4186x + 0.0573	0.9922	0.071	0.134

Table 2. Precision of the proposed method for three levels of concentration

Compound	Concentration (μg/spot)	Scale	Peak area/volume mean			Standard error of mean			RSD (%)		
			1	2	3	1	2	3	1	2	3
Ethylparaben	0.400	grey	366.80	6125.00	1.55	6.09	417.15	0.07	1.66	6.81	4.44
		red	953.68	15925.00		18.89	1168.02		1.98	7.33	
	0.600	grey	485.80	7696.80	1.99	1.77	170.96	0.02	0.37	2.22	1.19
		red	1263.08	20011.68		5.49	529.97		0.44	2.65	
	0.800	grey	649.20	9928.80	2.30	17.52	227.26	0.11	2.70	2.29	4.86
		red	1687.92	25814.88		54.32	704.49		3.22	2.73	
Propylparaben	0.400	grey	289.60	5710.40	1.38	7.03	364.16	0.04	2.43	6.38	3.00
		red	752.96	14847.04		21.78	1128.88		2.89	7.60	
	0.600	grey	397.60	7424.80	1.84	7.50	126.56	0.08	1.89	1.71	4.07
		red	1033.76	19304.48		23.25	392.34		2.25	2.03	
	0.800	grey	489.60	8920.40	2.13	17.72	297.48	0.06	3.62	3.34	2.70
		red	1272.96	23193.04		54.94	922.19		4.32	3.98	
Butylparaben	0.400	grey	304.80	5472.00	1.02	8.36	231.64	0.05	2.74	4.23	4.96
		red	792.48	14227.20		25.91	718.08		3.27	5.05	
	0.600	grey	414.20	6806.20	1.42	16.47	132.12	0.06	3.98	1.94	3.98
		red	1076.92	17696.12		51.06	409.56		4.74	2.31	
	0.800	grey	489.60	8081.00	1.75	18.68	273.42	0.06	3.81	3.38	3.22
		red	1272.96	21010.60		57.89	847.61		4.55	4.03	

1 – ImageDecipher-TLC; 2 – Sorbfil; 3 – JustTLC

Table 3. Recovery studies carried out for two levels of concentration

Compound	Concentration (µg/spot)	Scale	Found concentration (µg/spot)*			Recovery (%)*		
			1	2	3	1	2	3
Ethylparaben	0.400	grey	0.341	0.293	0.311	85.13	73.36	77.87
		red	0.330	0.297		82.54	74.21	
	0.600	grey	0.585	0.581	0.540	97.58	96.83	89.96
		red	0.557	0.562		92.82	93.61	
Propylparaben	0.400	grey	0.359	0.366	0.368	89.79	91.56	91.97
		red	0.360	0.367		89.93	91.83	
	0.600	grey	0.549	0.577	0.579	91.44	96.19	96.52
		red	0.555	0.576		92.49	96.16	
Butylparaben	0.400	grey	0.432	0.417	0.421	108.03	104.18	105.33
		red	0.441	0.413		110.18	103.15	
	0.600	grey	0.598	0.601	0.578	99.73	100.13	96.39
		red	0.610	0.588		101.67	97.95	

* data are mean of five replicate spots
1 – ImageDecipher-TLC; 2 – SorbfilTLC; 3 – JustTLC

Table 4. Quantitative evaluation of parabens in pharmaceutical suspension

Compound	Added concentration (mg/100 mL)	Scale	Observed concentration (mg/100 mL)			Obtained concentration (mg/100 mL)		
			1	2	3	1	2	3
Propylparaben	0.000	grey	52.410	46.479	48.162	52.410	46.479	48.162
		red	53.508	47.128		53.508	47.128	
	10.000	grey	63.811	54.683	57.176	53.811	44.683	47.176
		red	63.015	56.324		53.015	46.324	

1 – ImageDecipher-TLC; 2 – Sorbfil; 3 – JustTLC

The pharmaceutical suspension labeled with propylparaben content in no specified concentration was analyzed after a sample preparation step (including centrifugation) developed as described in the experimental part. The results obtained for the unspiked and spiked samples of pharmaceutical suspension are presented in Table 4. As it is shown, no statistical significant differences were obtained between values of propylparaben concentration using both the spiked and unspiked samples with ImageDecipher-TLC and JustTLC software respectively.

CONCLUSIONS

In this study a new chromatographic method based on image analysis of TLC plates was developed for simultaneous determination of parabens in pharmaceutical suspensions. For the quantitative evaluation of the chromatographic spots three diffrent software that combines 2D and respectively 3D image analysis were investigated. The obtained results indicated the new ImageDecipher-TLC software based on 2D image analysis as being the most appropriate for simultaneous determination of parabens. Also, the results obtained working in grey scale, proved to be more precise and accurate, comparing to those obtained working in red scale. The proposed sample preparation methodology and the new UV-Vis scanner device for TLC analysis with ImageDecipher-TLC software proved to be a valuable alternative for rapid routine analysis of parabens in pharmaceutical suspensions. The new developed method offer several advantages regarding the effective cost and comparative short analysis time made in reliable and easy reproducible mode.

EXPERIMENTAL SECTION

Reagents

The analytical purity ethyl, propyl and butylparaben, used in this study, were obtained from Sigma-Aldrich (Steinheim, Germany). The analytical grade methanol was obtained from Chemical Company (Iaşi, Romania).

Equipment and software

The standard and sample spots were applied using a semi-automatic sample applicator for qualitative and quantitative TLC analysis (Linomat 5, Camag). The quantitative evaluation of the chromatographic plates was made using BioDit Thin Layer Chromatography (TLC) Scanner (the second-generation instrument for quantitative measurements in TLC) equipped with high qualified Micortek® 3-linear color CCD. ImageDecipher-TLC version 2.0 (BioDit Technology, Co. www.biodoit.com), Sorbfil TLC Videodensitometer (Sorbpolymer,

Krasnodar, Russia) and JustTLC (Sweday, Sweden, www.sweday.com) software were used for digital processing of images and quantification of parabens on the TLC plates. The limit of detection and the limit of quantification (LOD and LOQ) were calculated using SMAC (Statistical Methods in Analytical Chemistry) and Statistica 8.0 software package was used for statistical data treatment.

Standard and Sample Preparation

The stock solution, mixture of ethyl, propyl and butylparaben was prepared by dissolving 0.200 g from each standard in 100 mL ethanol. Six different volumes (with a concentration between 0.300 – 0.800 µg/spot for each of the parabens) of standard stock solution were spotted on the chromatographic plates in duplicate. For the isolation and concentration of the parabens from a pharmaceutical suspension (Maalox suspension, Theraplix France) a centrifugation step was done. 5 mL sample of pharmaceutical suspension was centrifuged 3 times with 5 mL of methanol, at 4000 rpm. After each centrifugation the liquid phase was collected in a flask and filled with methanol to 25 mL. This solution was next used for the TLC analysis.

HPTLC procedure

HPTLC was performed using RP-18WF_{254S} chromatographic plates (20cm x 10cm, Merck, Darmstadt, Germany) and mixture of methanol-water as mobile phase. For a good separation of the parabens, the plates were developed twice: firstly the plates were developed using 60% methanol in mobile phase composition. Then the plates were dried at room temperature for 30 min to eliminate any trace of water, and they were developed again, in the same direction, using 30% methanol in mobile phase composition. In both cases the ascending technique (in a developing chamber saturated for 15 minutes with vapors of mobile phase) and a developing distance of 8 cm were used. After the second elution, the plates were dried at room temperature for 30 min and prepared for scanning process.

Image Analysis

The chromatographic plates were scanned using the BioDit TLC Scanner under UV light at 254 nm and an optical resolution of 300 dpi in order to obtain images of chromatographic plates (bmp file format). The image of the TLC plate was imported directly from the scanner using ImageDecipher-TLC software and the evaluation of the plates was performed by digitalization of images, after their conversion into grey and red scale. For a comparative analysis, the images in grey and red scale, bmp files, were then converted in 'jpg' format and processed by Sorbfil TLC Videodensitometer software in order

to calculate the spots area. Also the images were processed by JustTLC, an advanced digital image analysis software packed with features for editing, quantifying and comparing spots by their automatically detection, only in grey scale. Unlike to the first two investigated software that evaluate the chromatograms in two dimensions (by spot area), the new one truly compare chromatograms in three dimensions performing quantitative analysis based on the spot volumes.

In all cases, the obtained results were based to the fact that both area and volume of the chromatographic spots are proportional with the amount of compound applied on the TLC plate.

Method Validation

For the calibration procedure, six different volumes of stock solution were used and the calibration curve was constructed for each of the parabens, by plotting the measured peaks area or volume versus applied amount of compound. The linearity was characterized by the linear range, the regression equation, and the coefficient of determination value (R^2).

The precision of the method, expressed as relative standard deviation (RSD), was determined at three concentration levels by analyzing five replicate spots for each concentration.

The accuracy of the method, expressed as recovery, was investigated at two concentration levels for five replicate spots using the standard addition method. Known amounts of paraben standards were added to the sample matrix and the sample was processed and analyzed as described above.

REFERENCES

1. M.G. Soni, I.G. Carabin, G.A. Burdock, *Food and Chemical Toxicology*, **2005**, *43*, 985.
2. P.W. Harvey, D.J. Everett, *Journal of Applied Toxicology*, **2004**, *24,* 1.
3. R. Golden, J. Gandy, G. Vollmer, *Critical Reviews in Toxicology*, **2005**, *35*, 435.
4. R.L. Elder, *Journal of the American College of Toxicology*, **1984**, *3*, 147.
5. P. Majlát, E. Barthos, *Journal of Chromatography A*, **1984**, *294*, 431.
6. P. Canosa, I. Rodriguez, E. Rubi, M.H. Bollain, R. Cela, *Journal of Chromatography A*, **2006**, *1124*, 3.
7. L.E. Koundourellis, E.T. Malliou, T.A. Broussali, *Journal of Pharmaceutical and Biomedical Analysis,* **2000**, *23,* 469.

8. R. Hajkova, P. Solich, J. Dvorak, J. Sicha, *Journal of Pharmaceutical and Biomedical Analysis,* **2003**, *32*, 921.
9. G.A. Shabir, *Journal of Pharmaceutical and Biomedical Analysis*, **2004**, *34*, 207.
10. E. Marengo, V. Gianotti, S. Angioi, M.C. Gennaro, *Journal of Chromatography A*, **2004**, *1029*, 57.
11. M. Thomassin, E. Cavalli, Y. Guillaume, *Journal of Pharmaceutical and Biomedical Analysis*, **1997**, *15*, 831.
12. D. Casoni, I.A. Tuhuţiu, C. Sârbu, *Journal of Liquid Chromatography & Related Technologies*, **2011**, *34*, 805.
13. R. Hamoudová, M. Pospisilová, A. Kavalirová, P. Solich, J. Sicha, *Journal of Pharmaceutical and Biomedical Analysis*, **2006**, *40*, 215.
14. S. He, Y. Zhao, Z. Zhu, H. Liu, M. Li, Y. Shao, Q. Zhuang, *Talanta*, **2006**, *69*, 166.
15. B. Baalbaki, M. Blanchin, H. Fabre, *Analytica Chimica Acta*, **2002**, *463*, 15.
16. H. Huang, Y. Lai, C. Chiu, J. Yeh, *Journal of Chromatography A*, **2003**, *993*, 153.
17. L. Zhang, X. Lin, *Journal of Chromatography A*, **2006**, *1109*, 273.
18. I. Vovk, M. Prošek, *Journal of Chromatography A*, **1997**, *779*, 329.
19. C.F. Poole, *Journal of Chromatography A*, **1999**, *856*, 39.
20. F. Soponar, A.C. Moţ, C. Sârbu, *Journal of Chromatography A*, **2008**, *1188*, 295.
21. L. Cieśla, M. Waksmundzka-Hajnos, *Journal of Chromatography A*, **2009**, *1216*, 1035.
22. F. Soponar, A.C. Moţ, C. Sârbu, *Chromatographia*, **2009**, *69*, 151.
23. F. Soponar, A.C. Moţ, C. Sârbu, *Journal of AOAC International*, **2010**, *93*, 804.

STUDIA UBB CHEMIA, LVII, 2, 2012 (p. 95 - 102)

HYDROMETALLURGICAL FLOW FOR ZINC RECOVERY FROM Zn-MnO_2 WASTE BATTERIES. I. ZINC SOLUBILIZATION FROM ANODIC REMNANTS

M.S. ANTON[a], A. L. MANCIULEA[a], U. SCHMIDT[b], A. BUND[b], P. ILEA[a]

ABSTRACT. The present study is focused on the electrochemical recovery of zinc anodic remnants from Zn-MnO_2 waste batteries and the development of a combined flow scheme that allows the recovery of zinc by electrodeposition with satisfactory energy consumption related to the amount of Zn deposited. Batch laboratory experiments were performed to evaluate the electrochemical dissolution/winning parameters (electrolyte composition, pH, current density) in acidic medium. The proposed flow scheme aims at the electrodissolution of anodic remnants from waste batteries. Using the electrochemical method were achieved a high cathodic current efficiencies, approximately 98 % for Zn electrodeposition and also an improvement of the solubilization degree in comparison with the chemical solubilization using as anode Zn remnants in 0.5 M H_2SO_4.

Keywords: *Zn-MnO_2 batteries, electrochemical dissolution, energy consumption*

INTRODUCTION

The solubilization of spent battery components is of great scientific and economic interest, on account of recycling requirement of wastes and ~~of~~ valuable materials recovery. After the solubilization of electrodic inactive material from Zn-MnO_2 batteries, solutions with a zinc content between 5 and 30 g/L were obtained, depending on the H_2SO_4 concentration [1]. Subsequent to a previous solubilisation of the anodic remnants, the solution can be further processed for electroextraction of high purity zinc. Electrowinning of zinc from relatively concentrated solutions with 160 g/L of Zn^{2+}, could be achieved, successively, with acceptable current efficiencies down to a concentration of 40 g/L [2].

Generally, during the solubilization process of the metal anode, several different phenomena, such as active dissolution, passivation, pitting and trans-passivation, etc., can occur with the change of potential and concentration

[a] Babes Bolyai University, Faculty of Chemistry and Chemical Engineering, 11 Arany Janos Str., Cluj-Napoca, Romania
[b] Fachgebiet Elektrochemie und Galvanotechnik II, Technische Universität Ilmenau, Germany

of the anion [3]. Metal dissolution takes place essentially at the base of pores of a conductive layer of oxidation products which is progressively degraded by the anodic current [4]. However, concerning the anodic polarization processes of some metals, there is no passivation but only active dissolution, and the anodic reaction current increases with the positive shift of potential until ultimately reaches a diffusion limited current. Hence, the electrochemical solubilization rate of metal is controlled by the diffusion rate of the salt layer formed on the surface of the metal [5, 6].

One of the most important aspects for the electrowinning process is the selection of the electrolyte system [7]. The zinc solubilization process was studied in different electrolyte solutions: NH_3-NH_4Cl [7], NaOH [8, 9], NaCl [8], H_2SO_4 [10]. In alkaline electrolytes, the polarization is more significant than in acidic solutions, probably due to $Zn(OH)_2$ precipitation in the pores of the anode [8]. According to Z. Huajun et al. [7], the anodic dissolution in NH_3-NH_4Cl medium can go along quite well as long as the Zn concentration of the electrolyte is well controlled, under 60 g/L Zn^{2+}. At higher concentrations of Zn^{2+}, a white film, mainly composed of Zn(OH)Cl, appeared on the surface of the zinc anode, preventing further dissolution. In NaCl electrolyte, and the formation of ZnO on the zinc surface suggests the passivation of zinc [8].

We have studied previously [1, 11] the experimental conditions for Zn solubilization from the inactive electrodic material of the battery in H_2SO_4. The 2 M H_2SO_4 concentration ensures 98 % of zinc solubilization, together with 30 % manganese and 20 % iron. The resulting aqueous solution contains about 20 g/L Zn^{2+}, 6 g/L Mn^{2+} and 0.1 g/L Fe^{2+}. Experiments on the electrodeposition of zinc from these solutions showed low cathodic current efficiencies [12,13]. This is mainly due to the low concentration of zinc in the solution. As an alternative for increasing the Zn concentration in the electrolyte, the solubilization of Zn anodic remnants from the battery is proposed.

In this study, the solubilization process of zinc from the anodic remnants of Zn-MnO_2 waste batteries was studied in H_2SO_4 medium, through chemical and electrochemical methods. To determine the best conditions for the solubilization process, chemical (acid concentration, solid liquid mixing ratio) and electrochemical parameters (electrolyte composition, applied anodic current density) were assessed.

RESULTS AND DISCUSSIONS

1. Chemical dissolution of anodic remnants

The preliminary chemical leaching studies were carried out without agitation, using different concentrations of H_2SO_4 and mixing ratios (S: L) between 1:10 and 1:50 as shown in Table 1.

Table 1. Influence of the solid: liquid ratio and H_2SO_4 concentration on the solubilization degree of Zn anodic remnants

H_2SO_4 concentration (M)	Solid: liquid ratio (g/mL)	Solubilization degree (%)	
		24 hours	48 hours
1.5	1:10	53	86
	1:20	73	96
	1:50	91	96
2	1:10	98*	-
	1:20	99*	-
	1:50	99*	-
4	1:10	64	72
	1:20	71	75
	1:50	76	76

* Completely dissolved after 20 hours.

In 20 hours, chemical dissolution ensures 99 % dissolution of Zn anodic remnants in 2 M H_2SO_4, regardless of the mixing ratios. In 1.5 M H_2SO_4 a total dissolution was achieved only in 48 hours at mixing ratios higher than 1:10. The increase in H_2SO_4 concentration leads to a decrease in zinc dissolution, due to the passivation process.

2. Combined electrodissolution and electrodeposition of zinc

Given the relatively long duration of the waste's dissolution, an electrochemical process was developed, allowing anodic dissolution of waste and the zinc cathodic recovery.

Electrochemical dissolution of zinc remnants was focused on obtaining high solubilization degrees and low specific energy consumption. The effects of electrolyte composition and current densities on zinc dissolution in acidic sulphate electrolyte have been investigated.

The electrochemical dissolution of zinc remnants using an aqueous solution (H_2SO_4 and low concentration of Zn^{2+} ions) is determined by the following possible reactions:

(i) Direct anodic solubilization:

$Zn - 2e^- \rightarrow Zn^{2+}$ and

(ii) Electroless solubilization:

$Zn_{(s)} + H^+_{(aq)} \rightarrow Zn^{2+}_{(aq)} + H_{2(g)}$.

The electroless solubilization triggers an alkalinization of the solution near the anode surface, causing the formation of a white precipitate of $Zn(OH)_2$:

$Zn^{2+} + 2OH^- \rightarrow Zn(OH)_2$.

This hydroxide re-dissolves in acidic medium:

$Zn(OH)_2 + 2H_2SO_4 \rightarrow ZnSO_4 + H_2O$

Under these conditions, the following reactions take place at the cathode:

$Zn^{2+} + 2e^- \rightarrow Zn$

In acidic solutions, the hydrogen evolution reaction, HER also occurs:

$2\,H^+_{(aq)} + 2e^- \rightarrow H_{2(g)}$

To determine the best conditions for the solubilization tests the optimal current density has to be established, as well as the optimal composition of the leaching solution.

2.1. The influence of the anodic current density

The influence of the anodic current density on the current efficiencies and power consumptions was investigated under the following conditions: 0.5 M H_2SO_4, electrical charge fixed at 1485 C (which ensures the solubilization of approximately 50 % of Zn remnants). The anodic current density was between 217 and 1087 A/m^2. In order to diminish the acid consumption due to hydrogen evolution reaction, in the initial electrolyte solution were dissolved approximately 2 g/L Zn^{2+}. At the end of electrochemical solubilization the composition of the solutions was determined.

The evolution of parameters in electrochemical (chemical) solubilization for different anodic current densities, in 0.5 M H_2SO_4 solutions is summarized in Table 2.

Table 2. *The evolution of parameters during the electrochemical solubilization at different anodic current density, in 0.5 M H_2SO_4 solutions, electrical charge* 1485 C

Anodic current density	Electrochemical solubilization		Zinc electrodeposition	
	Solubilization degree	Energy consumption	Current efficiency	Energy consumption
A /m^2	%	kWh/kg Zn	%	kWh/kg Zn
1087	34	1.85	50	4.0
870	38	1.36	50	3.1
652	44	1.19	51	2.6
434	45	0.72	61	1.5
217	45	0.37	75	0.7

The solubilization process is slow and cannot be accelerated by increasing the current density. Low current densities give better process parameters (solubilization degree, current efficiency and specific energy consumption). The best results were obtained at a current density of 217 A/m^2, when the

solubilization degree was 45 %, after approximately 4 hours of electrolysis. In case of chemical solubilization, under similar conditions, the solubilization degree was only 17 %. At the same time, the cathodic current efficiencies increase with decreasing current densities. During these experiments, the final Zn concentration in the electrolyte increased to approximately 8 g/L.

2.2. The influence of zinc concentration

As mentioned above (see section 2.1), the electrochemical solubilization was studied in the presence of a quantity of zinc in the initial solution in order to accelerate the electrodeposition process by decreasing the acidity of the solution. At the same time, the electrochemical solubilization increases the concentration of zinc in the solution, so it was considered necessary to study the influence of Zn^{2+} concentration on the process parameters.

The effect of zinc concentration (see Figures 1 and 2) on current efficiencies and power consumptions were investigated under the following conditions: current density of 217 A/m^2, different zinc concentrations (2, 10, 20 and 40 g/L) in 0.5 M H_2SO_4.

Figures 1 and 2 illustrate that high cathodic current efficiencies were obtained in the zinc concentration range of 10–40 g/L. The specific power consumptions, between 0.5 and 0.7 kWh/kg Zn, were much lower than in conventional zinc electrowinning (3 – 4.3 kWh/kg Zn) [14,15].

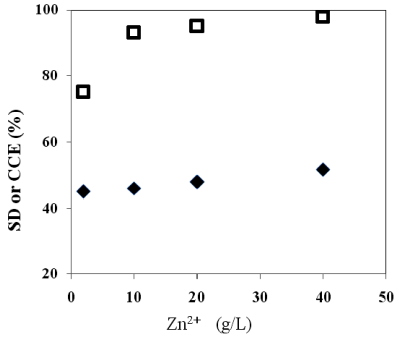

Figure 1. The effect of Zn^{2+} concentration on the solubilization degree (♦) and cathodic current efficiency (□)

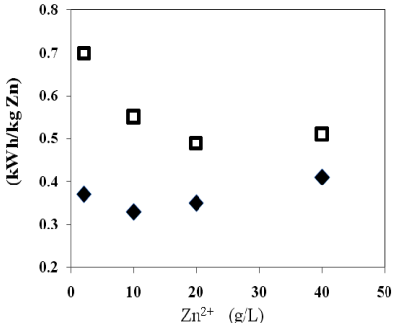

Figure 2. The effect of Zn^{2+} concentration on the specific energy consumption for the solubilization process (♦) and for Zn electrodeposition (□)

2.3. The influence of acid concentration

To study the effect of acid concentration on process parameters, the H_2SO_4 concentration was increased to 2 M. Figure 3 shows that the solubilization degree increases up to 75 %, while at the same time the cathodic current efficiency drastically drops. At high acid concentration a massive hydrogen evolution occurs, leading to low cathodic current efficiency and an excessive consumption of the zinc anode, thereby increasing the solubilization degree.

Furthermore, to assess the global parameters of the process, a complete solubilization test of the anodic Zn remnants was done using a solution containing 10 g/L Zn^{2+} in 0.5 M H_2SO_4 medium. For this test the amount of electrical charge was 1600 C. A solubilization degree of 100 % was achieved after 4.5 hours, demonstrating that the electrochemical process is more advantageous compared to the chemical one.

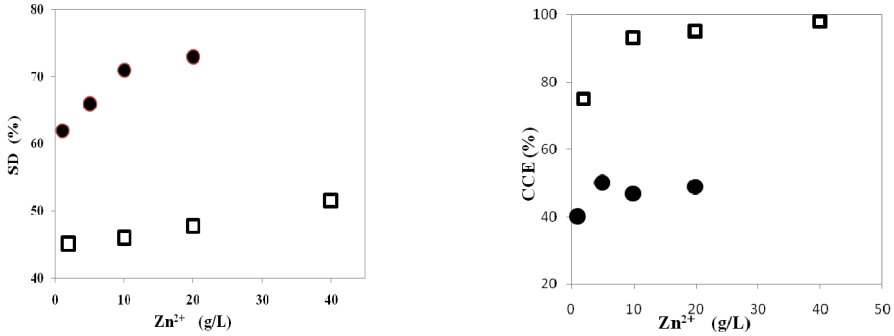

Figure 3. The evolution of the electrochemical parameters, CCE and SD, in 0.5 M (□) and 2 M H_2SO_4 (●) for different concentrations of Zn^{2+}, i =217 A/m^2

CONCLUSIONS

The electrochemical recycling of zinc reduces the amount of exhausted Zn–MnO_2 batteries in urban waste and protects the environment from contamination with toxic metals.

High current efficiencies, approximately 98 % for Zn electrodeposition process and an increase of the solubilization degree with 20 % in comparison with the chemical process were achieved using Zn remnants as anodes in 0.5 M H_2SO_4. Increasing the concentration of acid to 2 M decreased the current efficiency for electrodeposition (~50 %) and increased the solubilization degree to 69 % in comparison with the chemical process.

The results for the electrolyte's composition of Zn electrodeposition show that cathodic current efficiency decreased dramatically when the zinc content in the electrolyte decreases below 10 g/L in 0.5 M H_2SO_4. Electrowinning of Zn from such diluted solutions becomes uneconomical due to the poor quality of the recovered zinc, affected by the massive hydrogen production.

Electrochemical recovery of zinc anodic remnants allows shortening the dissolution time of the wastes and increases the solubilization degree with low specific energy consumption. This allows the recovery of pure metallic zinc, with high current efficiency and lower energy consumption than in conventional electrowinning cases.

EXPERIMENTAL SECTION

The electrochemical measurements were performed at room temperature (25 °C) in a conventional four electrode cell. The counter electrode (CE) was an aluminium plate, the working electrode (WE) were Zn anodic remnants recovered after dismantling the waste batteries and as reference electrodes (RE) we used $Ag/AgCl/KCl_{sat}$.

Aluminium is used as cathode because it forms no alloys with zinc, thus facilitating zinc separation at the end of the electrolysis [16]. For the cleaning of aluminium surfaces, electrodes were soaked in 6 M NaOH bath for 2 minutes. Prior to immersion in the electrolytic bath, the electrodes were rinsed with distilled water, dried and weighted, to determine the mass of deposited metal. In all experiments, the current efficiency was assessed by the difference in mass of the electrode before and after the experiment.

The electrolyte used was a synthetic solution containing different concentrations of Zn in different H_2SO_4 concentrations. All chemicals used ($ZnSO_4 \cdot 7H_2O$, H_2SO_4) were of analytical grade (Merck) and all solutions were prepared with Milli-Q water.

A Voltcraft current supply and multimeters were used to control and monitor the electrochemical processes. The solubilization degree (SD) and cathodic current efficiencies (CCE), as well as the specific current consumption (Ws) were evaluated.

Due to the fact that in the absence of polarization deposited zinc could dissolve in acid medium, at the end of the experiment the polarization was maintained until the deposit was washed with double distilled water. Dry electrodes were weighed before and after the experiment, to determine the mass of metal deposited, respectively dissolved. Based on these weights the cathodic current yields, respectively the solubilization degrees were calculated. The current efficiencies, CCE were evaluated using the expression:

$$CCE = \frac{m}{m_t} \cdot 100$$

where: m is the mass of substance deposited at the electrodes, and

m_t- theoretical mass calculated from Faraday's law:

$$m_t = \frac{I \cdot t \cdot M}{z \cdot F}$$

where: z is the number of electrons transferred in the reduction of zinc ions (z=2), F-Faraday's constant (F=96500 C/mol), M-molecular weight (65 g/mol), I- the total electric current (A) and t- electrolysis time (s).

The solubilization degree of zinc anodic remnants obtained in the electrochemical process was evaluated taking in consideration the amount of zinc chemically dissolved, under similar experimental conditions (average mass of 0.4626 g Zn chemically dissolved), as shown in the formula:

$$SD = \frac{m_{Zn,f} \cdot 100}{m_{Zn,i} - 0.4626}$$

where: $m_{Zn,i}$, respectively $m_{Zn,f}$ are the initial, respectively de final mass of zinc anodic remnants, weighed before and after the experiment.

The initial and final composition of the solutions was determined for each step of the process, using a Fischerscope X-ray System XDVM (Helmut Fischer GmbH, Sindelfingen, Germany).

ACKNOWLEDGEMENTS

The authors wish to thank for financial support the projects co-financed by the Sectorial Operational Program For Human Resources Development 2007 – 2013 - contract no.: **POSDRU/88/1.5/S/60185** – "Innovative doctoral studies in a Knowledge Based Society" and - contract no.: **POSDRU/89/1.5/S/60189** – "Postdoctoral Programs for Sustainable Development in a Knowledge Based Society".

REFERENCES

1. M. Anton, A. Manciulea, P. Ilea, *Studia UBB Chemia*, **2011**, *LVI (4),* 223.
2. A.E. Saba, A.E. Elsherief, *Hydrometallurgy,* **2000**, *54*, 91.
3. M. Ojaghi Ilkhchi, H. Yoozbashizadeh, M. Sadegh Safarzadeh, *Chemical Engineering and Processing,* **2007***, 46,* 757.
4. A.B. Velinchenko, J. Portillo, M. Sarret and C. Muller, *Journal of Applied Electrochemistry,* **1999***, 29,* 1119.
5. M. Datta, *Electrochemical Science and Technology,* **1993***, 37,* 207.
6. C.H.A.O. Liyan, M. Ishikawa, M. Okido, *Transactions of Nonferrous Metals Society of China*, **2002**, *03*, 757.
7. Z. Huajun, G. Zhenghai, Z. Jinhuan, *Hydrometallurgy*, **2007**, *89*, 369.
8. M. Mouanga, P. Berçot, J.Y. Rauch, *Corrosion Science*, **2010**, *52*, 3984.
9. M. Mokaddem, P. Volovitch, K. Ogl, *Electrochimica Acta*, **2010**, *55*, 7867.
10. M.B.J.G. Freitas, M.K. de Pietre, *Journal of Power Sources*, **2004**, *128*, 343.
11. M. Anton, F. Imre-Lucaci, S.-A. Dorneanu, P. Ilea, National Conference with international participation: "*Corrosion and AntiCorrosive Protection",* 16-18 September **2010**, Cluj-Napoca.
12. C.C.B. Martha de Souza, J. A.Soares Tenório, *Journal of Power Sources,* **2004**, *136,* 191.
13. Q.B Zhang, Y.Hua, *Hydrometallurgy,* **2009**, *99,* 249.
14. Francesco Ferella, Ida De Michelis, Francesco Veglio, *Journal of Power Sources,* **2008**, *183*, 805.
15. K.I. Popov, S.S. Djokic, B. N. Grgur, *Kluwer Academic Publishers, New York***, 2002**, 179.
16. A.Recéndiz, I. González, J. L. Nava, *Electrochimica Acta,* **2007**, *52*, 6880.

STUDIA UBB CHEMIA, LVII, 2, 2012 (p. 103 - 112)

NADH OXIDATION AT MELDOLA BLUE MODIFIED GLASSY CARBON ELECTRODES. A COMPARATIVE STUDY

CARMEN IOANA FORŢ[a,*], IONEL CĂTĂLIN POPESCU[b]

ABSTRACT. Three types of modified electrodes based on glassy carbon (powder and rod) and Meldola Blue (MB) were used for NADH electrocatalytic oxidation. MB was immobilized by simple adsorption on two different phosphates materials, crystalline zirconium phosphate (α-ZP) and crystalline titanium phosphate (α-TP), as well as on carbon aerogel (CA). The phosphate materials were incorporated in carbon paste, while CA was immobilized on a glassy carbon rod using a chitosan matrix. The basic electrochemistry of adsorbed MB and its ability to catalyze NADH electrooxidation have been investigated by cyclic voltammetry, performed in different experimental conditions (pH, potential scan rate, NADH concentration). The electroanalytical parameters of the investigated modified electrodes showed that: (i) irrespective the material, the formal standard potential of the immobilized MB was found pH dependent; (ii) the best electrocatalytic response was obtained for MB-αTP modified electrode.

***Keywords**: electrocatalysis, NADH electrooxidation, glassy carbon electrode, redox dyes*

INTRODUCTION

Dehydrogenases represent the majority of redox enzymes. They require for the operation the presence $NAD(P)^+$ / NAD(P)H coenzyme. Consequently, the electrochemical regeneration of this coenzyme - in fact the oxidation of the reduced form, NAD(P)H - is an important issue. Indeed, for many years the electrochemical oxidation of NADH was studied, and it was concluded that in order to achieve this process at different conventional electrode materials relatively high overpotentials are required [1, 2] or is necessary the presence of a suitable redox mediator [3]. It is worth to add, that the direct electrochemical oxidation of NADH is accompanied by the electrode fouling, which is due to the NAD^+ adsorption on the electrode surface or to the side reactions involving the radicals generated during the coenzyme oxidation.

[a] "Babes-Bolyai" University, Laboratory of Electrochemical Research and Nonconventional Materials, 11, Arany J. St., 400028 Cluj-Napoca, Romania, * iladiu@chem.ubbcluj.ro

[b] "Babes-Bolyai" University, Department of Physical Chemistry, 11, Arany J. St., 400028 Cluj-Napoca, Romania

One of the best mediators for NADH catalytic oxidation is Meldola Blue (MB), a phenoxazine compound involving two electrons and two protons [4, 5].

Excepting the water solubility of the MB, another reason for its immobilization onto different type of support materials is the shift of its formal standard potential (E°') towards more positive potentials, at a value allowing the operation of the modified electrode within the potential window essentially free of interfering reactions [6]. Previous studies showed that, when MB was directly adsorbed onto pyrolytic graphite, its E°' value was – 175 mV *vs.* Ag|AgCl (at pH 7) [4], which is outside of the optimum window for amperometric detection [7]. Additionally, an increase of this E°' value will indirectly induce an increase of the rate constant for NADH electrocatalytic oxidation, which, actually, is large enough to be limited by the mass transport process [8, 9].

Due to their peculiar properties crystalline phosphates were used in many research areas as catalysts, ion exchangers, molecular sieves, and electrode materials [10]. Thus, because of their negatively charged phosphate groups, crystalline phosphates are good ion conductors and good ion exchangers (strong acidic materials). Additionally, they are layered materials, which present two important features: (i) the interlayer spaces can be adjusted to accommodate guests of different size; (ii) they have the control over the orientation, aggregation and distribution of the adsorbed guests [11].

Recently, carbon aerogels (CAs) were used as support material for the immobilization of different chemical species with catalytic properties [12]. CAs have interesting properties, such as high specific surface area, porosity, and electrical conductivity, associated with a good chemical stability. Therefore, CAs are attractive materials for different applications such as electrode materials in supercapacitors and rechargeable batteries, catalyst supports, adsorbent materials and thermal insulators [13].

In the present work carbon aerogel (CA), a high mesoporous material, was compared with crystalline zirconium phosphate (α-ZP) and crystalline titanium phosphate (α-TP) when all were used as support material for MB immobilization. The resulting modified materials, MB-αTP, MB-αZP and MB-CA, were deposited on two types of glassy carbon, Sigradur K powder (SK) or glassy carbon rod (GC) in order to obtain two MB modified carbon paste electrodes, (MB-αTP-SK-CPE) and MB-αZP-SK-CPE, and MB modified glassy carbon electrodes (MB-CA/GCEs). Aiming to estimate and compare their electroanalytical parameters, the electrochemical behavior of the obtained modified electrodes and their ability to catalyze the electrooxidation of NADH have been investigated by cyclic voltammetry, performed in different experimental conditions (pH, potential scan rate, NADH concentration).

RESULTS AND DISCUSSIONS

Electrochemical behavior of the MB modified GC electrodes

A comparison between the cyclic voltammograms (CVs) recorded at MB modified electrodes with similar measurements performed at electrodes without immobilized MB lead to observe that, as expected, no redox process occurred at electrodes in the absence of MB, while MB-αTP-SK-CPE (Sigradur K : MB-αTP = 19:1; w/w), MB-αZP-SK-CPE (Sigradur K : MB-αZP = 19:1; w/w), and MB-CA/GCE present one voltammetric peaks pair, which is due to the oxido-reduction process involving the mediator redox couple (Figure 1).

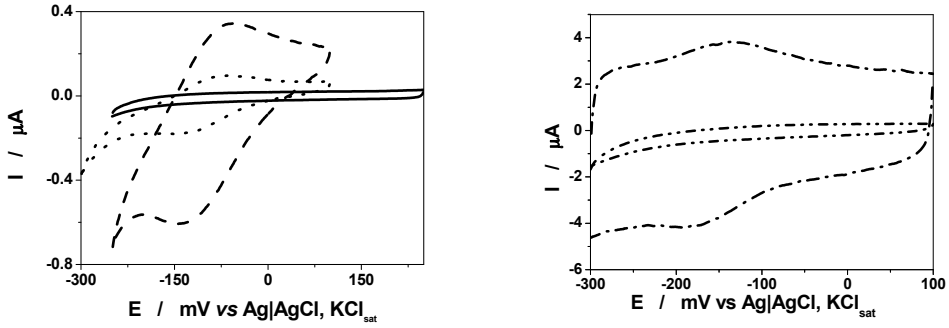

Figure 1. Cyclic voltammogram recorded at MB-αTP-SK-CPE (⋯⋯), MB-αZP-SK-CPE (----), SK-CPE (—), MB-CA/GCE (-·-·-) and GCE (-··-). Experimental conditions: scan rate, 20 mV/s, supporting electrolyte Tris buffer, 0.1 M, pH 7.

The background current observed on the recorded CVs was higher for all MB modified electrodes than that evidenced for the corresponding unmodified electrodes (SK-CPE or GCE) (Figure 1). A plausible explanation of this fact should take into consideration that all support material used for mediator immobilization (α-TP, α-ZP, and CA), have high specific surface area, conferring a high electrochemical active surface to the modified electrodes. Indeed, the highest background current among the compared modified electrodes was observed in the case of the electrode modified with CA, which is a high mesoporous material (Figure 1) [14].

The electrochemical parameters of the MB modified GCEs are summarized in Table 1. In all cases, the peak separation values (ΔE_p), the width at half maximum current intensity ($W_{1/2}$) and the ratio between the intensity of the cathodic and anodic peaks (I_{pa}/I_{pc}) point to a quasi-reversible redox process [15].

The values of the formal standard potential (E°') for all MB modified GCEs (Table 1) are in the optimal potential range for electroanalytical applications [7], and assure an efficient production of enzyme active NAD^+ [6, 8]. Among the prepared modified electrodes, the MB-αZP-SK-CPE and MB-αTP-SK-CPE exhibit identical values of (E°') for MB redox couple, which are slight lower than that corresponding to MB-CA/GCE.

Table 1. Electrochemical parameters of the investigated GC modified electrodes.

Electrode	E°' (mV)	ΔE_p (mV)	$W_{1/2}$ (mV)		I_{pa}/I_{pc}
			anodic	catodic	
MB-CA/GCE	-140	40	110	100	1.1
MB-αZP-SK-CPE	-100	65	120	100	1.07
MB-αTP-SK-CPE	-100	60	100	90	0.87

$\Delta E_p = E_{pa} - E_{pc}$, where E_{pa} and E_{pc} are the cathodic and anodic peak potentials.

The short-term stability of the modified electrodes was estimated by continuous voltammetric cycling within the potential window of practical interest. The time evolution of the recorded CVs revealed that the peak current and the peak potential corresponding to the MB redox wave show a good stability. Thus, by using the relation $\frac{(I_{pa})_{100^{th}\ cycles}}{(I_{pa})_{1^{st}\ cycle}} \times 100\%$, the current stability was found as follows: ~80% for MB-αTP-SK-CPE; ~101% for MB-αZP-SK-CPE was; and ~105% for MB-CA/GCE. These results show a low decrease or even an increase of the electrode activity due to its activation induced by the continuous potential cycling. Consequently, the simple adsorption of MB on the α-TP, α-ZP or CA support materials, followed by the incorporation MB / support material in the electrodes composition, lead to stable and functional modified electrodes.

For all prepared modified electrodes based on MB-αTP, MB-αZP and MB-CA the *E°'* value depends on the pH in the same manner as that reported for MB dissolved in aqueous solution [16], MB adsorbed on spectrographic graphite [4] or on α-ZP [17]. In good agreement with previously published results [4], the E°' *vs.* pH dependence shows two linear regions: one with the slope of ~60 mV/pH, and the second having the slope of ~30 mV/pH unit (Figure 2). This behavior indicates that, irrespective of the support material, the pK_a value for the adsorbed MB is around 4 [4]. Indeed, all experimental data were well fitted to the following nonlinear regression equation: $E = E^{0'} - 0.059 * pH + 0.029 * \log(1 + 10^{pH - pK_a})$. The calculated pK_a values for MB-αTP-SK-CPE, MB-αZP-SK-CPE and MB-CA/GCE are presented in Table 2. These pK_a values are lower than that reported for MB adsorbed on spectrographic graphite (pK_a = 5) [4]. This difference suggests that, due to the interactions with the support materials the MB immobilized onto α-ZP, α-TP or CA becomes more acidic than when adsorbed onto graphite.

The cyclic voltammograms recorded at pH 7, in a wide range of potential scan rates (0.001 – 18 Vs^{-1}), showed a linear dependence of the peak currents (I_{pa}) on the scan rate (*v*). Thus, the slopes of log(I_{pa}) *vs.* log(v)

dependencies (Figure 3) were close to the theoretical value (1), confirming the immobilization of the redox mediator MB on the support material (α-ZP, α-TP or CA) (Table 3).

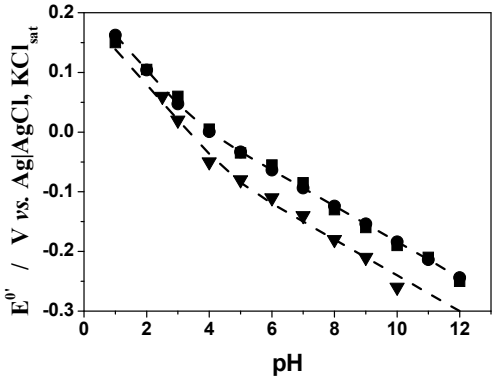

Figure 2. pH influence on the E°' value of MB adsorbed on: α-ZP [SK : MB-αZP = 19:1 (w/w)] (●) [18]; α-TP [SK : MB-αTP = 19:1 (w/w)] (■) and CA (▼).

Table 2. pK_a calculated values for MB-αTP-SK-CPE, MB-αZP-SK-CPE, and MB-CA/GCE

Electrode	pK_a	chi^2	R^2	N
MB-αZP-SK-CPE	4.3 ± 0.4	0.0002	0.9866	11
MB-αTP-SK-CPE	3.6 ± 0.2	0.00007	0.9963	12
MB-CA/GCE	4.7 ± 0.3	0.0001	0.9899	9

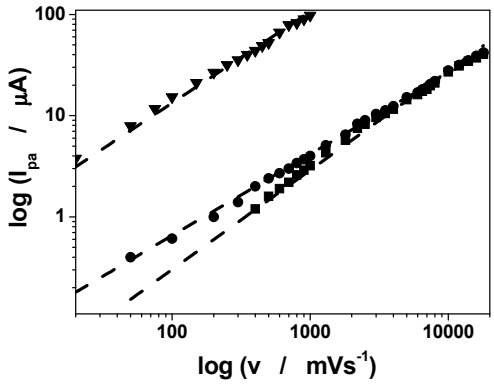

Figure 3. Influence of the potential scan rate on the anodic peak current recorded at MB-αTP-SK-CPE (■), MB-αZP-SK-CPE (●), and MB-CA/GCE (▼). Experimental conditions: supporting electrolyte, 0.1 M Tris buffer (pH 7).

Table 3. The slopes of the log(I_{pa}) *vs.* log(v) for MB-αZP-SK-CPE, MB-αZP-SK-CPE and MB-CA/GCE modified electrodes.

Electrode	Slope	R	N
MB-CA/GCE	0.90 ± 0.02	0.994	19
MB-αZP-SK-CPE	0.80 ± 0.01	0.997	32
MB-αTP-SK-CPE	0.98 ± 0.01	0.994	26

Electrocatalytic NADH oxidation at MB modified GC electrodes

MB-αZP-SK-CPE, MB-αTP-SK-CPE and MB-CA/GCE showed clear electrocatalytic activity for NADH oxidation. Thus, the cyclic voltammograms recorded at these electrodes in the presence of NADH (Figure 4, solid lines) present all the features of an electrocatalytic process: the oxidation peak is drastically increased, simultaneously with the disappearance of the reduction peak.

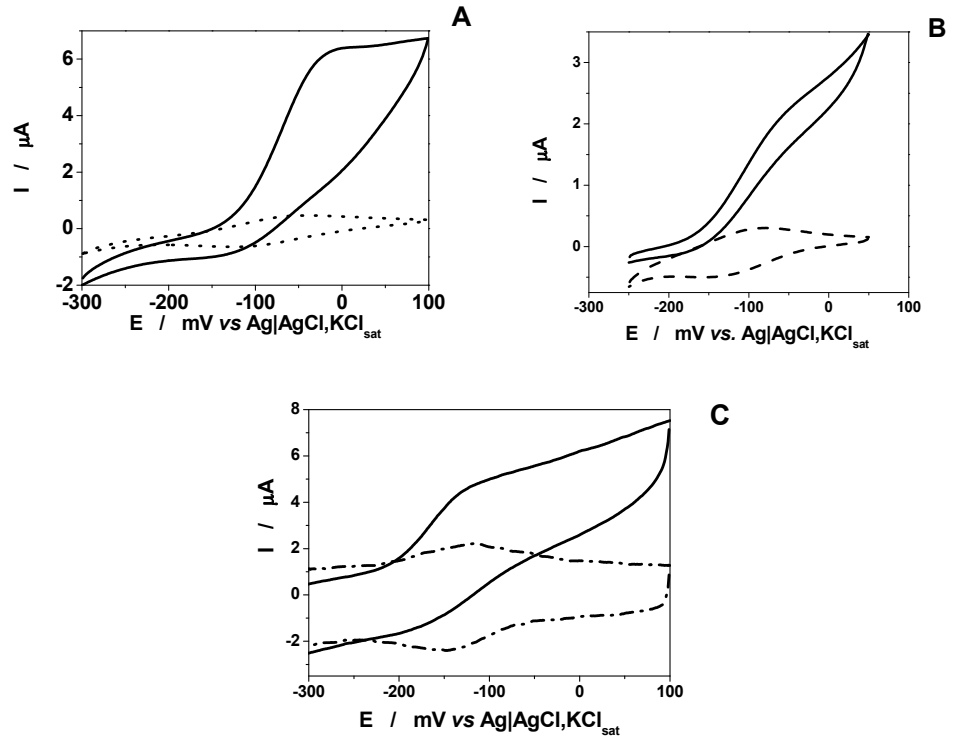

Figure 4. Electrocatalytic oxidation of NADH at MB-αTP-SK-CPE (A), MB-αZP-SK-CPE (B) and MB-CA/GCE (C) in the absence and in the presence of 5 mM NADH. Experimental conditions: scan rate, 20 mV/sec; supporting electrolyte, 0.1 M Tris buffer, (pH 7).

The efficiency (*Eff*) of the electrocatalytic oxidation of NADH at the investigated modified electrodes (MB-αTP-SK-CPE, MB-αZP-SK-CPE and MB-CA/GCE) was calculated according to the following relation: $\mathbf{Eff = (I_{cat} - I_0) / I_0}$, where I_{cat} is the oxidation current intensity in presence of 5 mM NADH and I_0 is the oxidation current intensity observed in its absence. Among the calculated electrocatalytic efficiencies, the highest value was obtained for MB-αTP-SK-CPE, and decrease in the following sequence: $Eff_{MB\text{-}\alpha TP\text{-}SK\text{-}CPE} > Eff_{MB\text{-}\alpha ZP\text{-}SK\text{-}CPE} > Eff_{MB\text{-}CA/GCE}$ (Table 4).

The surface coverage (Γ) was estimated by using the equation $\mathbf{\Gamma = Q / nFA}$, *w*here Q is the electric charge obtained by integrating the anodic peak, corrected for the background current; *n*, *F* and *A* are the number of electrons transferred in redox reaction, Faraday's constant and the electrode geometric area, respectively.

Table 4. Electrocatalytic efficiencies for NADH oxidation at modified GC electrodes.

Electrode	Eff	Γ 10^{10} mol cm^{-2}
MB-CA/GCE	2.2	1.85
MB-αZP-SK-CPE	7.5	0.32
MB-αTP-SK-CPE	19.4	0.08

Surprisingly, the MB coverage value for MB-αTP-SK-CPE was the lowest, comparing with those obtained for MB-αZP-SK-CPE or MB-CA/GCE, but is associated with the highest electrocatalytic efficiency. A plausible explanation for this behavior could due to the differences existing between the structure of the support material used for mediator immobilization. Therefore, when CA, a high mesoporous material, was used as support material the free access of NADH to the immobilized MB was more difficult due to some steric hindrances.

CONCLUSIONS

Two different types of glassy carbon (powder and rod) and three types of support materials have been successfully used for the preparation of MB-αZP-SK-CPE, MB-αTP-SK-CPE and MB-CA/GCE modified electrodes. The electrochemical parameters of the modified electrodes point out the presence of the immobilized MB species on the electrode surface. All E°' values are placed in the optimal potential range for the amperometric detection. The pH dependence of E°', for all investigated modified electrodes, was fitted using a nonlinear model, allowing the estimation of the pK_a value for the

immobilized MB. The electrochemical and electroanalytical parameters of the investigated electrodes recommend them as stable and reproducible sensors for NADH. Among them MB-αTP-SK-CPE presents the best electrocatalytic response for NADH electrooxidation.

EXPERIMENTAL SECTION

Synthesis of CA. CA was prepared using a mixture of resorcinol (98% purity, Aldrich), formaldehyde (37% solution, Aldrich), Na_2CO_3 (99.9% purity, Aldrich), and deionized water, according to a previously reported sol-gel method [14].

Synthesis of acidic alpha- zirconium phosphate (α-ZP) and alpha-titanium phosphate (α-TP). α-ZP and α-TP were prepared according to a previously reported method [17], and [19], respectively.

Immobilisation of the organic dye (Meldola Blue) on the support material surfaces. The immobilization process was carried out using an aqueous solution of the organic dye (Meldola Blue, MB; Sigma, St. Louis, MO, USA) in a concentration of 0.001% (w/v). The procedure of immobilization was as follows: 50 mg of support material (α-ZP, α-TP and CA) was added to 50 ml of dye solution and the mixture was shaken for 1 h. The precipitate (MB-αZP, MB-αTP and MB-CA) was filtered, washed with de-ionized water and dried at room temperature.

Preparation of the modified glassy carbon electrode. The carbon paste electrodes were prepared by thoroughly mixing glassy carbon powder (Sigradur K, HTW, Hochtemperatur-Werkstoffe GmbH, Bonn, Germany) and MB-αZP or MB-αTP with paraffin oil (Fluka, Buchs, Switzerland) in an agate mortar. For 20 mg of carbon powder and MB-αZP or MB-αTP mixture, with a ratio of glassy carbon powder to MB-αZP or MB-αTP of 19:1 (w/w), 5 μL of paraffin oil were added. The size of the spherical glassy carbon particles was 0.4 – 1.2 μm. The obtained pastes were put into the cavity of a Teflon holder, in the bottom of which a piece of pyrolytic graphite was used for electric contact. The Teflon holder then was screwed onto a rotating disc electrode device (EG-G PAR, model 616, Princeton, USA) and was used as working electrode for cyclic voltammetry.

The home made glassy carbon rod electrodes were prepared by introducing glassy carbon rod into a Teflon holder, then was screwed onto a rotating disc electrode device (Radiometer Analytical, France) and was used as working electrode for cyclic voltammetry. The glassy carbon rod was thoroughly polished on alumina (1 μm Stuers, Copenhagen, Denmark), then rinsed with Milli-Q water. Chitosan solution was prepared by adding 10 mg chitosan (Sigma-Aldrich) to 10 mL of acetic acid (glacial acetic acid, Sigma) 0.1 M. Then a suspension of 1 g/L MB-CA in this solution was prepared. 5 μL from this suspension were placed onto clean GC electrode surface, and let to dry at room temperature.

The geometrical area of the prepared modified electrodes was 0.049 cm^2.

Electrochemical measurements. The measurements were performed using a BAS 100 W Electrochemical Analyzer (Bioanalytical Systems, West Lafayette, IN, USA), which was connected to a PC microcomputer for potential control and data acquisition. The modified GCEs were used as working electrode, a platinum ring as the counter electrode, and Ag|AgCl,KCl_{sat} as reference electrode. Cyclic voltammetry was carried out in 0.1 M solution of Tris (Sigma). The pH of the electrolyte solutions was adjusted to the desired values by adding HCl or KOH (Merck).

All experiments were performed in deoxygenated electrolytes by bubbling argon for 20 min before each measurement. Al reagents were used as received.

For each prepared modified glassy carbon, the surface coverage (Γ, mol cm^{-2}) was estimated through integration of the area of the wave registered with cyclic voltammetry.

NADH electro-oxidation study. The electrocatalytic oxidation of NADH using MB adsorbed onto MB-αZP, MB-αTP or CA modified glassy carbon electrodes were investigated through addition of freshly prepared NADH (Sigma) solution to the electrolyte solution. Investigations on the electrocatalytic oxidation of NADH were performed using cyclic voltammetry. For cyclic voltammetry measurements, the initial potential was -300 mV *versus* Ag|AgCl,KCl_{sat} for MB-αTP and MB-CA and -250 mV *versus* Ag|AgCl,KCl_{sat} for MB-αZP. The experiments were performed in the potential range: -300 to 100 mV *versus* Ag|AgCl,KCl_{sat} for MB-αTP and MB-CA and -250 to 100 mV *versus* Ag|AgCl,KCl_{sat} for MB-αZP.

ACKNOWLEDGMENTS

This work was possible with the financial support of the Sectorial Operational Programme for Human Resources Development 2007-2013, co-financed by the European Social Fund, under the project number POSDRU 89/1.5/S/60189 with the title „Postdoctoral Programs for Sustainable Development in a Knowledge Based Society”.

REFERENCES

1. W.J. Blaedel, R.A. Jenkins, *Analytical Chemistry,* **1975**, *47*, 1337-1338.
2. J. Moiroux, P.J. Elving, *Analytical Chemistry,* **1978**, *50*, 1056-1062.
3. C.I. Ladiu, I.C. Popescu, L. Gorton, *Journal of Solid State Electrochemistry,* **2005**, *9*, 296-303.
4. L. Gorton, A. Torstensson, A. Jaegfeldt, G. Johansson, *Journal of Electroanalytical Chemistry,* **1984**, *161*, 103-120.

5. L. Gorton, *Journal of the Chemical Society, Faraday Transaction* **1986**, *1*, 1245-1258.
6. C. Trobajo, S.A. Khainakov, A. Espina, J.R. Garcia, *Chemistry of Materials*, **2000**, *12*, 1787-1790.
7. C.V. Kumar, A. Chaudgari, *Microporous and Mesoporous Materials,* **2000**, *41*, 307-318.
8. Y. Ando, K. Sasaki, R. Adzic, *Electrochemistry Communication*, **2009**, *11*, 1135-1138.
9. Y. Zhang, D. Kang, M. Aindow, C. Erkey, *Journal of Physical Chemistry B*, **2005**, *109*, 2617-2624.
10. L. Gorton, E. Csoregi, E. Dominguez, J. Emmeus, G. Jonsson-Pettersson, G. Marko-Varga, B. Persson, *Analytica Chimica Acta,* **1991**, *250*, 203-248.
11. L. Gorton, *Electroanalysis,* **1995**, *7*, 23-45.
12. L. Gorton, E. Dominguez, *Reviews in Molecular Biotechnology,* **2002**, *82*, 371-392.
13. L. Gorton, E. Dominguez, in G.S. Wilson (Ed.), *Encyclopedia of Electrochemistry*, Wiley, New York **2002**, *9*, 11-31.
14. L.C. Cotet, A. Roig, I.C. Popescu, V. Cosoveanu, E. Molins, V. Danciu, *Revue Roumaine de Chimie,* **2007**, *52*, 1077-1081.
15. M.J. Honeychurch, G. A. Rechnitz, *Electroanalysis,* **1998**, *10*, 285-293.
16. L.T. Kubota, F. Munteanu, A. Roddick-Lanzilotta, A.J. McQuillan, L. Gorton, *Quimica Analitica,* **2000**, *19*, 15-27.
17. C.I. Ladiu, I.C. Popescu, R. Garcia, L. Gorton, *Revue Roumaine de Chimie,* **2007**, *52*, 67–74.
18. C.I. Ladiu, R. Garcia, I.C. Popescu, L. Gorton, *Chemical Bulletin of "Politehnica" University of Timisoara,* **2004**, *49*, 51.
19. C.I. Ladiu, R. Garcia, I.C. Popescu, L. Gorton, *Revista de Chimie (Bucuresti)*, **2007**, *58*, 465-469.

STUDIA UBB CHEMIA, LVII, 2, 2012 (p. 113 - 118)

HPLC ANALYSIS OF POLYPHENOLIC COMPOUNDS, PHYTOESTROGENS AND STEROLS FROM *GLYCYRRHIZA GLABRA* L. TINCTURE

IBRAHIM KHALAF[a], LAURIAN VLASE[b], BIANCA IVĂNESCU[c,*], DOINA LAZĂR[a], ANDREIA CORCIOVĂ[a]

ABSTRACT. The presence and quantification of polyphenolic compounds, phytoestrogens and sterols from *Glycyrrhiza glabra* tincture, was assessed through HPLC methods. Phenol carboxylic acids were present in larger quantities than flavonoids in tincture. p-Coumaric acid, ferulic acid, luteolin and apigenin were found and quantified in both hydrolyzed and unhydrolyzed samples. Kaempferol, fisetin, myricetin, hyperoside, quercitrin, isoquercitrin and rutoside could not be found in the analyzed samples. Regarding the phytoestrogens content, significant quantities of ononin and its aglycone formononetin were detected. Among sterols, the largest amount recovered in the tincture was beta-sitosterol and the smallest ergosterol.

Keywords: *polyphenolic compounds, phytoestrogens, sterols, HPLC-DAD, HPLC-MS, Glycyrrhiza glabra*

INTRODUCTION

The roots and rhizomes of *Glycyrrhiza glabra* L., licorice, have been used as an herbal medicine for more than 4000 years. Licorice contains a biologically active complex composed of saponins, mostly triterpenoid saponins - glycyrrhizin, a mixture of potassium and calcium salts of glycyrrhizic acid, liquiritic acid, glycyrretol, glabrolide, isoglabrolide and licorice acid, flavonoids, chalcones and coumarins. Other compounds are stilbenoids, fatty acids, phenols, lactones, asparagines, glucose, sucrose, starch, polysaccharides, and sterols. Licorice root exhibits a variety of useful pharmacological activities such as anti-inflammatory, antimicrobial, antioxidant, anticancer, immunomodulatory, hepatoprotective, antiviral, antispasmodic, demulcent, diuretic, emollient, expectorant, mild estrogenic, tonic and cardioprotective [1-8].

[a] "Grigore T. Popa" University of Medicine and Pharmacy Iasi, Faculty of Pharmacy, Department of Drugs Analysis, 16 Universitatii Street, RO-700115 Iasi, Romania
[b] „Iuliu Hatieganu" University of Medicine and Pharmacy Cluj –Napoca, Faculty of Pharmacy, Department of Pharmaceutical Technology and Biopharmaceutics, 13 Emil Isac Street, RO-400023 Cluj–Napoca, Romania
[c] "Grigore T. Popa" University of Medicine and Pharmacy Iasi, Faculty of Pharmacy, Department of Pharmaceutical Botany, 16 Universitatii Street, RO-700115 Iasi, Romania, * biancaivanescu@yahoo.com

Glycyrrhiza glabra L. is widespread in Syrian spontaneous flora and it is widely used in therapy for its pharmacological actions and also as an ingredient of soft drinks. We continue our phytochemical studies on licorice by analyzing the tincture which is a widely marketed commercial preparation. In the present study, we employed three methods of analysis previously developed in our work [9-11] in order to characterize polyphenolic compounds, phytoestrogens and sterols from a pharmaceutical form of drug administration.

For all analyses we have used high performance liquid chromatography coupled with DAD and mass spectrometry [12-15]. Eighteen polyphenolic compounds have been researched: one hydroxybenzoic acid, six cynnamic acid derivatives, four quercetin glycosides, and seven aglycones of flavonol and flavone type. Eight compounds with phytoestrogenic activity (seven isoflavones and one coumestan) and four sterols were also determined.

RESULTS AND DISCUSSION

Considering the conditions of the methods described in our previous papers (retention time, parameters of calibration curves, characteristic ions) we obtained the following results for the tincture sample. The amounts of polyphenolic compounds found in *Glycyrrhiza glabra* tincture are presented in Table 1, expressed in µg/ml tincture.

Table 1. The content (µg/mL) of polyphenolic compounds in *Glycyrrhiza glabra* tincture

Compound	MS identified		Content (µg/ml)	
	NH	H	NH	H
Gentisic acid	Yes	Yes	-	-
Caffeic acid	Yes	Yes	-	-
p-coumaric acid	Yes	Yes	1.270	13.859
Ferulic acid	Yes	Yes	1.560	25.912
Luteolin	Yes	Yes	0.620	0.966
Apigenin	Yes	Yes	1.708	2.361
Sinapic acid	Yes	Yes	-	9.534

NH non hydrolyzed sample; H hydrolyzed sample

Results show that phenol carboxylic acids were primarily extracted in tincture. Ferulic acid and p-coumaric acid are found in appreciable quantities, especially as esters. Sinapic acid was determined only in the hydrolyzed sample. Gentisic and caffeic acid could not be determined quantitatively in any of the samples, the amount was below the limit of quantification. As for flavonoids, in none of the samples were found kaempferol, fisetin, myricetin,

hyperoside, quercitrin, isoquercitrin or rutoside. Luteolin and apigenin are present both as free aglycones and in glycosides form, being found in larger quantities after hydrolysis.

Results obtained for phytoestrogens compounds from *Glycyrrhiza glabra* are presented in Table 2, expressed in ng/ml tincture.

Table 2. The content (ng/mL) of phytoestrogen compounds in *Glycyrrhiza glabra* tincture

Sample / **Compound**	**Tincture unhydrolyzed sample**	**Tincture hydrolyzed sample**
Daidzin	884.3	286.8
Genistin	0.0	251.2
Ononin	13744.6	11620.5
Daidzein	2672.3	2682.1
Glycitein	1237.7	1907.6
Genistein	513.2	531.3
Coumestrol	948.8	211.1
Formononetin	12749.0	10030.7

Ononin and its aglycon formononetin are found in large quantities in tincture, followed by daidzein and glycitein. There are also smaller amounts of daidzin, genistein and coumestrol. Genistin is present only in the hydrolyzed sample.

Sterols content from *Glycyrrhiza glabra* tincture are presented in Table 3. The tincture contains all four analysed sterols: beta-sitosterol, ergosterol, stigmasterol, campesterol. Beta-sitosterol and stigmasterol are predominant. Much lower amounts of campesterol and ergosterol were detected.

Table 3. The sterols content (ng/mL) in *Glycyrrhiza glabra* tincture

Compound	**Content (ng/ml)**
Ergosterol	1856.3
Stigmasterol	14847.5
Campesterol	4704.0
Sitosterol	27549.2

CONCLUSIONS

It is a well known fact that plant extracts contain a great number of pharmacologically active compounds which together form the phytocomplex. Each substance in the phytocomplex contributes to the overall therapeutic effect of the extract. Few commercial preparations with plant extracts that are in use nowadays are characterised and their chemical composition is known.

In this context, the current research tried to determine three groups of phytochemicals present in licorice tincture: polyphenolic compounds, phytoestrogens, and sterols. Among the polyphenolic compounds, the phenol carboxylic acids were found in significant quantities in the preparations, especially ferulic acid and p-coumaric acid. As for phytoestrogens, ononin and its aglycon formononetin were detected in appreciable amounts in tincture. Regarding the sterols content, the largest quantity recovered in licorice tincture was beta-sitosterol.

Although in minor quantities, the compounds identified in *Glycyrrhiza glabra* tincture contribute to the therapeutic effect of the biologically active complex. Our results allow a better characterization of the active principles from an herbal drug preparation of *Glycyrrhiza glabra.*

EXPERIMENTAL SECTION

Plant material: The root parts of *Glycyrrhiza glabra* were collected from north of Syria and air-dried at room temperature. Plants were identified by one of the authors and a voucher specimen (no. GG-0509) was deposited at the Pharmaceutical Botany Department, Faculty of Pharmacy, University of Medicine and Pharmacy, Iasi.

Sample preparation: Over 2 g of finely pulverized plant material was added to 20 g 96 % ethanol in a tightly closed container. The vessel was kept at room temperature for ten days, stirring 3-4 times daily. The liquid extract obtained was decanted and the residue was pressed. Extraction fluids were collected and homogenized; they are left to settle out for 6 days at 5-10 ^{0}C and then filtrated. In order to study the aglycones that can be obtained by hydrolysis, 0.5 ml of the tincture were treated with 0.5 ml 2 N hydrochloric acid (to determine polyphenols) or with 0.5 ml 6 N hydrochloric acid (to determine phytoestrogens) in a centrifuge tube. In parallel, extracts were diluted with equal quantities of water. The samples obtained were heated 40 minute at 80^{0}C on a water bath, and then centrifuged at 10,000 rpm. Supernatants were diluted and centrifuged again at 8000 rpm, filtered through a filter with 0.45 mm diameter pores and then injected into the chromatographic system.

Chemicals*:* Methanol of HPLC analytical-grade, chloroform, ethanol, acetic acid and hydrochloric acid of analytical-grade were purchased from Merck (Germany). Standards: caffeic acid, chlorogenic acid, p-coumaric acid, kaempferol, apigenin, rutoside, quercetin, quercitrin, isoquercitrin, fisetin, hyperoside, myricetin, daidzin, genistin, ononin, daidzein, genistein, formononetin, glycitein, coumestrol, beta-sitosterol, stigmasterol, campesterol and ergosterol from Sigma (Germany), ferulic acid, gentisic acid, sinapic acid, patuletin, luteolin from Roth (Germany) and caftaric acid from Dalton (SUA) were used.

Apparatus and chromatographic conditions: The analyses were carried out using an Agilent 1100 HPLC Series system equipped with a degasser, binary pump, autosampler, column thermostat, UV detector. The

HPLC was coupled with an Agilent Ion Trap 1100 VL mass detector. For the separation we used a reversed-phased Zorbax SB-C18 analytical column (100 mm x 3.0 mm i.d., 3.5 µm particle – for polyphenols and 100 mm x 3.0 mm i.d., 5µm particle – for sterols and phytoestrogens) fitted with precolumn Zorbax SB-C18, both operated at 48^0C (polyphenols), 50^0C (phytoestrogens), 40^0C (sterols).

The mobile phase was prepared as follows:

- ***polyphenols analysis***: methanol:acetic acid 0.1% (v/v), the elution began with a linear gradient (started at 5% to 42% methanol for the first 35 minutes), followed by isocratic elution (with 42% methanol for the next 3 minutes).

- ***phytoestrogens analysis:*** methanol:acetic acid 0.1% (v/v), gradient elution, as shown in Table 4.

Table 4. Composition of the mobile phase employed in the HPLC analysis of phytoestrogens

TIME (MIN)	COMPOSITION OF MOBILE PHASE (%)	
	methanol	acetic acid 0.1%
0	20	80
2	20	80
10	40	60
10.5	40	60
11.5	45	55
12.5	45	55

- sterols analysis: methanol:acetonitril 30:70 (v/v), isocratic elution.

The flow rate was 1 mL/min and the injection volume was 5 µL (for polyphenols and phytoestrogens analysis) and 4 µL (for sterols analysis).

The detection was performed in the following manner:

Polyphenols analysis was carried out by MS, using a mass spectrometer equipped with a Turbo-Ionspray (ESI - electrospray ionization) interface, working in negative ion mode. ESI settings were: negative ionization, ion source temperature 360^0C, gas: nitrogen, flow rate 12 L/min, nebuliser: nitrogen at 70 psi pressure, capillary voltage 3000 V. The analysis mode was multiple reaction monitoring (MRM) and single ion monitoring (SIM). UV detection and quantification was performed at 330 nm for phenol carboxylic acids and at 370 nm for flavonoids using a G1315A diode array detector system.

Phytoestrogen were analysed by MS, ESI settings were: negative ionization, ion source temperature 360^0C, gas: nitrogen, flow rate 12 L/min, nebuliser: nitrogen at 65 psi pressure, capillary voltage 4500 V. For aglycones was used the Single Ion Monitoring (SIM) analysis mode and for glycosides the Single Reaction Monitoring (SRM) mode.

Sterols were analysed by MS, using an APCI interface, positive ion mode, gas – nitrogen, flow rate 7 L/min, ion source temperature 250^0C, nebuliser: nitrogen at 50 psi pressure, capillary voltage -4000 V.

All chromatographic data were processed using ChemStation (vA09.03) software and Data Analysis (v 5.3) from Agilent, USA.

REFERENCES

1. M.N. Asl, H. Hosseinzadeh, *Phytotherapy Research*, **2008**, *22*, 709.
2. J. Cheel, P. Van Antwerpen, L. Tumova, G. Onofre, D. Vokurkova, K. Zouaoui-Boudjeltia, M. Vanhaeverbeek, J. Neve, *Food Chemistry*, **2010**, *122*, 508.
3. L. Siracusa, A. Saija, M. Cristani, F. Cimino, M. D'Arrigo, D. Trombetta, F. Rao, G. Ruberto, *Fitoterapia*, **2011**, *82*, 546.
4. G. Chen, L. Zhu, Y. Liu, Q. Zhou, H. Chen, J. Yang, *Phytotherapy Research*, **2009**, *23*, 498.
5. K. Nakagawaa, K. Hosoea, T. Hidakab, K. Nabaec, M. Kawabec, M. Kitanod, *Nutrition Research*, **2010**, *30*, 74.
6. W. Xu-Yinga, L. Minga, L. Xiao-Dong, H. Pinga, *Chemico-Biological Interactions*, **2009**, *181*, 15.
7. B. Liu, J. Yang, Q. Wen, Y. Li, *European Journal of Pharmacology*, **2008**, *587*, 257.
8. E.H. Jo, S.H. Kim, J.C. Ra, S.R. Kim, S.D. Cho, J.W. Junga, S.R. Yanga, J.S. Parka, J.W. Hwanga, O.I. Aruomaa, T.Y. Kima, Y.S. Leea, K.S. Kanga, *Cancer Letters*, **2005**, *230*, 239.
9. I. Khalaf, L. Vlase, D. Lazar, A. Corciova, B. Ivanescu, M. I. Lazar, *Farmacia*, **2010**, *58*, 89.
10. I. Khalaf, L. Vlase, D. Lazar, A. Corciova, B. Ivanescu, M. I. Lazar, *Farmacia*, **2010**, *58*, 416.
11. I. Khalaf, L. Vlase, D. Lazar, B. Ivanescu, A. Corciova, *Studia UBB Chemia*, **2011**, *61*, 97.
12. D. Hanganu, L. Vlase, N. Olah, *Notulae Botanicae Horti Agrobotanici Cluj*, **2010**, *38*, 57.
13. S. Leucuta, L. Vlase, L. Radu, C. Fodorea, S. Gocan, *Journal of Liquid Chromatography & Related Technologies*, **2005**, *28*, 3109.
14. C.M. López Ortíz, M.S. Prats Moya, V. Berenguer Navarro, *Journal of Food Composition and Analysis*, **2006**, *19,* 141.
15. N.K. Olah, D. Hanganu, L. Vlase, C. Cobzac, *Studia UBB Chemia*, **2010**, *55*, 353.

STUDIA UBB CHEMIA, LVII, 2, 2012 (p. 119 - 127)

NOVEL PHOSPHAGERMAPROPENES, PRECURSORS FOR HETEROALLENES STABILIZED THROUGH INTRAMOLECULAR COORDINATION

PETRONELA M. PETRAR[a], RALUCA SEPTELEAN[a], AGOTA BARTOK[a], NOEMI DEAK[a], GABRIELA NEMES[a]

ABSTRACT. Potential precursors of phosphagermaallenes based on the use of dimethyl-benzyl-amine as a substituent on the group 14 element were designed. The proper orientation of the lone pair on the nitrogen towards the germanium atom could enhance the electron density around the germanium, thus stabilizing the –P=C=Ge< unit. Three novel phosphagermapropenes have been obtained and evidenced through NMR spectroscopy. The solid state structure of a novel organometallic germanium derivatives is also discussed.

Keywords: *phosphagermapropenes, heteroallenes, 2-substituted (N,N-dimethyl-aminobenzyl ligands, organogermanium derivatives*

INTRODUCTION

The synthesis of compounds in which two, or even three carbon atoms of an allene are formally replaced by heavier elements of group 14 or 15, has constituted a new challenge in organometallic chemistry [1-4]. Due to the presence of two unsaturations, such heteroallenes were thought to possess a rich and versatile chemistry and to be very useful building blocks in organometallic chemistry.

Unlike the 1,3-dimetallaallenes $>E_{14}=C=E_{14}<$, their phosphorus counterparts, 1,3-phosphametallaallenes $–P=C=E_{14}<$, have been experimentally investigated [5]. The recent studies reveal that for the stabilization of the P=C=Ge framework a greater steric shielding is required [6]. This was achieved by grafting bulky organic groups on the germanium atom. The 1,3-phosphagermaallene Mes*P=C=GeTip(*t*Bu) (Tip=2,4,6-tri-*iso*-propyl-phenyl), the first stable heteroallene that contains two heavy double-bonded group 14 and 15 elements, was obtained quantitatively as an orange solid by the dehalogenation of dihalophosphagermapropene with *tert*-butyllithium at -80 °C [5c].

[a] "Babeş-Bolyai" University of Cluj-Napoca, Faculty of Chemistry and Chemical Engineering, Arany Janos Street 11, 400028 Cluj-Napoca, Romania

While exploring new ways to further stabilize the -P=C=Ge< unit in phosphagermaallenes, we have envisaged the increase of the electron density on the germanium atom through its coordination with an electron-donor atom (scheme 1). The electronic influence, combined with the steric hindrance afforded by the coordinating atom can be enhanced by a chelate effect.

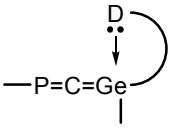

Scheme 1

This can be attained by functionalizing the germanium precursor with a pendant arm ligand containing a nitrogen atom as the electron-donor atom and it has already been used in the stabilization of various doubly-bonded compounds of germanium such as germathiones >Ge=S [7], germaselones >Ge=Se [8] and germatellones >Ge=Te [8].

RESULTS AND DISCUSSIONS

In order to obtain new products containing stable P=C-Ge or P=C=Ge units, the dimethyl-benzylamine group can be employed as a pendant arm ligand. To this purpose the synthesis of 2-(*tert*-butyldichlorogermyl)phenyl)-*N,N*-dimethylmethanamine **1** has been carried out through the series of reactions represented in scheme 2. The *ortho*-lithium N,N-dimehyl-benzylamine was first prepared according to the method of Noltes [9]. The selectivity of the *ortho*-lithiation was explained by a strong coordination between the nitrogen and lithium atoms. Addition to *t*BuGeCl$_3$ [10] afforded **1** in a good yield.

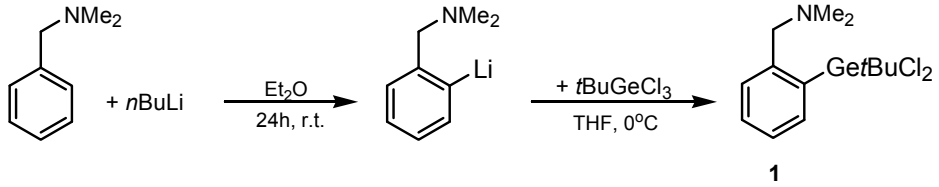

Scheme 2

A by-product of the reaction depicted in scheme 2 was the germane $(Me_2NCH_2C_6H_4)_2$(*t*Bu)GeCl **4**, for which the solid state structure was determined and will be discussed herein.

Derivative **1** was characterized through its proton and carbon NMR spectra. From the available data, it was impossible to determine if the nitrogen atom was coordinated to the germanium atom since in both cases

(coordination or lack of thereof) the two Me group and the two methylenic protons are equivalent.

Reaction of the dichlorogermane **1** with the lithium derivative of $Mes^*P=CCl_2$ at low temperature led to the phosphagermapropene **2** in a poor yield (scheme 3).

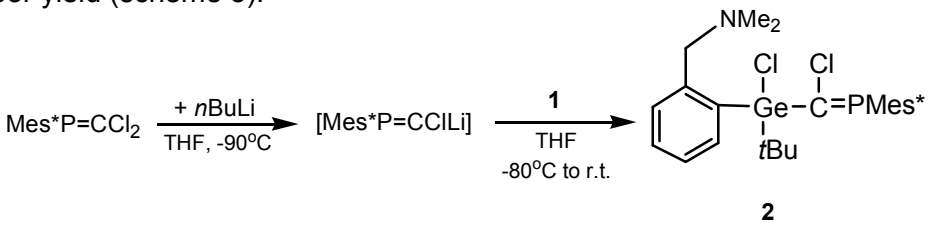

2

Scheme 3

One of the major by-products was Mes*P=C(Cl)H, due to the final hydrolysis of Mes*P=C(Cl)Li which had not reacted with **1**. The formation of **2** was evidenced through ^{31}P NMR spectroscopy. The signal appears at 300.4 ppm, as expected for a phosphagermapropene, along with the characteristic peak for Mes*P=C(Cl)H, in a 3.6:1 ratio. Although attempts to isolate compound **2** failed, its ^{1}H NMR spectrum shows a broad signal for the methylene protons on the pendant arm indicating in this case the coordination of the nitrogen atom to the germanium.

The N→Ge coordination should be less favorable in **2** than **1** for two reasons: the greater steric congestion which can prevent the approach of the NMe_2 moiety and the less electrophilic character of the germanium atom substituted by only one chlorine atom instead of two. As the coordination was proved in the case of **2**, we can reasonably postulate that such coordination also exists in **1** [11].

An alternative synthetic route involved the preparation of Mes*P=C($SnMe_3$)Cl **3**, as indicated in scheme 4, to obtain the phosphagermaallene precursor Mes*P=C($SnMe_3$)-Ge($Me_2NCH_2C_6H_4$)(*t*Bu)Cl. The latter could eliminate Me_3SnCl to afford the P=C=Ge unit without using a lithium compound.

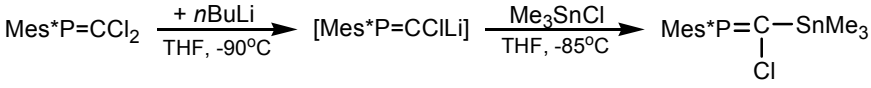

3

Scheme 4

Mes*P=C($SnMe_3$)Cl **3** was evidenced by ^{31}P NMR (with a chemical shift at 280.5 ppm) and the resulting reaction mixture was used without further purification. Treatment with *t*BuLi and the subsequent addition of ($Me_2NCH_2C_6H_4$)(*t*Bu)$GeCl_2$ does not lead to the expected stannylated-

phosphagermapropene, but affords a mixture of **2** and Mes*P=C(Cl)H, in about the same ratio as observed in the case of the previously described synthetic route (see scheme 5).

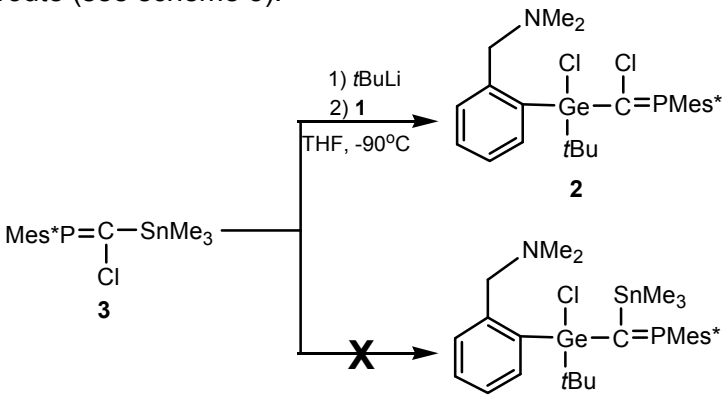

Scheme 5

The formation of **2** can be explained by the preliminary cleavage reaction of the weak C-Sn bond by *t*BuLi, leading to Me_3SnBu and Mes*P=C(Cl)Li followed by the subsequent reaction with **1** and/or hydrolysis.

Study of germane $(Me_2NCH_2C_6H_4)_2tBuGeCl$ 4

The structure of compound **4**, obtained as a by-product in the reaction between $C_6H_4(Li)CH_2NMe_2$ and $tBuGeCl_3$, was determined by X-ray diffraction (figure 1), showing that two halogen atoms of *t*BuGeCl$_3$ have been replaced by two $Me_2NCH_2C_6H_4$ moieties. The Ge(1)-C(1) (1.919(11) Å) and Ge(1)-C(10) (1.931(10) Å) distances lie in the normal range for such bonds between a germanium atom and the *ipso*-carbon of an aromatic ring. By contrast, the Ge(1)-C(19) distance was slightly elongated to 1.993(14) Å) due to the steric hindrance of the *t*Bu group.

The most interesting feature was the presence of a distorted tetrahedral geometry around the germanium atom: the sum of angles C(1)Ge(1)C(10), C(1)Ge(1)C(19) and C(10)Ge(1)C(19) was 350.5°, not too far from 360° for a planar geometry. In a tetrahedral structure, the sum of these angles should be 327.7°. The distance of the Ge atom to the C(1)C(10)C(19) plane was only 0.35 Å. Thus, the four atoms C(1), C(10), C(19) and Ge(1) are roughly in a plane. The Ge(1)-Cl(1) bond length (2.253 Å) is slightly elongated compared to standard Ge-Cl distances (2.09 to 2.21 Å) [14b]. The nitrogen atom N(1) is far from the germanium atom (4.724 Å), but the nitrogen atom N(2) is closer (3.107 Å). Even if the distance is long for an interaction between the Ge and N(2) atoms, the elongated Ge-Cl bond and the tendency to a planar geometry for the GeC_3 skeleton are in agreement with a weak coordination.

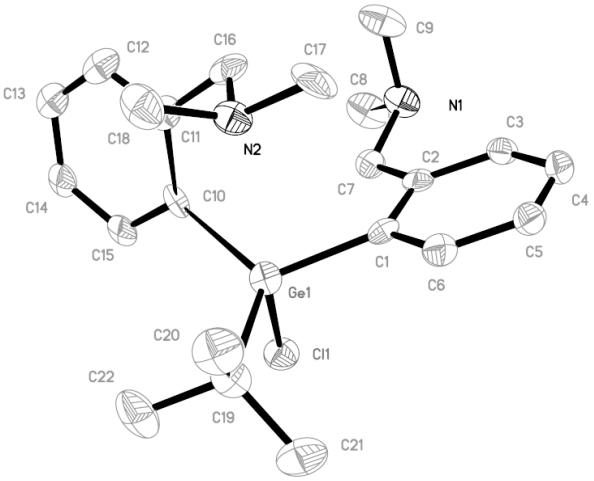

Figure 1. Molecular structure of **4** (thermal ellipsoids drawn at the 50% probability level); hydrogen atoms are omitted for clarity; selected bond lengths (Å) and angles (°).

Ge(1)-C(10): 1.919(11); Ge(1)-C(1): 1.931(10); Ge(1)-C(19): 1.993(14); Ge(1)-Cl(1) 2.253(4); C(2)-C(7): 1.515(14); C(7)-N(1): 1.451(16); C(11)-C(16): 1.517(15); C(16)-N(2); 1.473(14); C(10)-Ge(1)-C(1): 117.5(5); C(10)-Ge(1)-C(19): 117.3(5); C(1)-Ge(1)-C(19): 115.7(5); C(10)-Ge(1)-Cl(1): 100.6(4); C(1)-Ge(1)-Cl(1): 100.8(3); C(19)-Ge(1)-Cl(1): 99.6(4); Ge(1)-N(1): 4.724; Ge(1)-N(2): 3.107.

Action of tBuLi on derivative 2

The reaction of **2** with *tert*-butyllithium was followed by ^{31}P NMR techniques. After the addition of the lithium reagent and warming up to room temperature, the signal corresponding to the phosphagermapropene **2** disappears and two other peaks appear at 403.3 and 322.2 ppm (d, J_{PH} = 24.85 Hz). The more deshielded signal at 403 ppm could reasonably be assigned to the lithium compound **5** (scheme 6), stabilized by a possible interaction with the amino group (such a deshielded signal like the one at 441.4 ppm was observed in a phosphasilapropenyl derivative with a similar structure Mes*P=C(Li)SiCl [12].

When the reaction mixture was kept under an inert atmosphere, the amount of the compound corresponding to the signal at 322 ppm increased.

Although attempts to separate the mixture and further analyze the two derivatives are still in progress, we have assigned the signal at 322 ppm to **7**, the hydrolysis product of **5**, which can also be used as a precursor in the synthesis of the desired phosphagermaallene.

Subsequent treatment of **5** with Me_3SnCl led to the shift of the signal to a higher field (392.6 ppm), which could be explained by the formation of **6** (scheme 6).

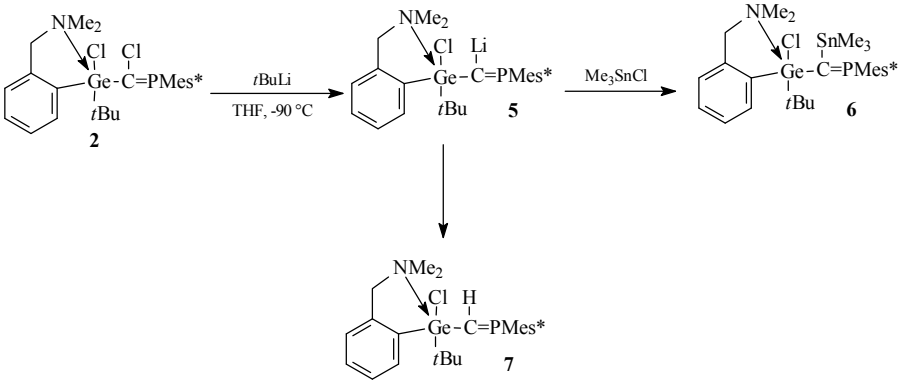

Scheme 6

A signal at this field was characteristic of a Mes*P=C derivative, with two electropositive groups on the doubly bonded carbon atom. For example Mes*P=C($SiMe_3$)$_2$ with two $SiMe_3$ group which have about the same electronic proprieties as Me_3Sn and R(*t*Bu)ClGe gives a signal at 393 ppm [13] and the rather similar derivative Mes*P=C($SnMe_3$)$_2$ gives a signal at 386.7 ppm [14].

Heating **5** or **6** to get the expected phosphagermaallene by elimination of LiCl or Me_3SnCl was unsuccessful. However, new attempts will be made using other solvents or involving heating in a sealed tube.

CONCLUSIONS

Several routes to obtain phosphagermaallenes stabilized through electronic effects induced by the presence of a pendant arm ligand on the germanium atom were investigated. The increased reactivity of the phosphagermapropenes and their lithium derivatives leads to poor yields and the reaction parameters are yet to be perfected, but three novel precursors in the synthesis of phosphagermaallenes, Mes*P=C(Cl)Ge(Me_2NR)*t*BuCl **2**, Mes*P=C($SnMe_3$)Ge(Me_2NR)*t*BuCl **6** and Mes*P=C(H)-Ge(Me_2NR)*t*BuCl **7** (R=$CH_2C_6H_4$) have been obtained and evidenced through NMR spectroscopy. A new organometallic derivative of germanium, ($Me_2NCH_2C_6H_4$)$_2$*t*BuGeCl **4**, has also been characterized and its structure in solid state has been determined through X-ray diffraction.

EXPERIMENTAL PART

General procedures

All experiments were carried out in flame-dried glassware under an argon atmosphere using high-vacuum-line techniques. Solvents were dried and freshly distilled on drying agents and carefully deoxygenated on a

vacuum line by several “freeze-pump-thaw” cycles. NMR spectra were recorded in $CDCl_3$ on the following spectrometers: ^{1}H, Bruker Avance 300 (300.13 MHz) and Avance 400 (400.13 MHz); $^{13}C\{^{1}H\}$, Bruker Avance 300 (75.47 MHz) and Avance 400 (100.62 MHz) (reference TMS), ^{31}P, Bruker AC200 at 81.02 MHz (reference H_3PO_4). Melting points were determined on a Wild Leitz-Biomed apparatus. Mass spectra were obtained on a Hewlett-Packard 5989A spectrometer by EI at 70 eV.

Synthesis of 2-(tert-butyldichlorogermyl)phenyl)-N,N-dimethylmethan-amine 1

To 4.5 ml (4 g, 29 mmol, 10% excess) of $PhCH_2NMe_2$ in 30 ml of ether, 16.25 ml *n*BuLi 1.6 M (26 mmol) were added dropwise and then the reaction mixture was stirred at room temperature for 24 hours, when a white precipitate appeared, and then it was cooled down to 0 °C. A solution of 6.25 g of *t*BuGeCl_3 (26 mmol) in 40 ml of THF was cooled to 0 °C and then cannulated drop by drop to the lithium derivative of the amine. The mixture was allowed to react for ½ hours and then the solvents were removed under vacuum and replaced with 40 ml of pentane. Lithium salts were separated by filtration and the solution was stored at -25 °C for 24 hours. The solution was concentrated until **1** precipitates as a white solid (7 g, η = 60 %).

δ **^{1}H** (300 MHz): 1.33 (s, 9H, *t*Bu, C(C$\underline{H}_3$)$_3$); 2.17 (s, 6H, methyl, C$\underline{H}_3$); 3.61 (s, 2H, methylene, C$\underline{H}_2$); 7.39-8 (m, 4H, arom H)

δ **^{13}C** (75.5 MHz): 27.08 (*t*Bu, C(C$\underline{H}_3$)$_3$) 38.26(*t*Bu, $\underline{C}$(CH$_3$)$_3$); 45.35 (Me, $\underline{C}$H$_3$); 63.43(methylene, $\underline{C}$H$_2$); 127.30-144.84 (arom C)

Transparent crystals are obtained from the pentane solution stored at room temperature and were later identified by X-ray crystallography as derivative **4**.

δ **^{1}H** (300 MHz, C_6D_6): 1.48 (s, 9H, *t*Bu, C(C$\underline{H}_3$)$_3$), 1.70 (s, 12H, NC$\underline{H}_3$), 2.92 (d, 2H, C$\underline{H}_2$, $^{2}J_{HH}$ = 12 Hz), 3.26 (d, 2H, C$\underline{H}_2$, $^{2}J_{HH}$ = 12 Hz), 7.15-7.20, 8.13-8.19 (broad signals, 8H, arom H)

Synthesis of ($Me_2NCH_2C_6H_4$)tBuGe(Cl)C(Cl)=PMes 2*

To 2.6 g (7.2 mmol) of Mes*P=CCl_2 in 40 mL of THF cooled at -95 °C, 4.95 mL of *n*BuLi 1.6 M in hexane (10% excess) were added dropwise. The reaction mixture was stirred at low temperature (-75 °C) for 45 minutes. A solution of 2.4 g of **1** in 30 ml of THF was cannulated slowly on to the lithium derivative, after it had been previously cooled down to -70 °C. The reaction mixture was then allowed to gradually warm up to room temperature and THF was removed under vacuum. Replacement with pentane allowed for the precipitation and separation of the lithium salts. ^{31}P-NMR spectra indicates the formation of **2**, which could not be separated from the by-product Mes*P=CHCl. The estimated yield (in ^{31}P NMR) was 40%.

δ **^{31}P** (121.5 MHz): 300.3 ppm

*Attempted Synthesis of ($Me_2NCH_2C_6H_4$)tBuGe(Cl)C($SnMe_3$)=PMes**

To a solution of 2.6 ml of Mes*P=CClLi in 20 ml THF, prepared as described above, 10 ml of a THF solution of Me_3SnCl_2 (0.52 g, 2.6 mmol) were added dropwise at -70 °C. The resulting mixture was used without any further purification; as Mes*PCCl($SnMe_3$) was identified by ^{31}P NMR to form in almost quantitative yield. 2 ml of *t*BuLi 1.5M in hexane were then added at low temperature and after 15 minutes, 0.9 g (2.6 mol) of **1** in 15 ml THF were cannulated. The solution was allowed to slowly warm up at room temperature. The formation of the expected Mes*P=C($SnMe_3$)Ge($Me_2NCH_2C_6H_4$)(Cl)*t*Bu was not evidenced, instead, derivative **1** was formed (δ^{31}**P** :300.3 ppm).

Action of tBuLi on 2

To the THF solution of a mixture of **2** and Mes*P=CHCl (1.55 g, in a 3.6:1 molar ratio), 2 ml *t*BuLi 1.5M in pentane were added at -90 °C. The solution was allowed to warm up to room temperature, and then the reaction products were characterized by ^{31}P-NMR and the lithium derivative **5** was assigned the peak at 403 ppm. At room temperature, only the hydrolysis product of the lithioderivative, compound **7**, was observed in phosphorus NMR (δ ppm: 322.2 ppm (d, J_{PH} = 24.85 Hz)). Upon adding an excess of Me_3SnCl to a sample solution of **5**, the signal shifted at higher fields, which was consistent with the formation of **6**.
δ^{31}**P** (121.5 MHz): 147 ppm

ACKNOWLEDGEMENTS

The authors wish to thank Dr Jean Escudié for useful discussions. R.S. thanks CNCSIS for funding through project PD-438. A.L. is funded by a Ph.D. scholarship through contract no. POSDRU/88/1.5/S/60185 – "Innovative Doctoral Studies in a Knowledge Based Society" Babeş-Bolyai University, Cluj-Napoca, Romania.

N.D. thanks Babeş-Bolyai University for the awarded scholarship.

REFERENCES

[1] J. Escudié, H. Ranaivonjatovo, *Organometallics*, **2007**, *26,* 1542.

[2] For reviews on heteroallenes, see refs: (a) J. Escudié, H. Ranaivonjatovo, L. Rigon, *Chem. Rev.,* **2000**, *100*, 3639. (b) B. Eichler, R. West, *Adv. Organomet. Chem.,* **2001**, *46*, 1. (c) M. Yoshifuji, K. Toyota, in *The Chemistry of Organosilicon Compounds*; Z. Rappoport, Y. Apeloig, Eds.; Wiley: Chichester, U.K., **2001**; Vol. 3, p. 491. (d) J. Escudié, H. Ranaivonjatovo, M. Bouslikhane, Y. El Harouch, L. Baiget, G. Cretiu Nemes, *Russ. Chem. Bull.,* **2004**, *53*, 1020.

[3] R. Appel, *Multiple Bonds and Low Coordination in Phosphorus Chemistry*, Georg Thieme Verlag: Stuttgart, Germany, **1990**, p. 157.

[4] J. Escudié, G. Nemes, *Comptes Rendus Chimie*, **2010**, *13*, 954.

[5] (a) L. Rigon, H. Ranaivonjatovo, J. Escudié, A. Dubourg, J.-P. Declercq, *Chem. Eur. J.,* **1999**, *5*, 774. (b) H. Ramdane, H. Ranaivonjatovo, J. Escudié, S. Mathieu, N. Knouzi, *Organometallics,* **1996**, *15*, 3070. (c) Y. El Harouch, H. Gornitzka, H. Ranaivonjatovo, J. Escudié, *J. Organomet. Chem.,* **2002**, *643-644*, 202.

[6] D. Ghereg, E. Andre, H. Gornitzka, J. Escudie, F. Ouhsaine, N. Saffon, K. Miqueu, J.M. Sotiropoulos, *Chem. Eur. J.*, **2011**, *45*, 12763. (b) D. Ghereg, H. Gornitzka, J. Escudie, *Eur. J. Inorg. Chem.*, **2011**, *2*, 281. (c) D. Ghereg, H. Gornitzka, J. Escudie, S. Ladeira, *Inorg. Chem.*, **2010**, *49*, 10497. (e) G. Dumitru, E. Andre, J. M. Sotiropoulos, K. Miqueu, H. Gornitzka, J. Escudie, *Angew. Chem. Int. Ed. Engl.*, **2010**, *49*, 8704. (f) P.M. Petrar, G. Nemes, I. Silaghi-Dumitrescu, H. Ranaivonjatovo, H. Gornitzka, J. Escudie, *Chem. Commun.*, **2007**, 4149.

[7]. a) W.-P. Leung, K.-H. Chong, Y.-S. Wu, C.-W. So, T.C.W. Mak, *Eur. J. Inorg. Chem.*, **2006**, *4*, 808. (b) W.-P. Leung, K.-H. Chong, Z.-Y. Zhou, T.C.W. Mak, *Organometallics*, **2000**, *19*, 293. (c) M. Veith, A. Rammo, Z. *Anorg. Allg. Chem.*, **1997**, *623*, 861.

[8] G. Ossig, A. Meller, C. Brönneke, O. Müller, M. Schafer, R. Herbst-Irmer, *Organometallics*, **1997**, *16*, 2116.

[9] G. Van Koten, J.T.B.H. Jastrzebski, J.G. Noltes, W.M.G.F. Pontenagel, J. Kroon, A.L. Spek, *J. Am. Chem. Soc.*, **1978**, *100*, 5021.

[10]. H. Puff, S. Franken, W. Schuh, W. Schwab, *J. Organomet. Chem.*, **1983**, *254*, 33.

[11] C. Brelière, F. Carré, R.J.P. Corriu, A. De Saxce, M. Poirier, G. Royo, *J. Organomet. Chem.*, **1981**, *205*, C1.

[12] G. Nemes, H. Ranaivonjatovo, J. Escudié, I. Silaghi-Dumitrescu, L. Silaghi-Dumitrescu, H. Gornitzka, *Eur. J. Inorg. Chem.*, **2005**, 1109.

[13] A.H. Cowley, R.A. Jones, J.G. Lasch, N.C. Norman, C.A. Stewart, A.L. Stuart, J.L. Atwood, W.E. Hunter, H.-M. Zhang, *J. Am. Chem. Soc.*, **1985**, *106*, 7015.

[14] S.I. Goede, F. Bickelhaupt, *Chem. Ber.*, **1991**, *124*, 2677.

STUDIA UBB CHEMIA, LVII, 2, 2012 (p. 129 - 137)

MULTI-SUBSTRATE KINETIC RESOLUTION SCREENING METHOD FOR LIPASE BIOCATALYSTS

MARTON ŐSZE[a], DIÁNA WEISER[a], GÁBOR HORNYÁNSZKY[a], LÁSZLÓ POPPE[a, b,*]

ABSTRACT. Development of efficient screening methods has increasing significance in rapid evaluation of novel biocatalysts. Our study reveals the scopes and limitations of a novel GC-based multi-substrate screening method for initial characterization of the activity and selectivity of lipase biocatalysts. The multi-substrate kinetic resolution of four different racemic alcohols **1-4a** by native and immobilized biocatalysts were analyzed by GC using enantiomer selective stationary phase.

Keywords: *lipase, immobilization, biocatalysis, multi-substrate screening*

INTRODUCTION

The use of enzymes in industrial processes is of growing interest due to its potential for the straightforward selective synthesis of many complex chemicals [1]. Discovery of novel biocatalysts or further development and optimization of the already known ones require efficient and robust screening methods. Our goal was to develop a rapid and efficient method for screening various lipases in their native or immobilized form to select the most promising biocatalyst candidates for enantioselective biotransformations.

An example was found for HPLC-based multi-substrate screening of lipase-catalyzed kinetic resolution of arylalkylethanols with succinic anhydride as acylating agent [2]. In our hands, a GC-based multi-substrate kinetic resolution method proved to be efficient in testing the bioimprinting effect in sol-gel immobilization of lipases [3]. The multi-substrate mixture consisted of a series of racemic, aliphatic alcohols of various chain lengths. In this study our goal was to explore the generality, the scopes and limitations of the GC-based multi-substrate kinetic resolution screening method to characterize the biocatalytic performance of various forms of lipases.

[a] Budapest University of Technology and Economics, Department of Organic Chemistry and Technology, and Research Group for Alkaloid Chemistry of HAS, Műegyetem rkp 3, H-1111, Budapest, Hungary, * poppe@mail.bme.hu
[b] SynBiocat Ltd., Lázár Deák u. 4/1, H-1173 Budapest, Hungary

RESULTS AND DISCUSSION

Four different racemic alcohols of (*rac*-**1-4a**) were selected as components of a multi-substrate system for rapid screening the biocatalytic behavior of various lipase biocatalysts (*Scheme 1*).

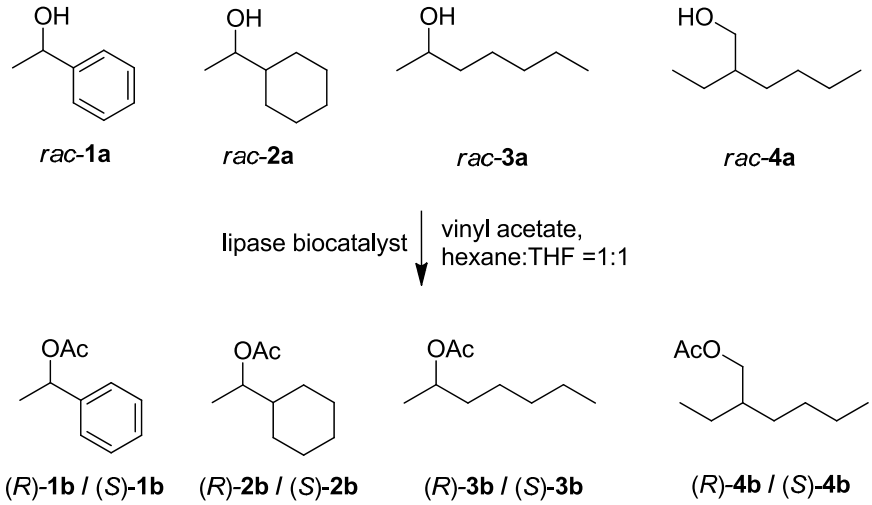

Scheme 1. The multi-substrate screen for lipases

The test system for screening lipase biocatalysts was based on acylation reaction of a mixture of four racemic alcohols, namely 1-phenylethanol (*rac*-**1a**), 1-cyclohexylethanol (*rac*-**2a**), 2-heptanol (*rac*-**3a**) and 2-ethyl-1-hexylethanol (*rac*-**4a**). Importantly, all enantiomers of the test substrates **1-4a** and all enantiomers of the product acetates **1-4b** proved to be separable by GC in reasonably short time (*Figure 1*).

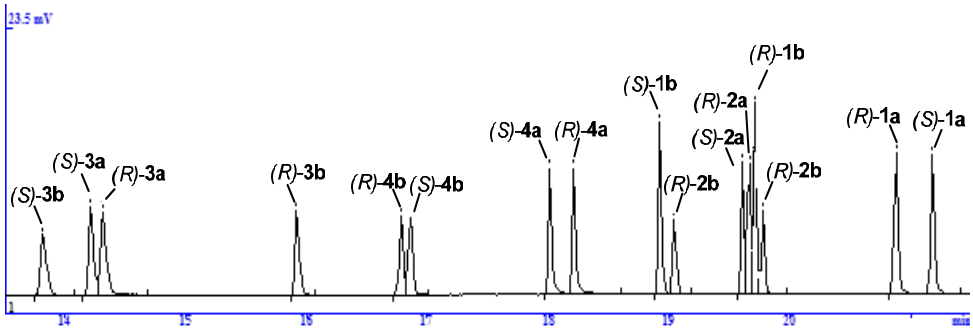

Figure 1. A chromatogram of rac-**1-4a** and rac-**1-4b** by enantiomer selective GC

After adjusting the GC method by racemic substrates, we demonstrated the performance of this method by using commercial and in-house-made lipase biocatalysts.

First, the method for was validated by comparing single-substrate (*1SS*) and the two-substrate screening (*2SS*) results. The kinetic resolution of 1-phenylethanol (rac-**1a**) and 2-heptanol (rac-**3a**) with lipase AK as biocatalyst were carried out in hexane:tetrahydrofuran solvent mixture using vinyl acetate as acylating agent. Good accordance were found in the conversion (*Figure 2*) and the enantiomeric excess (*Figure 3*) of single-substrate and two-substrate systems.

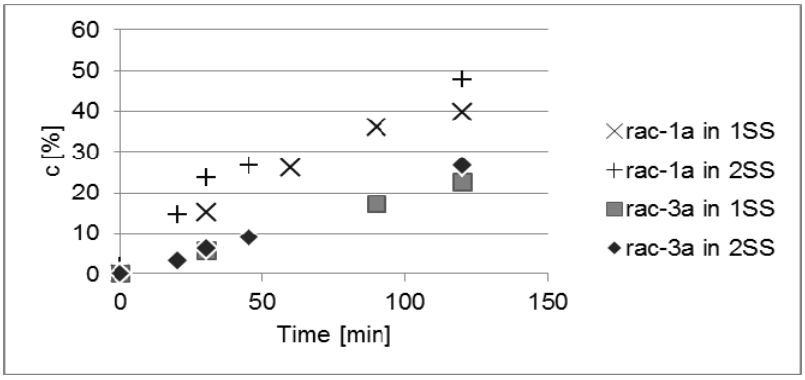

Figure 2. Comparison of the conversion course of the single (1SS) and the two-substrate (2SS) reactions by lipase AK catalyst

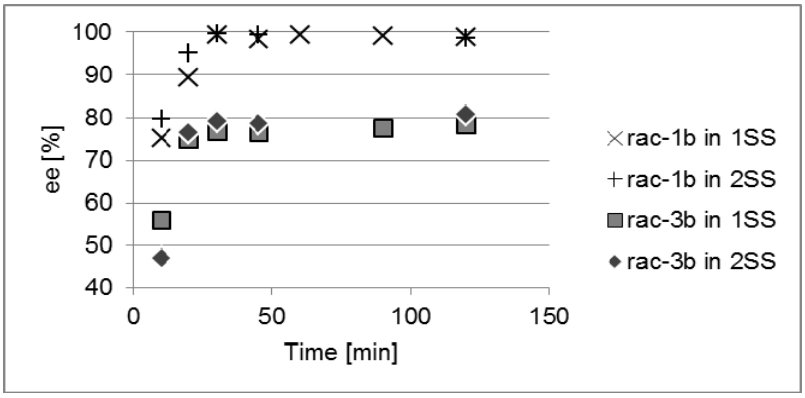

Figure 3. Comparison of the enantiomeric excess of products **1b** and **3b** of the single- (1SS) and the two-substrate (2SS) reactions by lipase AK catalyst

Next, a hydrolysis test with **1b** and **3b** was performed to determine its influence on the screening method (*Figure 4*). The hydrolysis test indicated that *rac*-**1b** hydrolyzed rapidly: more than 10% of the racemic acetate was transformed into its alcohol form (*R*)-**1a** after 8 hours due to the sensitivity of the forming ester (*R*)-**1b** to hydrolysis (i.e. the reverse process of the screening reaction). Consequently, only the results from the first 4 hours period were considered as reliable in our further investigations.

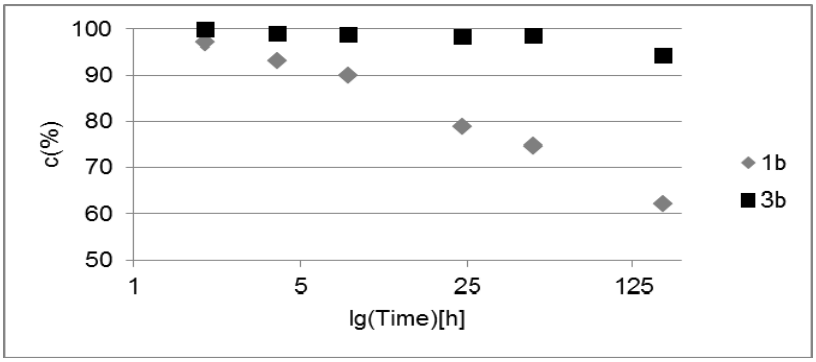

Figure 4. Hydrolysis of **1b** and **3b** catalyzed by lipase AK

All tested lipases proved to be active but non-selective towards *rac*-**4a** (0% ee for both **4a** and **4b**). Therefore, for sake of better transparency, the results with **4a** will not be shown in the following diagrams. Our multi-substrate test after 4 hours revealed that four lipases BUTE 3A, BUTE 3B, AK or NOV435 were significantly more active than other lipases (AYS, CCL, M, PPL, PS, R and TL IM) (*Figure 5*).

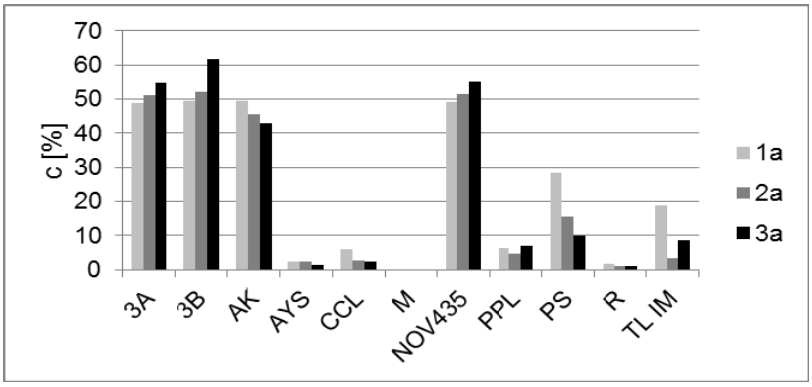

Figure 5. Conversions of **1-3a** with in-house-made and commercial lipases (4 h)

Most of the lipases were quite selective towards *rac*-**1a** and *rac*-**2a**, and less selective towards the acyclic alcohol *rac*-**3a** (*Figure 6*). Among the tested lipases, AYS, CCL, M, PPL and R showed significantly lower selectivity than the others (<80% ee for **1-3b** after 4 h) (*Figure 6*).

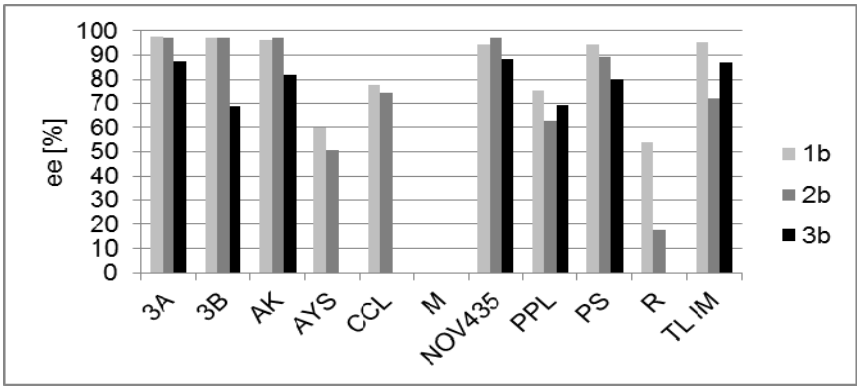

Figure 6. Enantiomeric excess of **1-3b** using in-house-made and commercial lipases (4 h)

Finally we demonstrated the performance of our method by characterization of eight various sol-gel immobilized lipase AK preparations (*Table 1*) by their productivity (*Figure 7*) and selectivity (*Figure 8*).

Table 1. Composition of the sol-gel immobilized lipase AK enzymes

Code	Composition		
173	Octyltriethoxy-silane:Phenyltriethoxy-silane:Tetraethoxy-silane preadsorbed on Celite	=	0.7:0.3:1
179	Octyltriethoxy-silane:Phenyltriethoxy-silane:Tetraethoxy-silane	=	0.7:0.3:1
188	Octyltriethoxy-silane:Phenyltriethoxy-silane preadsorbed on Celite	=	1:1
250	Octyltriethoxy-silane:Phenyltriethoxy-silane:Tetraethoxy-silane preadsorbed on Celite	=	0.6:0.4:1
251	Octyltriethoxy-silane:Phenyltriethoxy-silane:Tetraethoxy-silane preadsorbed on Celite	=	0.5:0.5:1
260	Propyltriethoxy-silane:Phenyltriethoxy-silane:Tetraethoxy-silane preadsorbed on Celite	=	0.5:0.5:1
261	Propyltriethoxy-silane:Phenyltriethoxy-silane:Tetraethoxy-silane preadsorbed on Celite	=	0.4:0.6:1
263	Propyltriethoxy-silane:Phenyltriethoxy-silane:Tetraethoxy-silane preadsorbed on Celite	=	0.2:0.8:1

The native lipase AK showed the highest activity but with moderate selectivity. The decrease in specific activity of the sol-gel biocatalysts is quite understandable as they contain considerably lower amount of enzyme entrapped in the sol-gel matrix than that present in the native form.

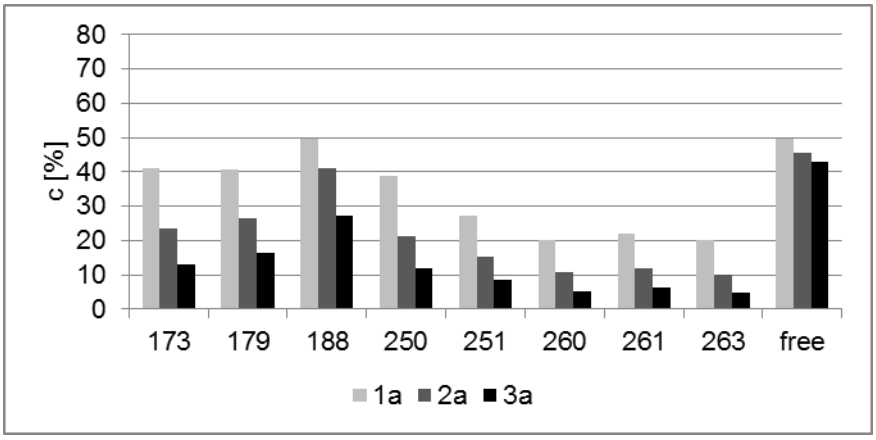

Figure 7. Conversions of **1-3a** with sol-gel immobilized and native lipase AK (4 h)

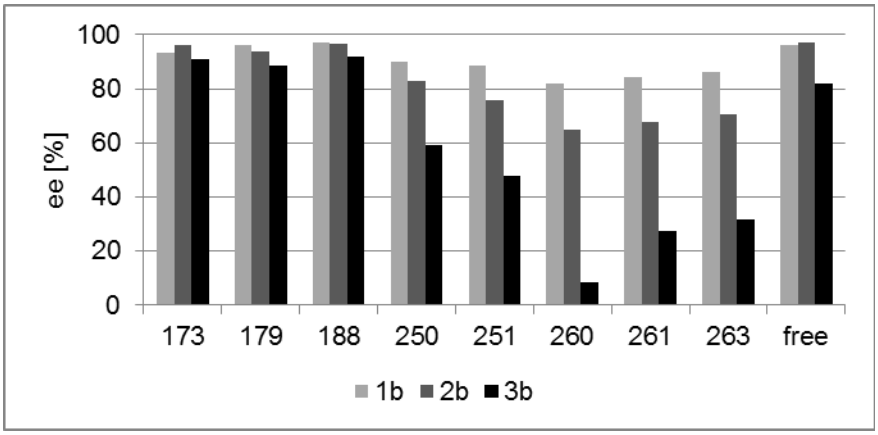

Figure 8. Enantiomeric excess of **1-3b** with sol-gel immobilized and native lipase AK (4 h)

In accordance with previous results [4,5], binary or ternary mixtures of silane precursors enabled the fine-tuning of matrix hydrophobicity of the forming sol-gel matrices. The most hydrophobic preparations (173, 179 and 188) were the most active and most selective forms on substrates *rac*-**1-3a** (*Figure 7* and *8*). Celite support allowed to omit the less hydrophobic tetraethoxy-silane precursor and to prepare the most hydrophobic matrix (188) which in fact resulted in the most productive and selective biocatalyst (*Figure 7* and *8*).

Decreasing the aliphatic character of the forming matrix (250, 251 and especially the propyl group containing systems 260, 261, 263) resulted in diminished activity and decreased selectivity towards aliphatic substrates **2a** and **3a** (*Figure 7* and *8*).

CONCLUSIONS

A rapid multi-substrate screening method was developed to characterize lipase biocatalyst based on enantiomer selective GC analysis of a reaction system including four racemic alcohols. Thorough comparison of the results from multi-substrate screening with single and two-substrate reactions revealed that the method was appropriate for rapid screening of the productivity and enantiomer selectivity of the lipases. This method, however was not adequate for exact determination of activity, selectivity, particularly at longer reaction times (over 4 h, due to reversible reaction of the forming ester **1b**). The robustness of the method was demonstrated by analysis of nine commercial and two in-house-made lipases. The fine-tunability of sol-gel biocatalysts was demonstrated also by the multi-substrate screening of lipase AK biocatalysts entrapped in eight various sol-gel matrices.

EXPERIMENTAL SECTION

Chemicals and enzymes

Racemic 1-phenylethanol *rac*-**1a**, racemic 1-cyclohexylethanol *rac*-**2a**, racemic 2-heptanol *rac*-**3a**, racemic 2-ethyl-1-hexanol *rac*-**4a**, vinyl acetate, acetyl chloride, triethylamine, tetrahydrofuran, hexane, toluene, acetone were products of Sigma Aldrich or Fluka. Lipase AK, Lipase PS, Lipase AYS, Lipase M and Lipase R were obtained from Amano Europe. Novozym 435 and Lipozyme TL IM were products of Novozymes, Denmark. *Mucor miehei* lipase, Lipase PPL, Lipase CcL were purchased from Sigma. Immobilized lipase from *Candida rugosa* (CRL T2-150) was obtained from Chiral Vision. Immobilized lipase PS was a kind gift of Iris Biotech GmbH. Lipases from a thermophilic fungi (BUTE 3A, BUTE 3B) were obtained from Fermentia Ltd [6]. The sol-gel immobilized lipases were prepared from native lipase AK as described earlier [4,7] (compositions are shown in Table 1).

Analytical methods

TLC was carried out on Kieselgel 60F_{254} (Merck) sheets. Spots were visualized under UV light (Vilber Lourmat VL-6.LC, 254 nm and 365 nm) or by treatment with 5% ethanolic phosphomolybdic acid solution and heating of the dried plates. GC analyses were carried out on Younglin ACME 6100 or

Agilent 4890D instruments equipped with FID detector and Hydrodex-β-TBDA column (50 m × 0.25 mm × 0.25 μm film with heptakis-(2,3-di-*O*-acetyl-6-*O*-*t*-butyldimethylsilyl)-β-cyclodextrin; Macherey&Nagel) using H_2 carrier gas (injector: 250°C, detector: 250°C, head pressure: 10 psi, 50:1 split ratio, column oven: 60°C/10 min, 60-130°C 7°C/min, 130°C/2 min). Retention times of the enantiomers of the four substrates **1-4a** and for the enantiomers of the four esters **1-4b** are listed in Table 2.

Table 2. Retention times of substrates and products

Compound	(*S*)-**3b**	(*S*)-**3a**	(*R*)-**3a**	(*R*)-**3b**	(*R*)-**4b**	(*S*)-**4b**	(*S*)-**4a**	(*R*)-**4a**
t_R (min)	13.81	14.20	14.30	15.91	16.78	16.86	18.00	18.20

Compound	(*S*)-**1b**	(*S*)-**2b**	(*S*)-**3a**	(*R*)-**3a**	(*R*)-**4b**	(*R*)-**2b**	(*R*)-**1a**	(*S*)-**1a**
t_R (min)	18.91	19.03	19.60	19.65	19.70	19.77	20.87	21.17

Preparation of the racemic acetates (rac-*1-4b*)

Acetyl chloride (6.25 mmol) was added dropwise to a solution of the racemic alcohol (*rac*-**1-4a**, 5 mmol) and triethylamine (7.5 mmol) in dry dichloromethane (10 mL) under argon atmosphere at 0°C and the reaction mixture was stirred for 2 h at this temperature. Then the resulting mixture was extracted with 5% HCl (35 mL), saturated $NaHCO_3$ (35 mL) and 40 mL saturated NaCl (40 mL), dried on Na_2SO_4. After evaporation of the solvent in vacuum, the residue was purified by column chromatography over silica gel (hexane:acetone 50:1) to give the corresponding product (*rac*-**1-4b**) as colorless oil.

Hydrolysis test for the acetates rac-*1b* and rac-*3b*

The racemic acetate (*rac*-**1b** or *rac*-**3b**, 50 μL) and lipase AK (50 mg) were added to a mixture of water saturated hexane and tetrahydrofuran (in 1:1 ratio; 2 mL) and mixture was shaken in screw-capped glass vial at 1000 rpm and 30°C. Samples (50 μL) were taken regularly (at 1, 2, 4, 8, 16 and 24 h). The diluted samples (with hexane, 500 μL) were analyzed by GC on Hydrodex-β-TBDA column.

Single-substrate tests with alcohols rac-*1-4a*

The racemic alcohol (*rac*-**1a**, *rac*-**2a**, *rac*-**3a** or *rac*-**4a;** 50 μL, each), vinyl acetate (100 μL) and the lipase biocatalyst (50 mg, in each case) were added to a mixture of hexane:tetrahydrofuran (in 1:1 ratio; 2 mL) and the resulting mixture was shaken in screw-capped glass vial at 1000 rpm and

30°C. Samples (50 µL) were taken regularly (at 1, 2, 4, 8, 16 and 24 h). The diluted samples (with hexane, 500 µL) were analyzed by GC on Hydrodex-β-TBDA column.

Multi-substrate screening of lipases with a mixture of alcohols rac-*1-4a*

An equimolar mixture of the racemic alcohols (*rac*-**1a**, *rac*-**2a**, *rac*-**3a** and *rac*-**4a**; 50 µL), vinyl acetate (100 µL) and the lipase biocatalyst (50 mg, in each case) were added to a mixture of hexane:tetrahydrofuran (in 1:1 ratio; 2 mL) and the resulting mixture was shaken in screw-capped glass vial at 1000 rpm and 30°C. Samples (50 µL) were taken regularly (at 1, 2, 4, 8, 16 and 24 h). The diluted samples (with hexane, 500 µL) were analyzed by GC on Hydrodex-β-TBDA column.

ACKNOWLEDGEMENTS

This research work was supported by the Hungarian National Office for Research and Technology (NKFP-07-A2 FLOWREAC) and is related also to the scientific program of "*Development of quality-oriented and harmonized R+D+I strategy and functional model at BME*" project (TÁMOP-4.2.1/B-09/1/KMR-2010-0002), supported by the New Hungary Development Plan. The authors thank Dr. György Szakács (Budapest University of Technology and Economics, Hungary) and Dr. Balázs Erdélyi (Fermentia Ltd, Budapest, Hungary) for the BUTE 3 lipase preparations.

REFERENCES

1. Tholey, A.; Heinzle, E., *Advances in Biochemical Engineering / Biotechnology,* **2002**, *74*, 1-19.
2. Debbeche, H.; Toffano, M.; Fiaud, J.-C.; Aribi-Zouioueche, L., *Journal of Molecular Catalysis B: Enzymatic,* **2010**, *66*, 319-324.
3. Hellner, G.; Boros, Z.; Tomin, A.; Poppe, L., *Advanced Synthesis & Catalysis,* **2011**, *353*, 2481-2491.
4. Tomin, A.; Weiser, D.; Hellner, G.; Bata, Z.; Corici, L.; Péter, F.; Koczka, B.; Poppe, L., *Process Biochemistry,* **2011**, *46*, 52-58.
5. Weiser, D.; Boros, Z.; Hornyánszky, G.; Tóth, A.; Poppe, L., *Process Biochemistry,* **2012**, *47*, 428-434.
6. Bódai, V.; Peredi, R.; Bálint, J.; Egri, G.; Novák, L.; Szakacs, G.; Poppe, L., *Advanced Synthesis & Catalysis,* **2003**, *345*, 811-818.
7. Weiser, D.; Tomin, A.; Poppe, L., *Studia UBB Chemia,* **2010**, *55*, 283-288.

STUDIA UBB CHEMIA, LVII, 2, 2012 (p. 139 - 146)

REACTION OF A HETEROTOPIC P,SAs LIGAND WITH GROUP 10 METAL(II) COMPLEXES: A THEORETICAL STUDY

IMOLA SÁROSI[a, b], MENYHÁRT B. SÁROSI[a], EVAMARIE HEY-HAWKINS[b] AND LUMINIŢA SILAGHI-DUMITRESCU[a]

ABSTRACT. Density functional calculations have been carried out in order to gain some insight into the electronic structure of 1-$Ph_2AsSC_6H_4$-2-PPh_2 (1) and to investigate the reactions of 1 with group 10 metal dihalides. The obtained results explain well the experimentally observed behaviour of 1 during the investigated complexation reactions and support the trends observed for the isomerisation of the resulted trinuclear trimeric compounds.

Keywords: *heterotopic P,SAs ligand, palladium complexes, platinum complexes, structural isomerism, DFT calculations.*

INTRODUCTION

Tertiary phosphine and arsine ligands derived from thiophenol have been shown to be very versatile ligands that form stable complexes with a wide range of transition metals [1]. The coordination chemistry of bidentate HSC_6H_4-2-EPh_2 ligands (E = P, As) was investigated thoroughly mainly due to their mixed-donor chelating compartments [1–3]. For EPh_2(SPh) ligands (E = P, As) [4,5], the metal-mediated E–S bond cleavage was studied in their reactions with metal carbonyls [6–13]. Based on our interest in designing and investigating the coordination properties of a heterotopic P,SAs ligand, the synthesis of 1-$Ph_2AsSC_6H_4$-2-PPh_2 (**1**) and reactions of **1** with group 10 metal dihalides were carried out and reported in a previous study done by our group [14]. Ligand **1** combines the properties of $AsPh_2$(SPh) and HSC_6H_4-2-PPh_2, bearing three donor atoms. However, reactions of **1** with [$PdCl_2$(cod)] and [PtI_2(cod)] (cod = 1,5-cyclooctadiene) in 1:1 ratio occurred with cleavage of the As–S bond and coordination of the resulting phosphanylthiolato ligand (SC_6H_4-2-PPh_2). Shorter reaction times (4 h, M = Pd; 1 week, M = Pt) led to trinuclear complexes [(*cis*-M{(μ-*S*-SC_6H_4-2-PPh_2)-κ^2*S,P*}$_2$)-MX_2-MX{(μ-*S*-SC_6H_4-2-PPh_2)-κ^2*S,P*}] [M = Pd, X = Cl (**3**); M = Pt, X = I (**5**)], while the

[a] "Babeş-Bolyai" University of Cluj-Napoca, Faculty of Chemistry and Chemical Engineering, Arany Janos Street 11, 400028 Cluj-Napoca, Romania, lusi@chem.ubbcluj.ro

[b] Universität Leipzig, Institut für Anorganische Chemie, Johannisallee 29, D-04103 Leipzig, Germany, hey@uni-leipzig.de

trimeric trinuclear isomers [MX{(*μ*-*S*-SC_6H_4-2-PPh_2)-κ^2*S,P*}]$_3$ [M = Pd, X = Cl (**2**); M = Pt, X = I (**4**)] were obtained after reaction times of two weeks [14].The central fragments of **2** and **4** are comparable with that of the recently reported [PtI{(*μ*-*S*-SC_6H_4-2-$AsPh_2$)-κ^2*S,As*}]$_3$ [3] and [PtI{(*μ*-*S*-SC_6H_4-2-P(Biph)}-κ^2*S,P*}]$_3$ (Biph = 1,1'-biphenyl) [15] complexes. Density functional calculations have been carried out in order to gain some insight into the electronic structure of **1** and to investigate the observed reactions which resulted in the formation of transition metal complexes **2**–**5**.

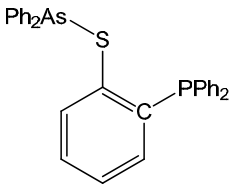

1

Scheme 1. 1-$Ph_2AsSC_6H_4$-2-PPh_2 (**1**).

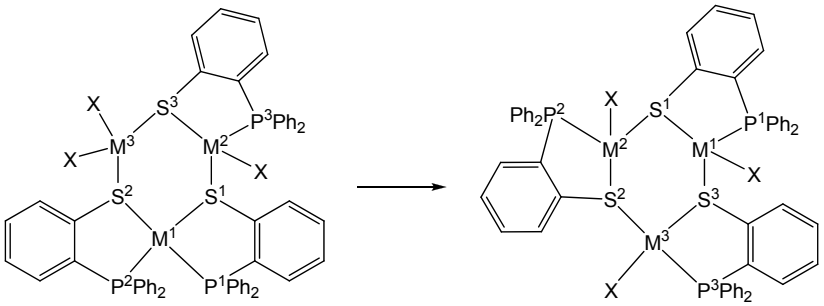

3, **5** **2**, **4**

Scheme 2. Isomerisation of **3** to **2** and **5** to **4**.

RESULTS AND DISCUSSION

The optimised geometry parameters of **1** (Table 1) are in excellent agreement with the experimental values [14]. Figure 1 shows the highest occupied molecular orbital (HOMO) of **1**, which is predominantly made of the phosphorus and sulfur lone pairs. This specific nature of the HOMO makes the P,S chelating pocket of **1** most suitable for an electrophilic attack. This is also supported by the electrostatic potential surface, where the negative regions correspond to the lone pairs at sulfur and phosphorus (Figure 2). The formation of complexes **2**–**5** undoubtedly proves that only the P,S chelating pocket coordinates to the transition metal centres. The lability of the As–S

bond is also suggested by the electronic structure calculations. The lowest unoccupied molecular orbital (LUMO) of **1** is predominantly an As–S antibond (Figure 1). However, the cleavage of the As–S bond might also be induced by the coordination of sulfur to the metal centre, which withdraws an electron from the As–S bond. The eliminated $AsPh_2$ group was observed by MS-ESI spectrometry in the filtrate solutions after isolation of **2**–**5**, which showed different oxidised species of dimerised $AsPh_2$ [1]

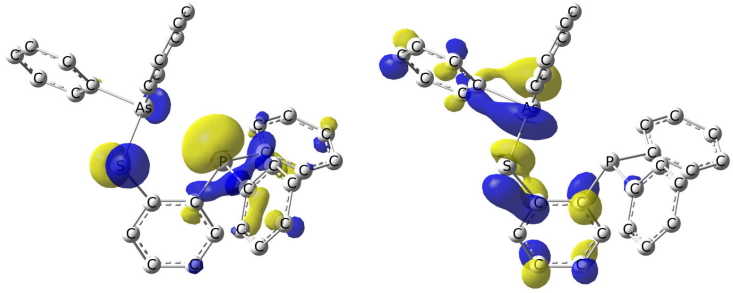

Figure 1. Frontier molecular orbitals of **1**. Isovalue: 0.5, positive orbital contour: yellow, negative orbital contour: blue, hydrogen atoms are omitted for clarity.

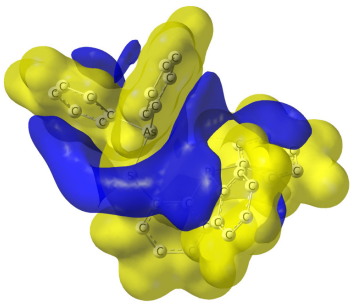

Figure 2. Electrostatic potential surface of **1**. Isovalue: 0.02, positive contours: yellow, negative contours: blue, hydrogen atoms are omitted for clarity.

Table 1. Selected bond lengths in pm for **1**.

Bond length	exp. [14]	calcd.
As(1)–S(1)	226.6(1)	228.1
S(1)–C(13)	178.4(4)	180.4
P(1)–C(19)	183.7(4)	185.0
P(1)–C(14)	183.8(4)	186.1
P(1)–C(25)	184.3(4)	185.5

Furthermore, the gas phase As–S and P–C bond dissociation energies for both homolytic and heterolytic bond cleavage were also calculated. In both cases the energy for the homolytic bond cleavage, resulting in two radical fragments (processes 1a and 2a in Table 2), is significantly smaller than the heterolytic bond dissociation energies. Not surprisingly, the P–C homolytic bond dissociation energy is significantly higher than the energy required to cleave the As–S bond. The corrections for the description of the solvation in toluene do not alter these trends. However, the bond dissociation energies are predicted to be lower than without corrections for solvent effects (Table 2).

Table 2. Bond dissociation energies for **1**, in kJ mol^{-1}.

Process	$\Delta G°$ (gas)	$\Delta G°$ (toluene)
1a: **1** → $[AsPh_2]^{\bullet}$ + $[1\text{-}PPh_2\text{-}2\text{-}SC_6H_4]^{\bullet}$	172.5	169.2
1b: **1** → $[AsPh_2]^{-}$ + $[1\text{-}PPh_2\text{-}2\text{-}SC_6H_4]^{+}$	579.5	390.6
1c: **1** → $[AsPh_2]^{+}$ + $[1\text{-}PPh_2\text{-}2\text{-}SC_6H_4]^{-}$	595.0	399.0
2a: **1** → $[PPh_2]^{\bullet}$ + $[S(AsPh_2)C_6H_4]^{\bullet}$	227.5	226.3
2b: **1** → $[PPh_2]^{-}$ + $[S(AsPh_2)C_6H_4]^{+}$	575.8	390.5
2c: **1** → $[PPh_2]^{+}$ + $[S(AsPh_2)C_6H_4]^{-}$	568.8	369.9

The optimised geometry parameters of **2**–**5** (Tables 3 and 4) are in good agreement with the experimental values [14], and the observed covalent and coordinative M–S bonds are correctly reproduced theoretically. Independent of the used metal halide in both cases the trimeric forms **2** and **4** are energetically favoured over their trinuclear counterparts (i.e., **3** and **5**). The relative energy differences between the trinuclear and trimeric forms are very similar: 15.7 kJ mol^{-1} and 10.5 kJ mol^{-1} for **2**/**3** and **4**/**5**, respectively. The corrections for the description of the solvation in tetrahydrofuran predict lower relative energy values for the differences between the trinuclear and trimeric forms (9.2 kJ mol^{-1} and 5.4 kJ mol^{-1} for **2**/**3** and **4**/**5**, respectively). Thus, solvation seems to lower the energy difference between the trinuclear and trimeric forms of both Pd- and Pt- substituted complexes. The trinuclear to trimeric interconversion from **3** to **2** might be facilitated by an intramolecular HOMO-LUMO interaction in **3**. The HOMO of **3** is mainly composed of the Cl(3) lone pair of electrons, which could interact with the σ*(Pd–E) LUMO (E = S, P) located on Pd(1), and trigger the isomeric rearrangement. The HOMO of **5** is composed mainly from the I(2) and I(3) lone pairs of electrons and has a similar character as the HOMO of **3**. However, the LUMO of **5** is shared between all three platinum centres, with the highest atomic orbital coefficient located at Pt(2) (Figure 3).

This might be one of the reasons for the experimentally observed differences between the two isomeric rearrangement reactions [14]. Furthermore, the gas phase Gibbs free energies ($\Delta G°_{gas}$) of the two isomeric rearrangements

also suggest differences between the two processes. The conversion from **3** to **2** is more exothermic (ΔG_{gas} = –68.5 kJ mol^{-1}) than the isomerisation from **5** to **4** ($\Delta G°_{gas}$ = –36.4 kJ mol^{-1}). The corrections for solvent effects do not alter this trend. However, the $\Delta G°_{THF}$ values are lower (–44.2 kJ mol^{-1} for the conversion from **3** to **2** and –32.1 kJ mol^{-1} for the isomerisation from **5** to **4**). The lower Gibbs free energies for the *trinuclerar*/*trimer* isomerisation in solution, together with the lower relative energy differences between the two isomers in THF, clearly indicate that the solvation effects facilitate the observed isomerisations.

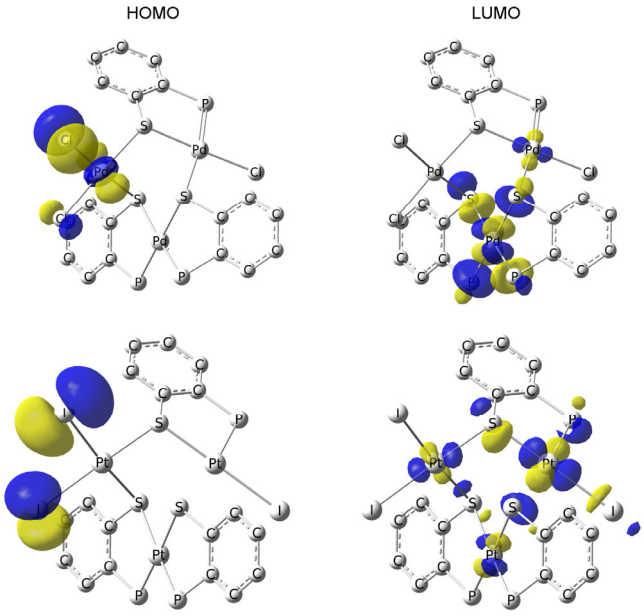

Figure 3. Frontier molecular orbitals of **3** (top) and **5** (bottom). Isovalue: 0.5, positive orbital contour: yellow, negative orbital contour: blue, hydrogen atoms and terminal phenyl rings are omitted for clarity.

Table 3. Selected bond lengths in pm for **2** and **4**.

	2 (M = Pd)		**4 (M = Pt)**	
Bond length	exp. (from [14])	calcd.	exp. (from [14])	calcd.
M(1)–P(1)	223.0(6)	229.9	222.8(1)	229.5
M(1)–S(1)	228.8(6)	237.0	230.2(1)	237.3
M(1)–S(3)	242.5(6)	251.7	242.8(1)	251.5
M(2)–P(2)	223.4(6)	230.0	223.6(1)	228.6
M(2)–S(2)	227.3(5)	235.7	227.3(1)	237.2
M(2)–S(1)	237.3(6)	246.6	237.3(1)	245.8
M(3)–P(3)	223.4(7)	229.3	223.5(2)	229.1
M(3)–S(3)	228.7(6)	237.9	228.8(1)	238.9
M(3)–S(2)	240.5(6)	247.6	238.7(1)	246.8

Table 4. Selected bond lengths in pm for **3** and **5**.

	3 (M = Pd)		**4 (M = Pt)**	
Bond length	exp. (from [14])	calcd.	exp. (from [14])	calcd.
M(1)–P(2)	225.9(2)	233.6	225.3(9)	232.3
M(1)–P(1)	227.5(2)	234.9	225.7(8)	233.1
M(1)–S(1)	234.6(2)	243.9	235.7(8)	242.7
M(1)–S(2)	233.9(2)	240.1	236.1(8)	242.1
M(2)–P(3)	222.3(2)	229.8	222.4(9)	228.6
M(2)–S(3)	227.6(2)	237.6	228.6(8)	238.6
M(2)–S(1)	237.1(2)	246.5	237.8(8)	246.0
M(3)–S(2)	228.6(2)	240.9	230.7(8)	239.7
M(3)–S(3)	230.7(2)	241.0	231.0(8)	240.6

CONCLUSIONS

Theoretical calculations on **1** predict that the P,S chelating pocket will be favoured over the As,S unit during an electrophilic attack, which is in agreement with the previously reported experimental results. The lability of the As–S bond is suggested by the electronic structure of **1** and the bond dissociation energies. The observed trinuclear to trimeric interconversions might be facilitated by intramolecular HOMO-LUMO interactions in the trinuclear isomers. Furthermore, the nature of the metal halide strongly influences the electronic structure of the trinuclear species and the progress of the isomerisation reactions.

EXPERIMENTAL SECTION

Density functional calculations were carried out with the GAUSSIAN 09 program package [16]. The starting geometries of **1**–**5**, obtained from X-ray structure data, have been optimized with the B3LYP density functional [17] using the LANL2DZ basis on Pd, Pt and I (along with the effective core potential of Hay and Wadt [18, 19, 20]) and the 6-31G(d,p) basis set [21] on all other atoms. Corrections for the description of the solvation were carried out by employing the Polarisable Continuum Model (PCM) method of Tomasi and coworkers [22].

ACKNOWLEDGMENTS

I.S. acknowledges financial support provided by programs co-financed by the Sectoral Operational Program Human Resources Development, Contract POSDRU 6/1.5/S/3, "Doctoral studies: through science towards society".

REFERENCES

1 J.R. Dilworth, N. Wheatley, *Coord. Chem. Rev.*, **2000**, *199*, 89.

2 E. Block, G. Ofori-Okai, J. Zubieta, *J. Am. Chem. Soc.,* **1989**, *111*, 2327.

3 A. Hildebrand, I. Sárosi, P. Lönnecke, L. Silaghi-Dumitrescu, Menyhárt B. Sárosi, I. Silaghi-Dumitrescu, E. Hey-Hawkins, *Inorg. Chem.*, **2012**, submitted.

4 H. Fritzsche, U. Hasserodt, F. Korte, *Angew. Chem. Int. Ed.*, **1964**, *3*, 64; H. Fritzsche, U. Hasserodt, F. Korte, *Angew. Chem.*, **1963**, *75*, 1205.

5 R. Fusco, C.A. Peri, V. Corradini, Montecatini, *Patent*, **1963**, BE621008.

6 G. Le Borgne, R. Mathieu, *J. Organomet. Chem.*, **1981**, *208*, 201.

7 A.J. Edwards, A. Martin, M.J. Mays, P.R. Raithby, G.A. Solan, *J. Chem. Soc., Chem. Commun*., **1992**, 1416.

8 A.J. Edwards, A. Martin, M.J. Mays, D. Nazar, P.R. Raithby, G.A. Solan, *J. Chem. Soc., Dalton Trans*., **1993**, 355.

9 A. Martin, M.J. Mays, P.R. Raithby, G.A. Solan, *J. Chem. Soc., Dalton Trans*., **1993**, 1431.

10 S.L. Ingham, M.J. Mays, P.R. Raithby, G.A. Solan, B.V. Sundavadra, G. Conole, M. Kessler, *J. Chem. Soc., Dalton Trans*., **1994**, 3607.

11 G. Conole, M. Kessler, M.J. Mays, G.E. Pateman, G.A. Solan, *Polyhedron*, **1998**, *17*, 2993.

12 G. Conole, J.E. Davies, J.D. King, M.J. Mays, M. McPartlin, H.R. Powell, P.R. Raithby, *J. Organomet. Chem*., **1999**, *585*, 141.

13 J.D. King, M.J. Mays, G.E. Pateman, P.R. Raithby, M.A. Rennie, G.A. Solan, N. Choi, G. Conole, M. McPartlin, *J. Chem. Soc., Dalton Trans*., **1999**, 4447.

14 I. Sárosi, A. Hildebrand, P. Lönnecke, L. Silaghi-Dumitrescu, E. Hey-Hawkins, *Dalton Trans.*, **2012**, DOI:10.1039/C2DT12506D.

15 A. Hildebrand, I. Sárosi, P. Lönnecke, L. Silaghi-Dumitrescu, Menyhárt B. Sárosi, I. Silaghi-Dumitrescu, E. Hey-Hawkins, *Dalton Trans.*, **2012**, submitted.

16 M.J. Frisch, G.W. Trucks, H.B. Schlegel, G.E. Scuseria, M.A. Robb, J.R. Cheeseman, G. Scalmani, V. Barone, B. Mennucci, G.A. Petersson, H. Nakatsuji, M. Caricato, X. Li, H.P. Hratchian, A.F. Izmaylov, J. Bloino, G. Zheng, J.L. Sonnenberg, M. Hada, M. Ehara, K. Toyota, R. Fukuda, J. Hasegawa, M. Ishida, T. Nakajima, Y. Honda, O. Kitao, H. Nakai, T. Vreven, J. Montgomery, J.A., J.E. Peralta, F. Ogliaro, M. Bearpark, J.J. Heyd, E. Brothers, K.N. Kudin, V.N. Staroverov, R. Kobayashi, J. Normand, K. Raghavachari, A. Rendell, J.C. Burant, S.S. Iyengar, J. Tomasi, M. Cossi, N. Rega, J.M. Millam, M. Klene, J.E. Knox, J.B. Cross, V. Bakken, C. Adamo, J. Jaramillo, R. Gomperts, R.E. Stratmann, O. Yazyev, A.J. Austin, R. Cammi, C. Pomelli, J.W. Ochterski, R.L. Martin, K. Morokuma, V.G. Zakrzewski, G.A. Voth, P. Salvador, J.J. Dannenberg, S. Dapprich, A.D. Daniels, O. Farkas, J.B. Foresman, J.V. Ortiz, J. Cioslowski, D.J. Fox, *Gaussian 09, Revision A.02*, Gaussian, Inc., Wallingford CT, **2009**.

17 P.J. Stephens, F.J. Devlin, C.F. Chabalowski and M.J. Frisch, *J. Phys. Chem.*, **1994**, *98*, 11623.
18 P.J. Hay, W.R. Wadt, *J. Chem. Phys.*, **1985**, *82*, 270.
19 P.J. Hay, W.R. Wadt, *J. Chem. Phys.*, **1985**, *82*, 284.
20 P.J. Hay, W.R. Wadt, *J. Chem. Phys.*, **1985**, *82*, 299.
21 R. Ditchfield, W. Hehre, J.A. Pople, *J. Chem. Phys.*, **1971**, *54*, 724.
22 J. Tomasi, B. Mennucci, R. Cammi, *Chem. Rev.*, **2005**, *105*, 2999.

STUDIA UBB CHEMIA, LVII, 2, 2012 (p. 147 - 156)

CHARACTERISATION OF GENERATED ASH FROM HAZARDOUS WASTE INCINERATION

EMANUELA ADINA COCIŞ[a], VASILE FILIP SOPORAN[a], PETRU ILEA[b], FLORICA IMRE-LUCACI[b], BIANCA MICHAELA SOPORAN[a], PAUL BERE[c], OVIDIU NEMEŞ[a, *]

ABSTRACT. Ash from hazardous waste incineration represents the most important residue of the total products resulted from the incineration process. International literature contains many references to research that characterize ash as dangerous, not dangerous, or inert, in an effort to diagnose its proper management and disposal. For this reason, this study focuses on the characterization of ash. Samples were collected from a typical hazardous waste incineration and a series of tests were conducted, including a particle size distribution analysis, humidity content, surface morphology, elemental composition, chemical composition and heavy metal content.

Keywords: *hazardous waste, incineration, ash, metals, elements.*

INTRODUCTION

Waste generation has increased considerably worldwide in the last few decades [1]. One of today's major concern and problem is represented by the increasing amount of waste and the decreasing available areas for landfilling. The harmful products of chemical processes produced from either industries or hospitals are called hazardous waste. Hazardous waste is also generated in recycling centers, where waste from industries is recycled. Hazardous waste can be explosive, oxidizing, highly flammable, corrosive, infectious, mutagenic, irritant, toxic, or carcinogenic. The common hazardous waste disposal methods are incineration, land disposal and new technologies like solar detoxification [2].

Incineration significantly reduces the volume of hazardous waste (by 95%) and has advantages such as pathogen inactivation and potential energy recuperation [3].The massive volume of hazardous waste in many countries

[a] Technical University of Cluj-Napoca, Faculty of Materials Engineering and Environment, Muncii Bd., No. 103-105, RO-400641, Cluj-Napoca, Romania, * ovidiu.nemes@sim.utcluj.ro
[b] Babes-Bolyai University, Faculty of Chemistry and Chemical Engineering, Janos Arany Str., No.11, RO-400028, Cluj-Napoca, Romania
[c] Technical University of Cluj-Napoca, Faculty of Mechanical Engineering, Muncii Bd., No. 103-105, RO-400641, Cluj-Napoca, Romania

is mostly reduced through incineration that leads to the generation of ash as a new type of waste.

Ash is a grey to black granular, porous, glasslike material which can be intermingled with ferrous and nonferrous metals and other incombustible materials contained in the waste composition before the incineration process it consists of fine, powdery particles, spherical or angular in shape, solid or hollow [4].

International literature contains many references to researches that characterize the resulted ash as dangerous, not dangerous, or inert, in an effort to diagnose its proper management and disposal. Reasons such as limited available land areas for the creation of specialized bottom ash burial grounds and, therefore, the necessity to reduce the quantities sent to landfills, channel research to finding ways of recycling bottom ash into products used in structural and construction materials. Thus, the impact on public health has once again become the focus of scientific research [5].

Unfortunately, only a limited amount of researches exists regarding the characteristics, particle size distribution, morphology and ash [6]. Further research is needed to investigate the characteristics and the toxicity of bottom ash in order to explore its potential use as construction material [7]. Limited space and high cost for landfilling, led to the development of recycling technologies and reuse bottom ash as an admixture material (in cement and concrete production) [8 - 11], in road pavement, embankment, soil stabilization, ceramics, glass and glass–ceramics [4].

Bottom ash and fly ash, produced from incinerated hospital waste, are used for the production of concrete and bricks [5]. In several European countries high quantities of ash are reused for the manufacture of pavements, bridges and structural stones but also as sub layer in the manufacture of motorways and as daily cover of landfills. On the contrary, in USA and Canada a general interest exists without constituting common practice to use ash as a construction material [5].

In the present work, nature of the ash has been examined through chemical analysis of samples collected from a hazardous waste incinerator. The main goal was to determine particle size distribution, humidity, heavy metals, morphology and elemental composition of ashes.

RESULTS AND DISCUSSION

The obtained grain sizes after particle size distribution were 1000 μm, 500 μm, 250 μm, < 250 μm (Figure 1).

The humidity content was between 5.86 - 9.84%.

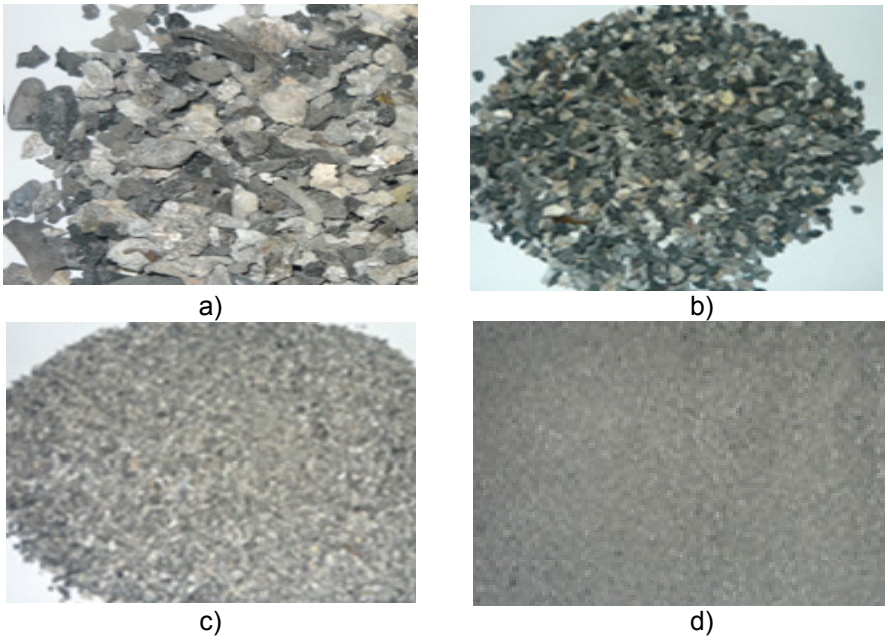

Figure 1. Granulometric sizes: a) 1000 μm; b) 500 μm; c) 250 μm; d) <250 μm

The metal elements determined were Pb, Zn, Cu, Cr, Ni, Ag, Sn and Mn. Figure 2 shows the metal concentrations in ash obtained by inductively coupled plasma mass spectroscopy (ICP-MS). The method used for the elementary analysis is based on SR EN ISO 17294-2/2005.

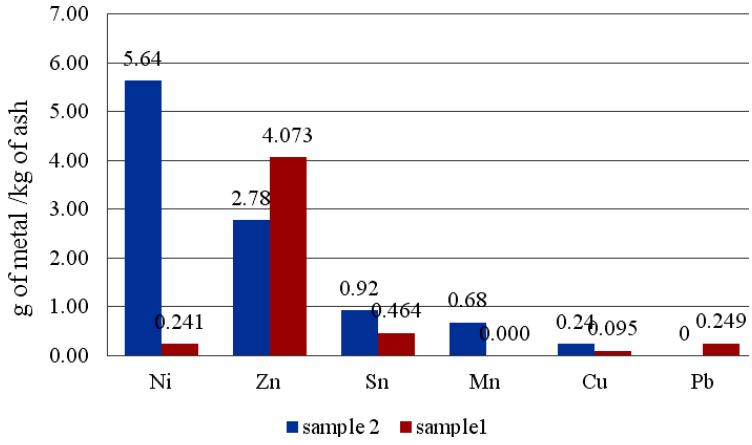

Figure 2. Metal concentrations in ash determined by ICP-MS

The obtained results were compared to the values indicated by the international literature in Table 1.

Table 1. Metal composition of ash

Element [g/kg]	Sample 1 [g/kg]	Sample 2 [g/kg]	Metal concentrations [g/kg] / Reference	Medium concentration according to literature [g/kg] [12]
Pb	0.249	0.00	4.76 / [13]	0.098 - 0.137
Zn	4.073	2.78	6.08 / [13]	0.613 - 7.77
Cu	0.095	0.24	0.97 / [13]	0.290 - 8.240
Ni	0.241	5.64	0.185 / [13]	0.007 - 4.28
Sn	0.464	0.92	5.87 / [13]	0.002 - 0.38
Mn	0.000	0.68	2.03 / [13]	1
Se	-	-	0.00005 / [15]	0.0003
Co	-	-	0.03 / [14]	0.008
Ag	-	-	0.004 / [14]	0.000005
As	-	-	0.001 / [15]	0.005
Cd	-	-	0.001 / [15]	0.00006
Hg	-	-	0.00007 / [15]	0.000003
Cr	-	-	0.00006 / [15]	0.1

As seen, the metal concentrations from or samples do not exceed the literature indicated limits. The difference between these results is due to the composition of waste before incineration. Another cause may be the ineffectiveness of incineration process.

The oxide composition of the ash was determined through alkaline decomposition, based on STAS 9163/7. The obtained data are presented in Figure 3. The loss on ignition was 31.71%, based on STAS 9163/3 – 73.

The obtained results were compared to the values indicated by the international literature in Table 2.

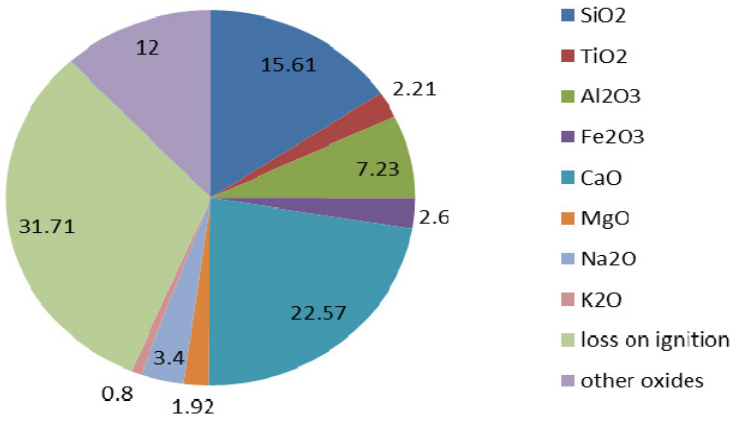

Figure 3. Oxide composition of the ash [%]

Table 2. Oxides identified in ash

Al_2O_3 [%]	SiO_2 [%]	CaO [%]	K_2O [%]	Na_2O [%]	MgO [%]	Fe_2O_3 [%]	Other oxides [%]	Reference
8.18	23.64	22.78	5.6o	5.28	-	-	5%	[13]
10.0	26.1	30.5	-	-	-	-	21%	[14]
17.83	0.18	22.90	-	3.68	1.04	11.39	-	[16]
14.34	0.39	33.18	0.6	3.64	2.81	4.64		[7]

As seen, the ash is mainly comprised from CaO, SiO_2 and Al_2O_3.

A morphology analysis by SEM is conducted to clearly understand how incineration process affects the ash surface structure [17].

The morphology of an ash particle is controlled by combustion temperature. The sizes of the observed particles are ranged from 9 μm to 1000 μm.

The micrographs showed agglomerated and irregularly shaped particles. This phenomenon occurs because of wastes containing impurities and complex components that may cause the particles to agglomerate at high temperature.

There were analyzed 20 areas (Z 1 ÷ Z 20) chose randomly, and depending on analyzed spectrum, we can observe smoother agglomerations and different shapes of ash particles (Figure 4).

The elemental composition of ash was determined by energy dispersive spectroscopy (EDS). The identified elements in the ash samples were C, O, Mg, Na, Al, Si, S, Cl, K, Ca, Ti, I, Zn, Ir, Zr, Fe (Table 3).

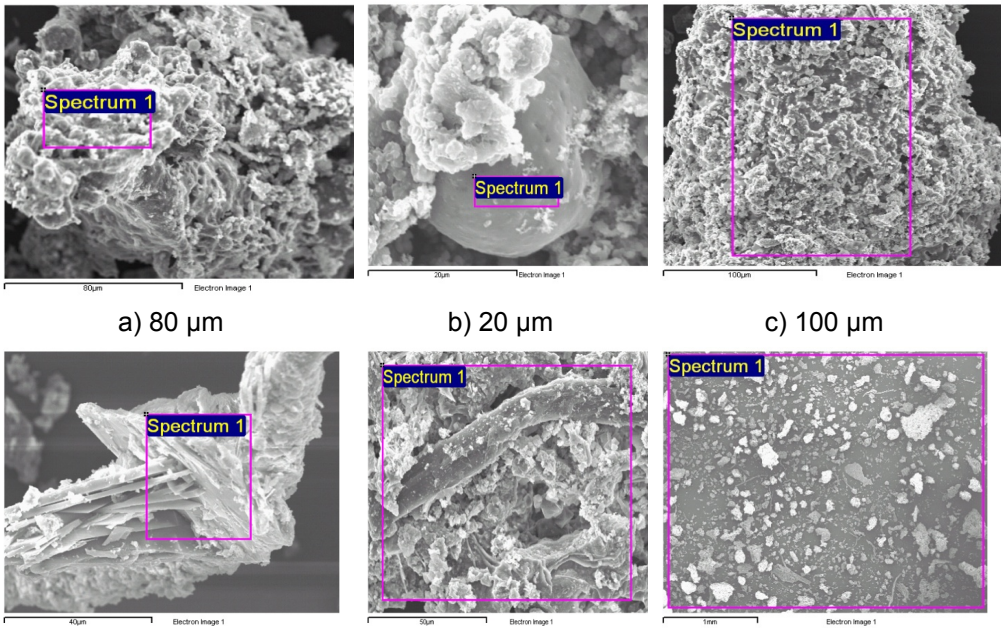

a) 80 μm b) 20 μm c) 100 μm

d) 40 μm e) 50 μm f) 1 mm

Figure 4. SEM images of ash

Based on the data given in the table we can observe that aluminum, silicon, calcium, chlorine and oxygen were identified in bigger percentage than other elements. We can also observe that the distribution of elements is heterogeneous and depends on the observed area (Figure 5).

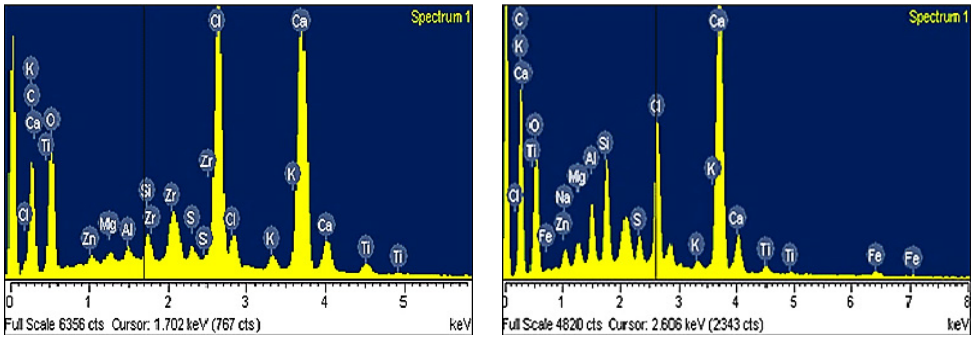

Figure 5. Elemental distribution determined by EDS

Table 3. Elemental composition of ash determined by EDS

Element [%] / Sample	C	O	Na	Mg	Al	Si	S	Cl	K	Ca	Ti	Fe	Zr	Ir	Zn
Z1	6.00	41.79	2.16	1.83	3.90	15.41	0.43	2.42	0.36	14.79	0.97	1.62	6.56	1.76	-
Z2	30.86	28.64	-	0.35	0.38	0.88	0.67	13.53	0.91	17.54	1.12	-	4.32	-	0.79
Z3	35.84	27.34	0.51	0.72	1.81	3.44	1.16	7.12	0.48	18.92	0.81	1.01	-	-	0.83
Z4	12.66	36.70	-	0.37	0.74	1.96	1.35	7.22	0.40	37.24	0.47	-	-	-	0.89
Z5	5.16	35.35	2.21	1.50	1.91	6.78	1.66	13.80	0.62	19.83	1.60	5.62	-	2.22	1.75
Z6	8.17	36.27	-	0.32	0.92	1.31	0.40	17.00	0.52	33.42	1.66	-	-	-	-
Z7	8.81	40.65	0.86	0.41	1.08	1.65	1.43	14.29	0.43	28.82	1.56	-	-	-	-
Z8	4.06	25.78	-	-	0.79	0.72	-	7.63	-	61.02	-	-	-	-	-
Z9	8.64	37.16	2.06	1.04	3.80	4.75	0.62	15.38	0.32	24.42	1.33	0.49	-	-	2.36
Z10	51.97	22.59	-	0.33	0.87	1.20	1.03	8.11	1.12	8.51	1.37	0.55	-	-	-
Z11	3.42	49.03	0.84	1.51	12.16	15.33	0.47	4.29	1.41	11.18	0.36	-	-	-	-
Z12	39.64	28.10	1.70	0.26	0.95	1.28	0.64	3.40	8.36	14.80	0.86	-	-	-	-
Z13	83.63	15.23	0.12	-	-	0.11	0.17	0.40	-	0.33	-	-	-	-	-
Z14	32.25	27.63	0.20	0.55	2.98	4.18	0.74	7.22	0.49	20.13	2.01	-	-	-	0.36
Z15	68.33	14.50	0.46	0.26	0.17	0.58	0.86	4.18	0.85	4.21	2.63	-	-	-	-
Z16	62.66	16.27	-	0.30	0.27	0.44	1.67	7.26	1.18	3.10	-	2.49	-	-	4.37
Z17	4.19	41.73	1.81	0.74	4.08	6.44	-	1.52	-	21.67	13.16	0.69	-	-	-
Z18	42.41	14.38	5.37	0.84	1.72	3.02	-	15.92	0.36	6.00	4.06	-	5.10	-	0.83
Z19	83.82	10.24	0.98	0.18	0.36	0.62	0.29	2.04	-	1.46	-	-	-	-	-
Z20	56.69	23.81	1.06	0.46	1.47	1.99	0.72	4.02	0.20	8.33	1.24	-	-	-	-

Studies showed that the EDS spectra of the surface and the interior of ash particles are similar, both having calcium and silicon as major elements, which is a typical elemental composition of combustion residues. Potassium, chlorine, sulfur, aluminum, iron, chromium, magnesium, phosphorus, titanium and zinc were also found at all points [18].

Other research showed that the elemental composition of ash was the following listed in Table 4.

Table 4. Elemental composition of ash

Element	Concentration sample 1 [%]	Concentration sample 2 [%]	Reference
C	41.6	38.7	[19]
O	27.5	29.0	
Na	0.5	1.0	
Mg	2.0	2.5	
Al	5.3	3.6	
Si	8.8	6.9	
S	0.6	0.9	
Cl	1.9	3	
K	3.7	2.2	
Ca	8.1	12.1	

Comparing these results with the ones from our sample (listed in Table 3), we can say that the elemental composition of ash is similar, because the same major elements can be observed.

CONCLUSIONS

Based on the information and data presented in this paper we can formulate the following conclusions:

The generated ash from hazardous waste incineration process represents the most important residue from the total resulted products.

Ash from waste incineration is a granular, porous, glasslike material which can be intermingled with ferrous and nonferrous metals and other incombustible.

Chemical analysis showed that the major components identified in ash were CaO, SiO_2, Al_2O_3, Fe_2O_3, MgO, TiO_2, Na_2O, K_2O. Metallic elements, such as Pb, Zn, Cu, Ni, Ag, Sn, Mn were determined.

The SEM images showed that particles are agglomerated and irregularly shaped.

As determined by EDS, the identified elements in the ash samples were C, O, Mg, Na, Al, Si, S, Cl, K, Ca, Ti, I, Zn, Ir, Zr, Fe .Distribution of elements is heterogeneous and depends on observed areas.

Aluminum, silicon and calcium were found in large quantities, being typical constituents of combustion residues.

EXPERIMENTAL SECTION

Two ash samples were collected from a typical hazardous waste incinerator functioning in Cluj-Napoca.

The samples were sieved by an auto sieve fitted with standard meshes of different sizes. The separated granulometric fractions were: 1000 μm, 500 μm, 250 μm, < 250 μm (figure 6).There were also two fractions, one containing oxidized needles, blades and other metal parts and one containing pieces of glass and unburned materials which were removed.

The humidity content was determined for each fraction using the gravimetric method in which the ash samples were dried in an oven (VO 500 oven) at 105 °C for 24 hours.

The determination of chemical composition was conducted on ash samples collected from the ash disposal place and straight from the furnace, due to water content difference. Each sample was divided into granulometric fractions as mentioned before. A quantity of 2 g of each fraction was accurately weighed into a 100 ml beaker. Twenty milliliters of aqua regia (HNO_3:HCl = 1:3) were added to the beaker. Then, the beaker was placed on a water bath for 24 hours and after that cooled at room temperature. The solution was filtered and then diluted with deionized water into a 100 ml volumetric flask. The element concentrations in the solutions were determined by inductively coupled plasma mass spectrometry (ICP-TOF-MS Optimass 9500 GBC, Australia, 2007) according to SR EN ISO 17294-2/2005.

The oxide composition of ash was determined through alkaline decomposition, based on STAS 9163/73 and the loss on ignition based on STAS 9163/3 – 73.

The morphology and shape of ash particles were determined using scanning electron microscopy (JOEL JSM5510 LV). A representative portion of ash was sprinkled onto double-sided carbon tape mounted on a SEM tub and coated with a thin layer of gold before examined. Each fly ash sample was characterized by randomly selecting 1 - 2 fields of view and examining all the ash particles observed within the selected fields. The elemental composition and morphology were noted for each particle and compiled for each sample [20].

ACKNOWLEDGEMENTS

This paper was funded by the Project "Doctoral studies in engineering science to develop knowledge - based society - "SIDOC" Contract POSDRU/88/ 1.5/S/60078.

REFERENCES

1. S.Javied, M. Tufail, Sofia Khalid, *Microchemical Journal*, **2008**, *90*, 77.
2. E. Emek, B. Kara, *Computers & Operations Research*, **2007**, *3*, 1424.
3. Y.C. Lin, J.H. Yen, S.K. Lateef, P.K.A. Hong, C.F. Lin, *Journal of Hazardous Materials*, **2010**, *182*, 337.
4. R. Siddique, *Resources, Conservation and Recycling*, **2010**, *55*, 84.
5. E. Gidarakos, Maria Petrantonaki, K. Anastasiadou, K.W. Schramm, *Journal of Hazardous Materials*, **2009**, *172*, 935.
6. J.D. Chou, M.Y. Wey, H.H. Liang, S.H. Chang, *Journal of Hazardous Materials*, **2009**, *168*, 198.
7. M. Ahmaruzzaman, *Progress in Energy and Combustion Science*, **2010**, *36*, 328.
8. C. Genazzini, G. Giaccio, A. Ronco, R. Zerbino, *Waste Management*, **2005**, *25*, 649.
9. J.E. Aubert, B. Husson, A. Vaquier, *Cement and Concrete Research*, **2004**, *34*, 958.
10. H.-S. Shi, L. Kan, *Construction and Building Materials*, **2009**, *23*, 2160.
11. A.Yilmaz, N. Degirmenci, *Waste Management*, **2009**, *29*, 1542.
12. IAWG, “Municipal Solid Waste Incinerator Residues”, *Elsevier Science*, **1997**, chapter 9.
13. X. Wan, W.Wang, T.Ye, Y. Guo, X. Gao, *Journal of Hazardous Materials*, **2006**, *B134*, 199.
14. L. Zhao, F.-S. Zhang, M. Chen, Z. Liu, D.B.J. Wu, *Journal of Hazardous Materials*, **2008**, *173*, 183.
15. R.D. Alorro, S. Mitani, N. Hiroyoshi, M. Ito, M. Tsunekawa, *Minerals Engineering*, **2008**, *21*, 1095.
16. F.Y. Chang, M.-Y. Wey, H, *Journal of Hazardous Materials*, **2006**, *B138*, 601.
17. B.G. Kutchko , Ann G. Kim, *Fuel*, **2006**, *85*, 2539.
18. A. Phongphiphat, C. Ryu, K.N. Finney, V.N. Sharifi, J. Swithenbank, *Journal of Hazardous Materials*, **2011**, *186*, 221.
19. R. Rajamma, R.J. Ball, L.A.C. Tarelho, G.C. Allen, J.A. Labrincha, V.M. Ferreira, *Journal of Hazardous Materials*, **2009**, *172*, 1054.
20. S.V. Vassilev, C.G Vassileva, *Energy Fuels*, **2005**, *19*, 1090.

STUDIA UBB CHEMIA, LVII, 2, 2012 (p. 157 - 167)

STUDIES ON THE PALLADIUM AND GOLD IONS EXTRACTION WITH SOME ESTER DERIVATIVES OF CALIX[N]ARENE

ALINA SAPONAR[a,*], ELISABETH-JEANNE POPOVICI[a], IOANA PERHAITA[a], GABRIELA NEMES[b]

ABSTRACT. The capability of *p-tert*-butyl calix[n]arene [n = 4,6,8] functionalized at the lower rim with a variable number of ethyl acetate groups to extract palladium and gold ions from aqueous medium has been investigated. The influence of reagent molar ratio, acidity of the medium and time on the extraction efficiency was investigated by monitoring the concentration of the metallic ions from aqueous solution. In most of the cases, the half substituted calix[n]arene derivatives show a relative high extraction efficiency and are of interest as liquid-liquid extraction reagents for precious metal ions.

Keywords: *Calixarene, liquid-liquid extraction, metal ions.*

INTRODUCTION

The design of new compounds that can act as extractants for toxic or valuable metals from waters and soils represent a continuous need, both in environmental and economical point of view. The challenge is to find ligands that efficiently and selectively extract commercially useful metals from aqueous medium and allow them to be released in pure form [1]. Calixarene is a class of compounds that successfully fulfill these requirements [2, 3]. They can be used as receptors for a large variety of ions and small molecules, forming host-guest or supramolecular complexes [4-12].

Calixarenes are a family of cyclic oligomers prepared from formaldehyde and *para*-substituted phenols via cyclic condensation under alkalin conditions [2]. They are characterized by a wide upper rim formed from the *para* substituents of the phenolic rings, a narrow lower rim formed from the phenolic hydroxyl groups and a central annulus i.e. a hydrophobic cavity consisting of aromatic rings [3]. Calixarene derivatives, with their large diversity of functional groups grafted at the upper or lower rims as well as with their cavity-shaped architecture, have been used extensively as selective ligands for metal ions in liquid-liquid extraction, in selective transport, as ionophores in ion-selective electrodes or as chromophores in optical sensing [13-24].

[a] Raluca Ripan Institute for Research in Chemistry, Babes Bolyai University, 400294, Cluj-Napoca, Romania, * salina@chem.ubbcluj.ro

[b] Faculty of Chemistry and Chemical Engineering, Babes-Bolyai University, 40084, Cluj-Napoca, Romania

The ability of the calix[n]arene molecules functionalized with electron donor groups to coordinate metal ions has been investigated by liquid-liquid extraction methods. These methods are based on the transfer of the analyte from the aqueous sample to a water-immiscible solvent [25]. The calix[n]arene derivatives dissolved in organic solvents (i.e. chloroform, dichloromethane, toluene, acetonitrile) are used as extractants for the recovery of the metals from aqueous solutions. They allow the exploitation of both the calixarene's cone-shape and the chelating ring of oxygen and nitrogen donor atoms that encircle the guests [26, 27].

Herein we present our studies referring to the extraction of precious metals using some calix[n]arene derivatives obtained by functionalization at the narrow rim with ethyl acetate donor groups, as already reported in our previous work [28]. We describe some calixarene-based compounds that were used as extracting agents in chloroform i.e. *p-tert*-butyl calix[4]arene grafted with two and four ethyl acetate groups, *p-tert*-butyl calix[6]arene grafted with two, three, four and six ethyl acetate groups and *p-tert*-butyl calix[8]arene grafted with four, six and eight ethyl acetate groups, respectively. Their capability to act as extraction agents for Pd^{2+} and Au^{3+} ions was investigated.

RESULTS AND DISCUSSION

The calixarene-based compounds used as extracting reagents are schematically presented in Figure 1 as follows: *bis*-ethylacetate-calix[4]arene (**C4Es2**), *tetra*-ethylacetate-calix[4]arene (**C4Es4**), *bis*-ethylacetate-calix[6]arene (**C6Es2**), *tris*-ethylacetate-calix[6]arene (**C6Es3**), *tetra*-ethylacetate-calix[6]arene (**C6Es4**), *hexa*-ethylacetate-calix[6]arene (**C6Es6**), *tetra*-ethylacetate-calix[8]arene (**C8Es4**), *hexa*-ethylacetate-calix[8]arene (**C8Es6**) and *octa*-ethylacetate-calix[8]arene (**C8Es8**).

The liquid-liquid extraction experiments were performed using $1x10^{-3}$ M aqueous solutions of $PdCl_2$ or $HAuCl_4$ and a $1x10^{-3}$ M solution of calixarene (Cx) in chloroform. The influence of the reagent molar ratio, acidity of the aqueous medium and time on the extraction efficiency was investigated by monitoring the concentration of metallic ions from the aqueous solutions, using Inductively Coupled Plasma Optical Emission Spectrometry.

Extraction of Pd^{2+} ions

The capability of *p-tert*-butyl-calix[n]arene esteric derivatives to extract Pd^{2+} ions from aqueous solutions was determined in a medium with variable pH (1.9, 2.6 and 3.1) using different molar ratios of reagents (Cx:Pd^{2+}= 2:1, 1:1 and 1:2), and a variable time of extraction (t = 30 - 360 min).

In a first stage, the extraction experiments were carried out at pH=2.6, using variable volumes of metal ions and calixarenes to achieve the Cx:Pd^{2+} molar ratios of 2:1, 1:1 and 1:2, respectively.

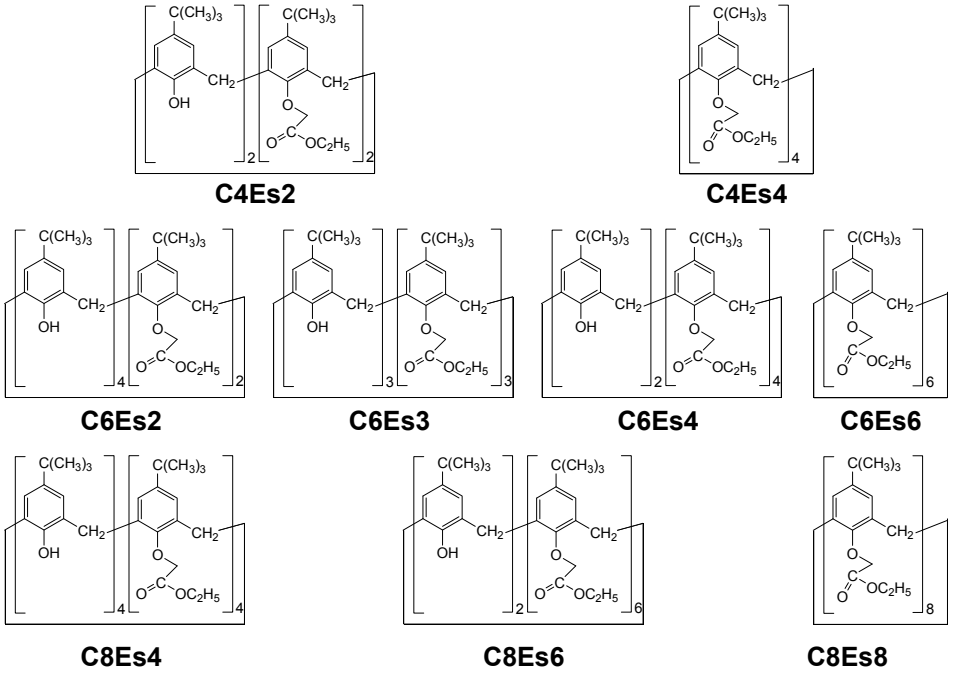

Figure 1. Calix[n]arene derivatives used as extracting agents

The dependence of the extraction yield (η) of the nine calixarene-based compounds on the ratios between the extractant and the extracted species is illustrated in Figure 2.

The yield for the extraction of Pd (II) ions from aqueous solution varies between 14.1% for **C6Es6** and 53.2% for **C6Es3**, in experiments with ratio Cx:Pd = 1:1, between 25.7% for **C8Es4** and 52.3% for **C4Es4** for Cx:Pd = 2:1 and between 18.2% for **C8Es6** and 40.9% for **C6Es3** for Cx:Pd = 1:2.

The highest extraction yield 53.2% was obtained for the **C6Es3** derivative, when calixarene:palladium ratio was 1:1.

The capability of calixarene-based compounds to "fix" palladium ions from aqueous medium can be estimated by the molar ratio **r** between the amount of extracted metal ion and the amount of extracting calixarene, a ratio that illustrates the number of mols of metal ion extracted by 1 mol of calixarene.

In our extraction conditions, the maximum extraction capability **r** was shown by the half- and totally substituted calix[6]arene, namely the compounds **C6Es3** (**r** = 0.82) and **C6Es6** (**r** = 0.93), when the ratio Cx:Pd^{2+} was 1:2.

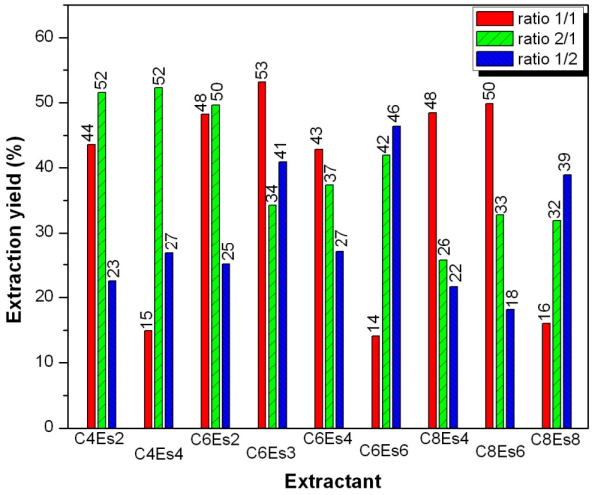

Figure 2. Extraction yield of Pd^{2+} with different calixarene-based compounds, using different Cx:Pd^{2+} ratios (pH=2.6, t=30 min)

The capability of *p-tert*-butyl calix[n]arene derivatives to extract palladium ions was also determined by liquid-liquid extraction experiments that were performed in an aqueous medium with variable pH, using equal volumes and equal concentrations of metal ions and calixarenes (Cx:Pd = 1:1). The results are summarized in Table 1.

Table 1. Extraction data for palladium ions, using different calixarene-based compounds at different pH (Cx:Pd^{2+} = 1:1; t=30 min)

Calixarene-based compounds	pH=1.9		pH=2.6		pH=3.1	
	η (%)	**r**	η (%)	**r**	η (%)	**r**
C4Es2	42.9	0.47	43.6	0.44	22.5	0.26
C4Es4	27.7	0.32	14.9	0.18	22.9	0.26
C6Es2	39.5	0.43	48.2	0.48	31.4	0.34
C6Es3	42.3	0.46	53.2	0.53	18.5	0.22
C6Es4	24.0	0.29	42.9	0.43	16.2	0.19
C6Es6	29.1	0.33	14.1	0.17	24.5	0.28
C8Es4	19.9	0.25	48.5	0.48	32.6	0.36
C8Es6	13.4	0.19	49.9	0.49	26.0	0.29
C8Es8	17.3	0.22	16.0	0.16	16.9	0.21

The extraction yield varies between 13.4% for **C8Es6** and 42.9% for **C4Es2** at pH 1.9, between 14.1% for **C6Es6** and 53.2% for **C6Es3** at pH=2.6 and between 16.2% for **C6Es4** and 31.4% for **C6Es2** at pH=3.1. It is obvious that the extraction yield of the Pd^{2+} ions with calixarene-based compounds depends on the acidity of the aqueous medium. Excepting the fully functionalized calix[n]arenes, all the calixarenele-based compounds show the maximum extraction efficiency at pH=2.6. For the calixarenes compounds **C4Es4**, **C6Es6** and **C8Es8,** the extraction efficiency is maximum at pH=1.9.

The highest extraction yield 53.2% was obtained for the **C6Es3** derivative, at pH=2.6. This compound shows the best extraction capability illustrated by the highest **r** value, namely 0.53. Good results were also obtained for **C4Es2** (η =42.9%, **r** = 0.47) at pH=1.9 and **C8Es4** (η =48.5%, **r** = 0.48) at pH=2.6.

It seems that the half-substituted compounds are more efficient as extracting reagents than the total functionalized compounds, whatever the pH. This could be due to a steric effect that is favourable for metal ion coordination.

The influence of the extraction time on the process efficiency was investigated for the totally functionalized calixarene derivatives, namely compounds **C4Es4**, **C6Es6** and **C8Es8**. The study was carried out in an aqueous medium with pH=2.6, using equal volumes and equal concentrations of metal ions and calixarenes (Cx:Pd = 1:1). The time of extraction was varied between 30 and 360 min (Figure 3).

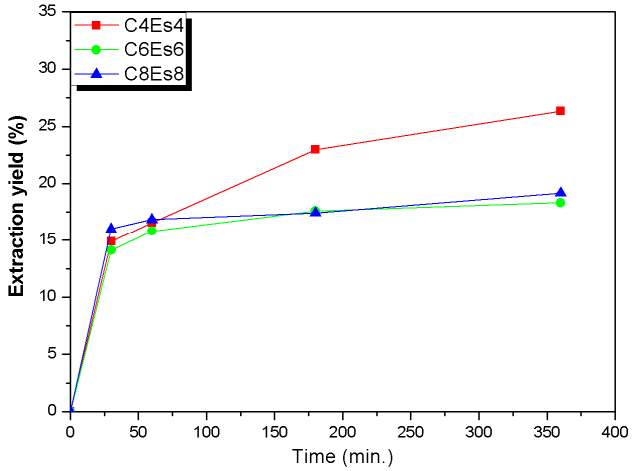

Figure 3. Variation of the extraction yield of Pd^{2+} with time, for some calixarene-based compounds (pH=2.6, Cx:Pd^{2+} =1:1)

For the tetraester calix[4]arene **C4Es4,** the extraction yield increases from 14.9% (30 min) to 16.6% (60 min) and 22.9% (180 min) and reaches the maximum value at 26.3% (360 min). Similar results are obtained for hexaester calix[6]arene and octaester calix[8]arene, when the efficiency varies between

14.1% (30 min) and 18.3% (360 min) for **C6Es6**, and 16.0% (30 min) and 19.2% (360 min) for the **C8Es8** compound.

In all cases, the extraction yield increases with time and tends toward saturation. The highest effect is observed for **C4Es4** compound which, in 6 hrs, extracts 0.29 mol Pd^{2+} ions/mol calixarene and attains the maximum **r** value.

Extraction of Au^{3+} ions

The capability of *p-tert*-butyl calix[n]arene ester derivatives to extract Au^{3+} ions from aqueous solutions was determined in a medium with variable pH (2.2, 3.2 and 4.1), using a variable time of extraction (t = 30 -1440 min).

First, the extraction of Au^{3+} ions was performed at a fix pH of 3.2, using equal volumes with equal concentrations of solutions of metal ions and calixarenes to achieve the ratio Cx:Au^{3+} = 1:1; the extraction time was 30 min (Figure 4).

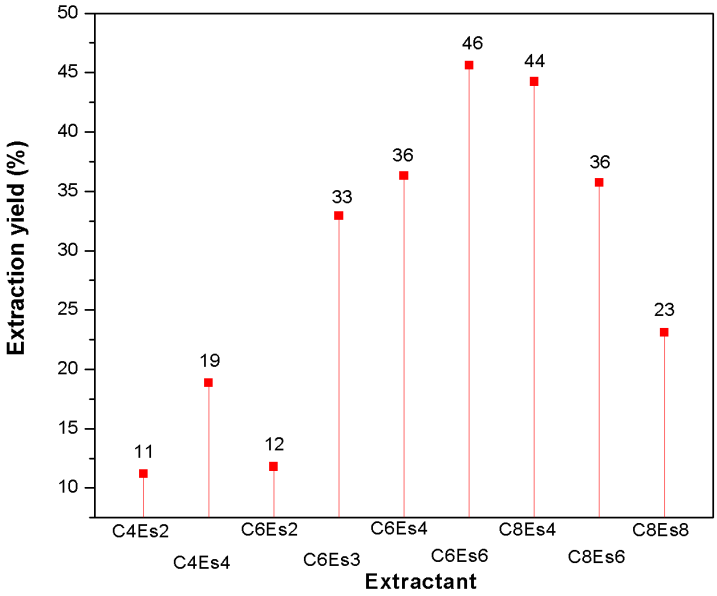

Figure 4. Extraction yield of Au^{3+} using different calixarene-based compounds (pH=3.2, Cx:Au^{3+} = 1:1, t = 30 min)

At pH=3.2, the highest extraction yield 45.6% was obtained for the hexaester calix[6]arene derivative. In our conditions, the extraction capability of the **C6Es6** compound is of 0.36 mol Au^{3+}/ mol calixarene. Relative good results were also obtained for compounds **C8Es4** (η =44.3%, **r** = 0.35), **C6Es4** (η =36.3%, **r** = 0.26) and **C8Es6** (η =35.8%, **r** = 0.25).

It seems that for Au^{3+} ions, the half substituted calixarenes exhibit the highest extraction capability only for the large-cavity compound **C8Es4**. The calixarene derivatives with four and six interconnected aromatic rings exhibit the maximum extraction efficiency when they are totally substituted. One can suppose that the highest extraction capability of the **C6Es6** compound is due to an optimum match between the trivalent charge of the gold ions and number of ligands i.e. six ester-groups grafted on the six interconnected aromatic rings.

The influence of the extraction time on the yield was investigated for the calixarene derivatives that show the maximum efficiency, namely compounds **C6Es6**, **C8Es4** and **C8Es8.** Experiments were carried out at pH=3.2, using equal volumes with equal concentrations of solutions of metal ions and calixarenes to achieve the ratio Cx:Au^{3+} = 1:1. The time of extraction was varied between 30 and 1440 min (Figure 5).

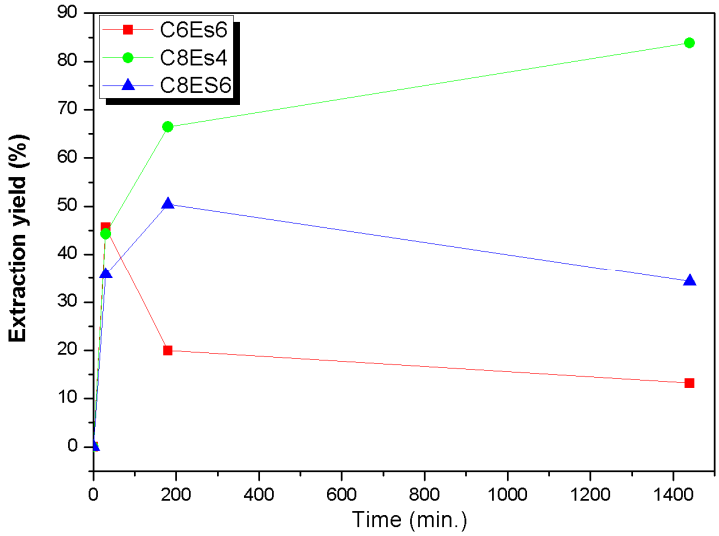

Figure 5. Dependence of the extraction yield of Au^{3+} on the time of extraction for some calixarene-based compounds (pH=3.2; Cx:Au^{3+} =1:1)

For the ester derivatives tested, the extraction yield shows an irregular dependence with time. For **C8Es4**, the yield increases from 44.3% (30 min) to 66.5% (180 min) and reaches the maximum values 83.9%, in 24 hrs.. For **C8Es6**, the yield increases from 35.8% (30 min) to 50.4% (180 min) and then decreases at 34.3% (1440 min). For **C6Es6**, the extraction efficiency decreases from 45.6% (30 min) to 19.9% (180 min) and reaches the minimum value, 13.2 % in 1440 min.

In our conditions, only the **C8Es4** compound shows a tendency toward saturation with time. This compound has the highest extraction capability (maximum **r** value), whatever the extraction time. Moreover, the **C8Es4** compound extracts in 24 hrs, 0.82 mol $Au^{3+/}$ mol calixarene.

It is obvious that for **C6Es6** and **C8Es8** compounds, the increase of the extraction time is unfavourable for the extraction process. It seems that, in our experimental conditions, a reverse process appears when the extraction lasts too much and part of the gold ions hosted by the calixarene is released in the medium.

The influence of the acidity of the aqueous medium on the extraction yield of Au^{3+} ions was also investigated. The liquid-liquid extraction experiments were performed for the triester and hexaester calix[6]arene derivatives, two compounds with a rather good extraction capability. Experiments were carried out for 30 min, using equal volumes with equal concentrations of solutions of metal ions and calixarenes to achieve the molar ratio Cx:Au^{3+} = 1:1. The dependence of the extraction yield on the pH of the medium is illustrated in Figure 6.

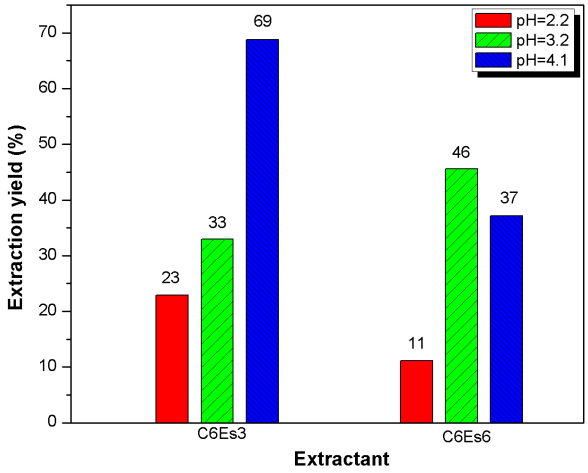

Figure 6. Variation of the extraction yield of Au^{3+} from solutions with variable pH, using different calixarene-based compounds
(Cx:Au^{3+} =1:1; t=30 min)

Compound **C6Es3** extracts between 22.9% (pH=2.2) and 68.8% (pH=4.1) of the amount of Au^{3+} ions from solution, while compound **C6Es6** pull out only from 11.2% (pH=2.2) to 37.2% (pH=4.1). For both calixarene compounds, the extraction efficiency increases with the pH of the medium (the only exception is **C6Es6**, which shows a relative lower value at pH=4.1).

In our extraction conditions, compound **C6Es3** exhibits the maximum extraction capability and efficiency at pH=4.1(**r** = 0.64; η = 68.8%) whereas compound **C6Es6** shows it at pH=3.2 (**r** = 0.36; η = 45.6%).

CONCLUSIONS

The capability of *p-tert*-butyl calix[n]arene functionalized at the lower rim with ethyl acetate groups to extract precious metallic ions has been investigated by liquid-liquid extraction experiments. Partial or total substituted calix[n]arenes with ester donor groups were used to extract Pd^{2+} and Au^{3+} ions from aqueous media, in different experimental conditions i.e. calixarene/ metal ratio, pH of the medium and time of extraction.

The highest extraction yield for palladium ions (53.2%) was obtained for **C6Es3** derivatives, when the calixarene:metal ratio was 1:1. Almost all calixarene-based compounds shows the maximum extraction efficiency at pH = 2.6. The highest extraction yield for gold ions was obtained for the **C6Es6** derivatives, namely 45.6% at pH=3.2.

The extraction yield can be considerably improved by modifying the extraction conditions: the time of extraction, pH of aqueous solution, etc. For example, for the extraction of palladium ions with the **C4Es4** derivative, when the time of extraction is modified, the extraction yield increase from 14.9% (30 min) to 26.3% (360 min). Also, for the extraction of gold ions with **C6Es3** derivative, at different pH of the aqueous medium, the extraction yield increase from 22.9% (at pH = 2.2) to 68.8% (at pH = 4.1).

In most of the cases, the half substituted calix[n]arene derivatives functionalized with ethyl acetate groups show a relative high extraction efficiency and are of interest as liquid-liquid extraction reagents for precious metal ions.

EXPERIMENTAL SECTION

Chemical reagents for extraction

The calixarene-based compounds were synthesized according to the methods described in our previous paper [28]. The following calixarene ester derivatives were used for the present study: 5,11,17,23 -tetra-*tert*-butyl-25, 27- bis[(ethoxycarbonyl) methoxy)]-26, 28 - dihydroxy-calix[4]arene (**C4Es2**); 5,11,17,23-tetra-tert-butyl-25,26,27,28-tetrakis[(ethoxycarbonyl)methoxy)]-calix[4]arene (**C4Es4**); 5,11,17,23,29,35 -hexa-*tert*-butyl-bis[(ethoxycarbonyl) methoxy)]-tetra hydroxy-calix[6]arene (**C6Es2**); 5,11,17,23,29,35-hexa-*tert*-butyl-37,38,39-tris[(ethoxycarbonyl)methoxy)]-40,41,42-trihydroxy-calix[6]arene

(**C6Es3**); 5,11,17,23,29,35-hexa-*tert*-butyl-tetrakis[(ethoxycarbonyl) methoxy)]-dihydroxy-calix[6]arene (**C6Es4**); 5,11,17,23,29,35-hexa-*tert*-butyl-37,38,39, 40,41,42-hexakis[(ethoxycarbonyl)methoxy]- calix[6]arene (**C6Es6**); 5,11,17,23, 29,35,41,47-*tert*-butyl-tetrakis-[(ethoxycarbonyl)methoxy)]-tetra-hydroxy-calix[8]arene (**C8Es4**); 5,11,17,23,29,35,41,47-*tert*-butyl-hexakis-[(ethoxycarbonyl) methoxy)]-dihydroxy-calix[8]arene (**C8Es6**) and 5,11,17,23,29,35,41,47-octa-*tert*-butyl-49,50,51,52,53,54,55,56-octakis[(ethoxycarbonyl)methoxy]-calix[8]arene (**C8Es8**).

$PdCl_2$ (p.a. Fluka) and $HAuCl_4x4H_2O$ (p.a. Merck) were used as supplier of Pd^{2+} and Au^{3+} metal ions ionic. Analytical-grade chloroform and deionized water were employed as solvents in the liquid-liquid extraction experiments.

Instrumentation and analysis

The metal concentration in aqueous medium was determined before and after extraction using Inductively Coupled Plasma Optical Emission Spectrometry. The analysis was performed with a Perkin Elmer ICP-OES spectrometer (OPTIMA 2100 DV), working with λ = 340.458 nm (D.L.= 0,003 mg/l) for palladium and λ = 267.595 nm (D.L.= 0,004 mg/l for gold.

Liquid-liquid extraction of metal ions

The organic solutions were prepared by dissolving the required amount of calixarene derivative in chloroform to obtain a solution with $1x10^{-3}$ M concentration.

The aqueous solution of metallic ions was prepared by dissolving the required amount of $PdCl_2$ or $HAuCl_4x4H_2O$ in acidulated water to obtain $1x10^{-3}$ mol/L solutions. The acidity of the aqueous medium was monitored with a pH-instrument. The pH was adjusted with HCl for Pd^{2+} or HNO_3 for Au^{3+} solution.

Liquid-liquid extraction experiments were carried out using different calixarene:metal Cx:M^{z+} ratios. For the ratio Cx:M^{z+} =1:1, the extraction was performed by introducing 15 mL of the organic solution and 15 mL of the aqueous solution into extraction funnels and vigorously shaking them, using a mechanical shaker. The aqueous phase was left to settle, washed with $CHCl_3$, separated and analysed.

The measurements were carried out with an ICP-OES instrument, using standard conditions calibration. The extraction yield (η%) was calculated from the equation [29]:

$$\eta = (A_0 - A) / A_0 \times 100\ \%$$

where A_0 and A are the initial and the final concentration (mg/L) of the metal salt before and after extraction, respectively.

ACKNOWLEDGEMENTS

This work was possible with the financial support of the Sectoral Operational Programme for Human Resources Development 2007-2013, co-financed by the European Social Fund, under the project number POSDRU 89/1.5/S/60189 with the title "**Postdoctoral Programs for Sustainable Development in a Knowledge Based Society".**

REFERENCES

1. C. Fontas, E. Antico, F. Vocanson, R. Lamatine, P. Seta, *Separation and Purification Technology*, **2007**, *54*, 322.
2. C.D. Gutsche, In *Calixarene revisited*, J.F. Stoddart, Ed., Royal Society of Chemistry: Cambridge, **1998**.
3. Z. Asfari, V. Bohmer, M.McB. Harrowfield, J. Vincens, *Calixarenes 2001*, Kluwer, Dordrecht, **2001**.
4. Y. Yang, G. Arora, F.A. Fernandez, J.D. Crawford, K. Surowiec, E.K. Lee, R.A. Bartsch, *Tetrahedron*, **2011**, *67*, 1389.
5. O.H. Altshuler, N.V. Malyshenko, G.J. Shkurenko, H.N. Altshuler, *Theoretical Foundations of Chemical Engineering*, **2009**, *43(1)*, 43.
6. S. Erdemir, M. Bahadir, M. Yilmaz, *Journal of Hazardous Materials*, **2009**, *168*, 1170.
7. M. Bayrakci, S. Ertul, M. Yilmaz, *Tetrahedron*, **2009**, *65*, 7963.
8. M. Atanassova, V. Lachkova, N. Vassilev, S. Varbanov, I. Dukov, *Polyhedron*, **2010**, *29*, 655.
9. L Elsellami, V. Chartron, F. Vocanson, P. Conchon, C. Felix, C. Guillard, L. Retailleau, A. Houas, *Journal of Hazardous Materials*, **2009**, *166*, 1195.
10. K. Ohto, H. Ishibashi, H. Kawakita, K. Inoue, T. Oshima, *Journal of Inclusion Phenomena and Macrocyclic Chemistry*, **2009**, *65*, 111.
11. A. Hamdi, R. Souane, L. Kim, R. Abidi, L. Mutihac, J. Vicens, *Journal of Inclusion Phenomena and Macrocyclic Chemistry*, **2009**, *64*, 95.
12. G. Daneshvar, A. Jabbari, Y. Yamini, D. Paki, *Journal of Analytical Chemistry*, **2009**, *64(6)*, 602.
13. N. Singh, D. Jang, *Supramolecular Chemistry*, **2009**, *21(5)*, 351.
14. A.V. Tenkovtsev, M.M. Dudkina, L.I. Scherbinskaya, V. Aseyev, H. Tenhu, *Polymer*, **2010**, *51*, 3108.
15. S. Sayin, F. Ozcan, M. Yilmaz, *Journal of Hazardous Materials*, **2010**, *178*, 312.
16. J. Kulesza, M. Guzinski, V. Hubscher-Bruder, F. Arnaud-Neu, M. Bochenska, *Polyhedron*, **2011**, *30*, 98.

17. V.I. Isaeva, A.L. Tarasov, O.P. Tkachenko, G.I. Kapustin, I.V. Mishin, S.E. Solov'eva, L.M. Kustov, *Kinetics and Catalysis*, **2011**, *52(1)*, 94.
18. P. Dinake, P.E. Prokhorova, V.S. Talanov, R.J. Butcher, G.G. Talanova, *Tetrahedron Letters*, **2010**, *51*, 5016.
19. M. Atanassova, N. Vassilev, I. Dukov, *Separation and Purification Technology*, **2011**, *78*, 214.
20. M. Atanassova, V. Lachkova, N. Vassilev, S. Varbanov, I. Dukov, *Polyhedron*, **2010**, *29*, 655.
21. B.B. Adhikari, K. Ohto, M. Gurung, H. Kawakita, *Tetrahedron Letters*, **2010**, *51*, 3481.
22. M. Atanassova, V. Lachkova, N. Vassilev, S. Varbanov, I. Dukov, *Polyhedron*, **2010**, *29*, 655.
23. M.C. Semedo, A. Karmali, P.D. Barata, J.V. Prata, *Journal of Molecular Catalysis B: Enzymatic*, **2010**, *62*, 97.
24. O. Karakus, H. Deligoz, *Analytical Letters*, **2010**, *43(5)*, 768.
25. F. Pena-Pereira, I. Lavilla, C. Bendicho, *Spectrochimica Acta Part B,* **2009**, *64*, 1.
26. X. Liu, K. Surowiec, R.A. Bartsch, *Tetrahedron*, **2009**, *65*, 5893.
27. M. Surowiec, R. Custelcean, K. Surowiec, R.A. Bartsch, *Tetrahedron*, **2009**, *65*, 7777.
28. A. Saponar, E.-J. Popovici, R.Grecu, I. Silaghi-Dumitrescu, N. Popovici, *Studia UBB Chemia,* **2009**, *LIV (4),* 203.
29. S. Sayin, M. Yilmaz, M. Tavasli, *Tetrahedron*, **2011**, *67*, 3743.